HIV-1: Identification of a Pathway for Virus release and Development of a New Nanotechnological Strategy to Counteract the Infection

D I S S E R T A T I O N

zur Erlangung des akademischen Grades

d o c t o r r e r u m n a t u r a l i u m

(Dr. rer. nat.)

im Fach Biologie

eingereicht an der Lebenswissenschaftlichen Fakultät

der Humboldt-Universität zu Berlin

von

M.Sc. Andrea Gramatica

Präsident der Humboldt-Universität zu Berlin:
Prof. Dr. Jan-Hendrik Olbertz

Dekan der Lebenswissenschaftlichen Fakultät:
Prof. Dr. Richard Lucius

Gutachter: 1. Prof. Dr. Andreas Herrmann

2. Prof. Dr. Thomas Sommer

3. PD Dr. Norbert Bannert

Eingereicht am: 06.05.2014

Datum der Promotion: 31.07.2014

Νὺξ ἱερὴ καὶ λύχνε, συνίστορας οὔτινας ἄλλους

ὅρκοις ἀλλ᾽ ὑμέας εἱλόμεθ᾽ ἀμφότεροι ˙

[...]

„Holy night and light, we chose you and none other as witnesses for our vows". *Meleager of Gadara (Greek Anthology book I chapter I part VII – Epigram LXVIII)*

Zusammenfassung

Das Humane Immundefizienz-Virus 1 (HIV-1) rekrutiert Wirtszellproteine und -Signalwege für seinen eigenen Lebenszyklus und beeinträchtigt viele Funktionen von Immunzellen, darunter die Phagozytose von Pathogenen durch Makrophagen. Diese Schwächung der Immunabwehr verursacht das *acquired immunodeficiency syndrome* (AIDS).

Der Zusammenbau von HIV-1 geschieht sowohl an der Plasmamembran als auch in endosomalen Kompartimenten und wird durch das Struktur-Polyprotein Gag kontrolliert, das auch für die Freisetzung virusähnlicher Partikel (VLPs) aus der Wirtszelle sorgt. Vorangegangene Studie haben gezeigt, dass durch hohe induzierte Calciumkonzentrationen im Zytoplasma die Anzahl an VLPs in endolysosomalen Kompartimenten steigt und die VLP-freisetzung drastisch zunimmt [1,2]. Der verantwortliche Mechanismus ist jedoch bisher unbekannt.

Die vorliegende Arbeit zeigt zunächst, dass Calciumausschüttung aus Lysosomen die Fusion von Endosomen und Lysosomen - und damit die Exozytose der in Lysosomen enthaltenen VLPs - auslöst. Dieser Prozess wird durch Synaptotagmin VII reguliert und verhindert den Abbau eines Teils der in späten Endosomen und Lysosomen eingschlossenen VLPs.

Der zweite Teil dieser Arbeit beschreibt die Entwicklung eines nanobiotechnologischen Systems zur Eliminierung von Env/Gag-VLPs (HIV-VLPs) mit Hilfe von Makrophagen. Dieses basiert auf Immunoliposomen, die HIV-VLPs über anti-Env-Antikörper binden und von Makrophagen dank membranständigem Phosphatidylserin (PS), einem apoptotischen Signal, phagozytiert werden. Die Liposomen imitieren apoptotische Zellen und induzieren ihre Internalisierung und die lysosomale Aufnahme von HIV-VLPs. Das System nutzt einen effizienten Internalisierungsweg, der während der HIV-1-Infektion nicht beeinträchtigt ist.

Diese Ergebnisse bieten neue Einblicke in die intrazellulären Prozesse der HIV-1 Freisetzung und präsentieren PS-Immunoliposomen als neuen potentiellen nanomedizinischen Ansatz zur Virusbeseitigung und HIV-Antigenpräsentation.

Schlagwörter: HIV-1, virusähnliche Partikel, Immunoliposomen, Phagozytose

Abstract

Human immunodeficiency virus 1 (HIV-1) hijacks proteins and signaling pathways of the host cell for its own life cycle, thereby impairing many functions of immune cells, including pathogen-phagocytosis by macrophages. The overall weakening of immune functions eventually results in the development of acquired immunodeficiency syndrome (AIDS).

HIV-1 assembly takes place at the plasma membrane as well as in endosomal compartments and is governed by the structural polyprotein Gag, which is also sufficient for the release of virus-like particles (VLPs) from the host cell. It was shown that an induced high cytoplasmic calcium concentration increases the amount of VLPs in endo-lysosomal compartments and results in a dramatic enhancement of VLP release [1,2]. However, the mechanism by which calcium can promote the release of VLPs remains to be determined.

The first part of this work shows that release of calcium from lysosomes causes fusion between endosomes and lysosomes as well as exocytosis of lysosome-entrapped VLPs. This mechanism is regulated by Synaptotagmin VII and prevents degradation of a part of the late endosome- and lysosome-entrapped VLPs.

The second part focuses on the development of a nanobiotechnological system for the clearance of Env/Gag-VLPs (HIV-VLPs) by macrophages. This system is based on immunoliposomes that (1) bind HIV-VLPs via anti-Env antibodies and (2) are phagocytosed by macrophages due to the presence of phosphatidylserine (PS), an apoptotic signal. Essentially, the PS-liposomes mimic apoptotic cells thereby inducing internalization and lysosomal delivery of bound HIV-VLPs. These immunoliposomes exploit an efficient internalization pathway not impaired upon HIV-1 infection.

The results of this thesis provide new insights into the intracellular pathways controlling HIV-1 release and demonstrate that PS-immunoliposomes can represent a novel nanomedical approach for viral clearance and HIV antigen presentation.

Keywords: HIV-1, Virus-like particles, Immunoliposomes, Phagocytosis

Content

The UNAIDS Global Report of AIDS epidemic 2013 declares that about 35 million people were living with human immunodeficiency virus (HIV) in 2012. This represents an increase from previous years and is owed to the fact that more people are receiving the life-saving antiretroviral therapy. In 2012 there were two million new HIV infections globally, showing a 33% decline in the number of new infections in 2001. The number of AIDS deaths is also declining with 1.6 millions AIDS deaths in 2012, down from 2.3 million in 2005. Despite the decrease of HIV infections and AIDS deaths in the last years, HIV/AIDS has remained on the top of the major causes of death during the past decade.

1 INTRODUCTION

1.1 The biology of HIV-1

HIV is a single-stranded, positive-sense, enveloped RNA virus, which belongs to the genus *Lentivirus,* family *Retroviridae*. This virus has probably originated through the evolution of a simian immunodeficiency virus (SIV) in non-human primates in West-central Africa and subsequently has been transferred to humans in the early 20th century [3]. Two types of the virus, HIV-1 and HIV-2, have been characterized. HIV-1 is the virus that was initially discovered (Figure 1): it is more virulent, more infective and is the cause of the majority of HIV infections globally. HIV-2, on the contrary, shows a lower infectivity, poor capacity to be transmitted and is mostly confined to West Africa regions. The transmission of HIV takes place mostly through sexual intercourse, contacts with infected blood and breast milk.

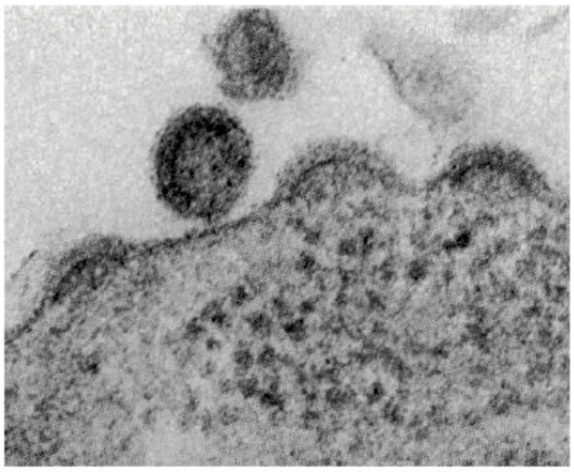

Figure 1. One of the first electron microscopy images of HIV-1 budding in lymphocytes. Electron microscopy image of a thin section of virus producing cord lymphocytes. The inset shows various stages of particles budding at the cell surface. Adapted from **[4]**.

1.1.1 Structure and genome

Mature viruses are composed by a viral envelope and a matrix [5]. In the interior part is enclosed a capsid, which itself encloses two copies of the single-stranded RNA genome and several enzymes (Figure 2). In the HIV-1 genome, starting from the 5'-end, are found the group-specific antigen (gag), the polymerase (pol), and the envelope glycoprotein (env) genes (Figure 3). The gag gene encodes a polyprotein precursor, which can be identified as Pr55, based on its molecular weight, or as "Gag", the structure-protein. Subsequently to the release of the newly produced virus, the Gag protein undergoes a maturation process, during which it becomes cleaved by the viral protease (PR) to the mature matrix protein (also known as MA or p17), capsid (CA or p24), nucleocapsid (NC or p7), and p6 (Figure 2) [5]. Two spacer peptides, p2 and p1, are also generated upon Gag processing. The pol gene encodes for different enzymes that are initially synthesized as part of a large polyprotein precursor, Pol (or Pr160, or "GagPol precursor"), whose synthesis results from a rare frame-shifting event during Gag translation. The pol-encoded enzymes, PR, reverse transcriptase (RT), and integrase (IN), are cleaved from Pr160 by the viral PR. The envelope glycoproteins are also synthesized as a polyprotein precursor (i.e. gp160). Gp160 is processed by a cellular protease during Env trafficking to the cell surface. The processing of gp160 results in the generation of the surface glycoprotein gp120 and the transmembrane glycoprotein gp41. Gp120 is responsible for the interaction with the CD4 receptor and the co-receptor(s), while gp41 anchors the gp120/gp41 complex in the membrane and performs the membrane fusion reaction between viral and host lipid bilayers, during the virus entry process. HIV-1 also encodes a number of regulatory and accessory proteins: Tat, Rev, Vpu, Vif, Vpr and Nef. Tat is critical for transcription of the viral genome, Rev plays a major role in the transport of viral RNAs from the nucleus to the cytoplasm. Vpu, Vif, Vpr and Nef have been recognized to be not uniformly required for virus replication, and therefore have been termed "accessory proteins".

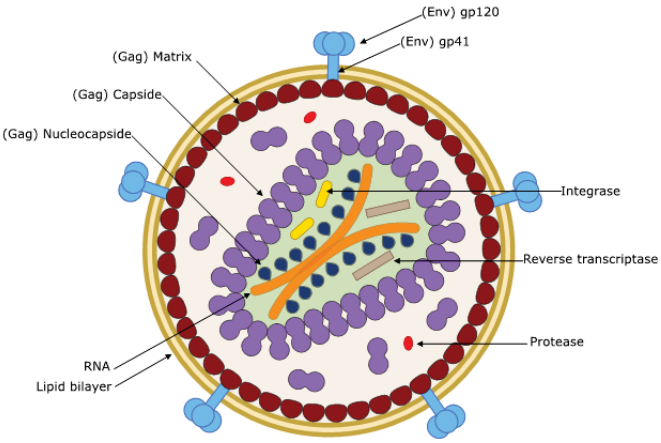

Figure 2. Schematic representation of HIV-1. From the outer part to the inner it can be found the spike proteins (Env), the lipid bilayer and the MA. Inside the particle the PR enzymes and the inner core of the virus, made by the CA proteins, can be found. Inside the core, there are the RT and IN enzymes and the viral RNA genome associated to NC residues. Adapted from **[6]**.

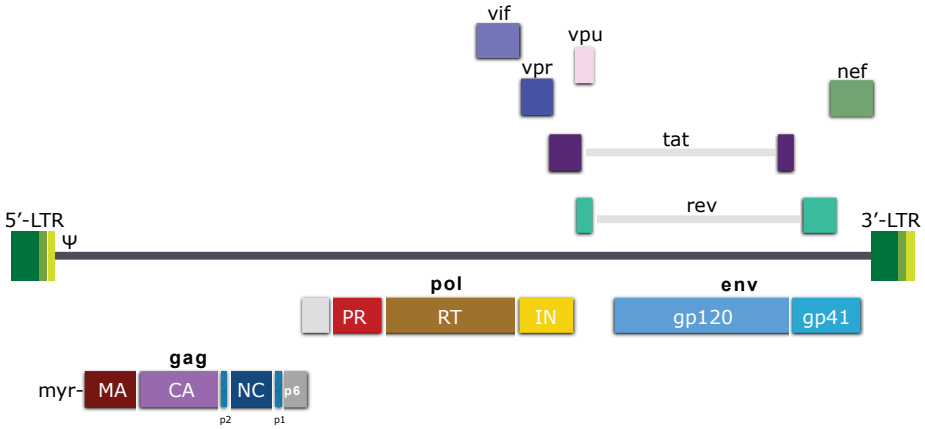

Figure 3. Schematic representation of the HIV-1 genome. The relative locations of the HIV-1 open reading frames gag, pol, env, vif, vpr, vpu, nef, tat, and rev are indicated. The 5' and 3' long terminal regions (LTRs) are shown. The ψ indicates the position of the RNA packaging signal. The major Gag domains (MA, CA, NC, p6) and the Gag spacer peptides (p2 and p1) are shown under the gag gene. The site of Gag N-terminal myristylation is denoted as "myr". Under the pol gene are indicated the PR, RT and IN coding regions. Sequences of the gp120 and gp41 Env glycoproteins are shown. Adapted from **[5]**.

1.1.2 Replication cycle

Once it has entered the host, HIV-1 can penetrate into specific target cells of the immune system and initiate its replication cycle (Figure 4): subsequent to the entry into the target cell, the viral RNA genome is first converted into a double-stranded DNA and subsequently integrated into the cellular genome. After integration into the host DNA, the virus may be either immediately activated, resulting in transcription of viral RNA, production of viral proteins and assembly and release of new viral particles, or become latent, avoiding the detection by the immune system.

Entry mechanism

HIV-1, as an enveloped virus, must fuse with the phospholipid bilayer of the host cell. This process, mediated by the spike-glycoprotein Env, leads to the disassembly of the viral core and the delivery of the viral genome to the cytoplasm and finally to the nucleus [7]. Fusion of HIV-1 with the target phospholipid bilayer mostly takes place at the plasma membrane (PM) [7]: a successful fusion between HIV-1 and target cell requires, initially, a high-affinity binding between gp120 and the T-lymphocyte receptor CD4. This association triggers conformational changes in Env that enable subsequent interactions with the so-called "co-receptor", which is a member of the seven-transmembrane chemokine-receptor family, usually CCR5 or CXCR4. This interaction, in turn, elicits more drastic changes in Env, releasing the fusogenic potential of gp41. Recently, it was shown that HIV-1 can also enter target cells via endocytosis [8]: after recognition and binding between Env and CD4/co-receptor (CXCR4 or CCR5), the virus can be endocytosed and then fuse with the endosomal membrane releasing its viral core into the cytoplasm. Besides these entry pathways, also described as "cell-free entry pathways" [9], in several physiologically relevant cells types (T-cells, macrophages, and dendritic cells), HIV-1 was shown to be able to enter target cells through points of cell-cell contact, the so-called "virological synapses" by analogy with similar structures–immunological synapses that form between antigen-presenting cells and T-cells. An HIV-1 virological synapse is characterized by polarization of the actin cytoskeleton and by accumulation of CD4, co-receptors, adhesion molecules, and tetraspanins, in addition to Gag and Env glycoproteins [10]. In macrophages, viral particles appear to assemble within an internal but surface-connected compartment [11]; in dendritic cells

(DCs), virus is thought to bind to the outer cell surface and then be taken into a similar compartment [12]. Such pre-assembled particles can subsequently move to the cell-cell junction on the way of synapse formation, allowing for efficient cell-cell transfer.

Assembly and budding

Following the integration into the host chromosome, the transcription of the viral RNAs, that ultimately encode the full complement of structural, regulatory, and accessory proteins used to direct virus replication, may start. The basal transcriptional activity from the provirus is initially very low: immediately after integration, only the host factors are responsible for the transcription process (e.g. RNA polymerase II, transcription factor IID, NF-kB). RNA synthesis is then greatly increased (by more than two logs) only when the transcriptional trans-activator protein Tat is present [5]. The produced viral RNAs can be then either: I) unspliced, which function as the mRNAs for the Gag and Pol polyprotein precursors, and are packaged into progeny viruses as genomic RNA, or II) partially spliced mRNA, which are around 5 kb in size and encode the Env, Vif, Vpu, and Vpr proteins, and III) small (1.7 to 2.0 kb), multiply spliced mRNAs, which are translated into Rev, Tat, and Nef. Following the synthesis of the full complement of viral proteins, the assembly process takes place. The major player in virus assembly is the precursor polyprotein Gag [13]. This protein contains determinants that target it to the PM [14], where it specifically binds to phosphatidylinositol(4,5)-bisphosphate (PIP_2) (Figure 6). Gag can also promote Gag-Gag interactions, encapsidate the viral RNA genome, associate with the viral Env glycoproteins, and finally stimulate budding from the cell [15,16]. The site of viral assembly has been shown to vary in respect of the infected cell: in T-cell Gag traffics as monomers or lower-order oligomers to the PM, where it undergoes higher-order multimerization and initiates particle assembly [17], while in macrophages or DCs Gag has been found to assemble in the lumen of late endosomes (LEs) or multivesicular bodies (MVBs) [18] (see further detail in the paragraph "trafficking to the assembly site"- section 1.1.3). Gag and Pol are synthesized by free ribosomes in the cytoplasm, while Env synthesis takes place in the endoplasmic reticulum (ER) [19]. Pol is produced as the result of a rare frame-shifting event during Gag translation. The enzymes encoded by pol are then packaged into virus via their Gag domain, largely using the same Gag-Gag interactions that drive Gag assembly. The Env precursor protein gp160 is co-translationally inserted into the ER membrane, exposing its ectodomain into the lumen of the ER, where it

forms intramolecular disulfide bonds and undergoes oligomerization [19]. Subsequently, during transport though the Golgi, the gp120 domain is heavily glycosylated. The Env glycoprotein complexes that reach the cell surface can be then either rapidly internalized, through recognition by host cell machinery of an endocytosis motif in the gp41 cytoplasmic tail, or are incorporated into virus particles [20]. The final step in the process of virus assembly involves the pinching off, or budding, of the virus particle from the host cell PM. As many other retroviruses and different enveloped viruses, HIV-1 encodes specific sequences that promote particle release. These sequences are collectively referred to as "late domains" or "L-domains" to reflect their role late in virus assembly [21]. The L-domains are usually encoded in the Gag sequence; in the case of HIV-1, the L-domain is present in the p6 domain. Deletion of p6, or mutations within the highly conserved Pro-Thr/Ser-Ala-Pro motif located near the N-terminus of p6, can strongly impair particle release [22]. The L-domain interacts with different host factors that play a fundamental role promoting the budding of viral particles. Specifically, the L-domain recruits the cellular endosomal-sorting complex required for transport-machinery (ESCRT), which normally assists budding and release of vesicles into the lumen of late endosomes [23]. The ESCRT machinery is known to comprise more than 25 proteins, organized into four complexes (ESCRT-0, -I, -II, and -III) that function sequentially along with several additional associated factors [24]. ESCRT-III and Vps4 (a protein required for the stripping of other ESCRT components) must be recruited to the bud neck to execute the final bud scission event and to release the ESCRT factors from the assemblage, for recycling back to the cytosolic pool [25]. The immature Gag shell, in which Gag molecules are radially arranged with their N-terminus in contact with the membrane and their C-terminus oriented toward the center of the virus, disassembles concomitant with particle release when the viral PR cleaves the Gag and GagPol polyproteins into their constituent proteins.

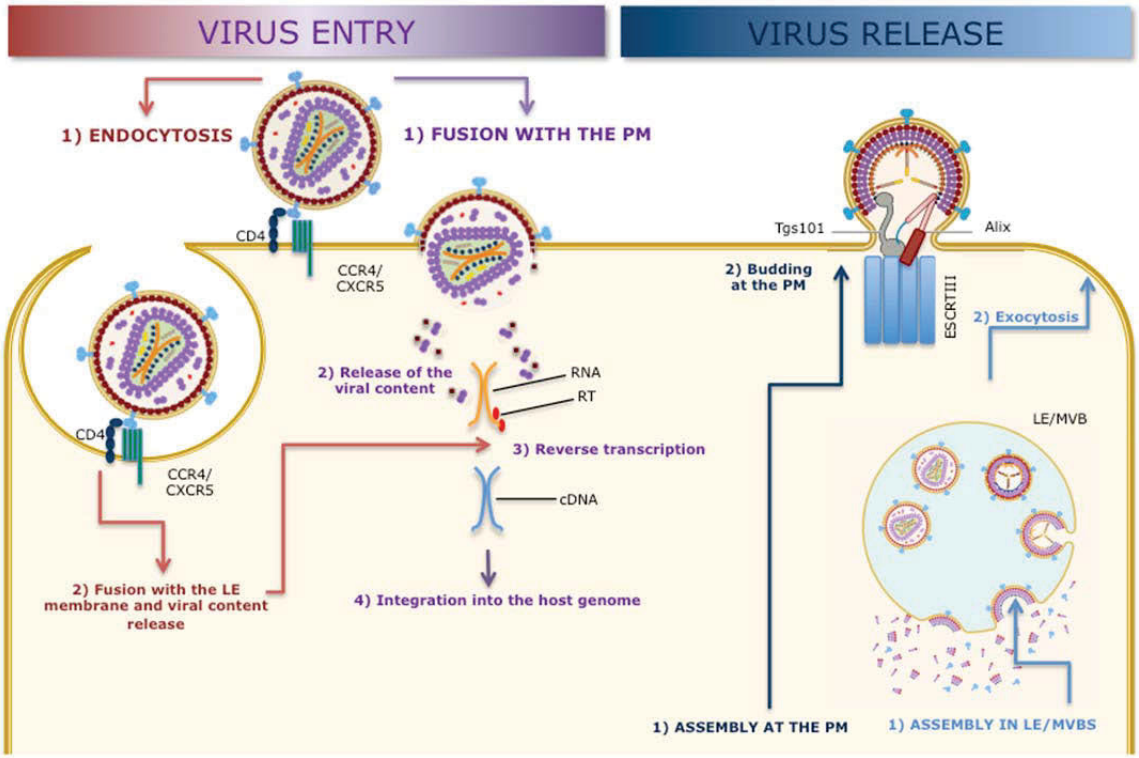

Figure 4. Schematic representation of the HIV-1 entry and release. On the left side are shown two entry mechanism: 1) endocytosis and subsequent fusion with the endosomal membrane and 2) direct fusion with the PM. Both entry mechanisms are followed by uncoating and release of the viral content, reverse transcription and HIV-DNA integration into the host genome. On the right side of the figure two exit mechanisms 1) direct assembly at the PM and 2) assembly in LEs/MVBs are shown. Mechanism 1: Gag traffics to the inner (cytoplasmic) leaflet of the PM where it initiates virus assembly and budding (typically observed in T-cells). Mechanism 2: Gag assembles on the cytoplasmic face of intracellular vesicles such as LE/MVBs, and the ensuing virus particles bud into the intraluminal space. The virus-harboring vesicles then traffic to and fuse with the PM, thereby resulting in the extracellular release of the virions. Adapted from **[6]**.

1.1.3 The structure-protein Gag

Gag (Figure 5) is the major structural protein and the building block of HIV-1 and comprises about 50% of the mass of a viral particle [26]. This protein, interacting with different host factors, is necessary and sufficient for orchestrating particle assembly, since its expression alone, in suitable eukaryotic cells, leads to the production of virus-like particles (VLPs) [27].

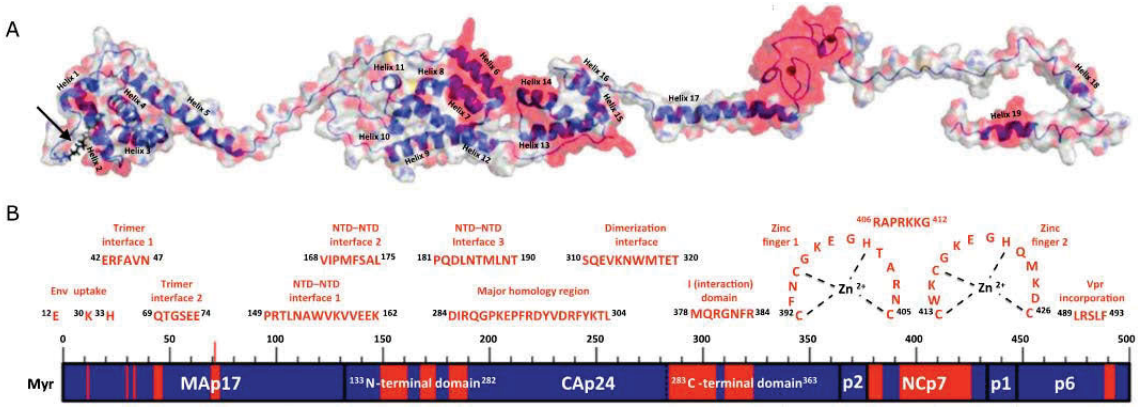

Figure 5. Schematic representation of the Gag polypeptide. (A) Tertiary structure of the myristoylated Gag. The Gag polypeptide, with helices (numbered from 1 to 19 starting from the N-terminal) and loops, is shown in blue with the respective atoms space-filling rendering. The regions responsible for the interaction of Gag with other viral proteins, as well as itself to form higher ordered structures, are highlighted in red. The position of the myristic acid is indicated by an arrow. (B) Schematic representation of the four major domain of Gag: MA, CA, NC, p6 and the two spacer-peptides (p2 and p1). N-terminal (NTD) and C-terminal (CTD) domains of CA are indicated highlighting their relevance in forming Gag-Gag interaction-interfaces. The specific amino acids involved in interactions between viral proteins (e.g. Env uptake, Vpr incorporation) and forming the two zinc-fingers are also indicated (orange). Adapted from **[28]**.

The MA domain is composed by 128 amino acids and comprises five alpha helices and a three strand mixed beta sheets [28]. The N-terminus Gly-2 is post-translationally myristoylated by covalent attachment of myristic acid by N-myristyltransferase within the consensus sequence MGXXX(S/T)XX (see position of myrtistic acid in the Gag polypeptide in Figure 5). Myristoylation is critical for PM targeting and viral assembly [29]: the MA domain binds specifically to PIP_2 in the inner leaflet of PM. This binding induces a conformational change in MA that exposes the N-terminus myristate moiety, which becomes inserted into the inner leaflet,

thereby stabilizing Gag-PM association. A PIP_2 recognition motif sequesters the unsaturated fatty acid of PIP_2 into the same hydrophobic pocket from which the myristic acid group is displaced allowing interaction of the myristic acid group with the PM and forming a bi-directional lipid anchor (Figure 6) [30]. The MA domain is also involved in interaction with the cytoplasmic tail of the Env gp41 protein to aid incorporation of Env into the viral particles [19]. Within the mature virus, the CA domains (231 amino acids) form the structural core, while CA–CA interactions are essential for the formation of the immature particles and any effector that can interfere with this process has a severe effect on viral replication. The proline-rich loop between helix 9 and 10 is a target for an innate immune factor, the tripartite motif-containing motif 5-alpha (TRIM5α) [31], which interferes with the early stages of viral uncoating during replication by targeting incoming virions to the proteasome. TRIM5α is a multimeric protein and forms hexameric lattices when stimulated by the presence of a CA lattice. HIV-1 overcomes the binding of TRIM5α by binding a molecule of cyclophilin A, a prolyl-peptidyl isomerase, to the same target site [32]. The NC region of Gag is constituted by 55 amino acids that form two zinc fingers separated by a functionally important basic domain. This region has two distinct roles during the assembly and maturation of the virus particle: I) to fulfill a major structural role within Gag–Gag interactions by forming the immature viral particle; and II) to play a role in nucleic acid recognition and interaction during viral replication [28]. The ALG-2-interacting protein X (ALIX), an ESCRT-associated protein that promotes viral budding, binds to both NC as well as p6 [33]. At the C-terminus of Gag the p6 domain is located, made up of a 52 amino acids forming two helices. Two functional regions have been mapped to the p6 domain: an N-terminal PTAP motif, which represents the late-domain and a C-terminal LXXLF sequence, which participates in the incorporation of Vpr into particles [34]. PTAP binds to the cellular tumor susceptibility gene 101 (Tsg101 or ESCRT-I), a protein involved in vacuolar cell sorting, which plays a fundamental role in the release of VLPs [35].

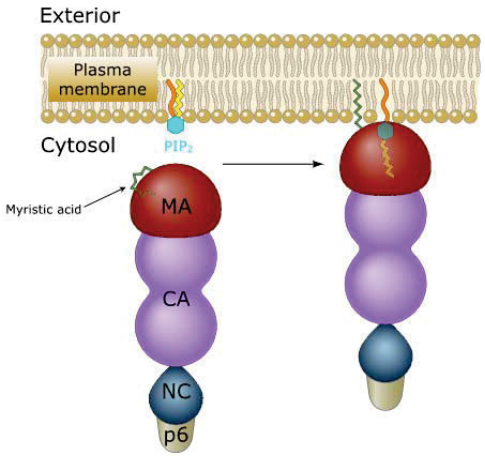

Figure 6. HIV-Gag association with PIP_2 at the plasma membrane. The N-terminal myristic acid moiety of MA is depicted in its sequestered conformation. PIP_2 embedded in the inner leaflet of the plasma membrane lipid bilayer is shown with its 1′ (orange) and 2′ (yellow) acyl-chains in the lipid bilayer. The arrows indicate the binding between MA and PIP_2, which leads to the flipping out of the myristate moiety into an exposed conformation and its subsequent insertion into the lipid bilayer. Adapted from **[6]**.

Trafficking to the assembly site

After its synthesis in the cytosol, Gag can traffic as monomer or lower-order oligomers to membranes, where it undergoes higher-order multimerization and initiates particle assembly. Interestingly, *in vitro* soluble Gag exists in monomer-dimer, monomer-trimer equilibrium, or can even assemble into a small sphere [36], suggesting that Gag may possess an intrinsic capability to build up into particles with a spherical shape. Gag binding to cell membranes (mostly PM) has been observed to take place already within 5–10 min post-synthesis [37]. The observations that cholesterol depletion diminishes PM binding of Gag, disrupts higher-order Gag multimerization and impairs virus production, together with other biochemical and microscopic data, implicate Gag association with lipid rafts [38]. Lipid rafts, also referred to as "membrane-rafts", are highly dynamic membrane microdomains that are rich in cholesterol and sphingolipids, display lateral heterogeneous protein distribution, and compartmentalize cellular processes [39]. The Env glycoproteins were also shown to be raft-associated, at least in part due to their association with Gag, and specifically the gp41 cytoplasmic tail has been reported to contain the determinants for Env association with rafts [40]. However, for a successful viral assembly at the PM, it is also required that all viral components traverse the cytoplasmic space and precisely target to the PM. In fact, it has been shown that in cells physiologically relevant for HIV-1 infection, like macrophages and T-lymphocytes,

but also in epithelial cells, Gag and, in some cases, VLPs are localized into intracellular compartments enriched in late endosomal and lysosomal markers [2,41]. A schematic representation of the suggested pathway for viral assembly is reported in Figure 7.

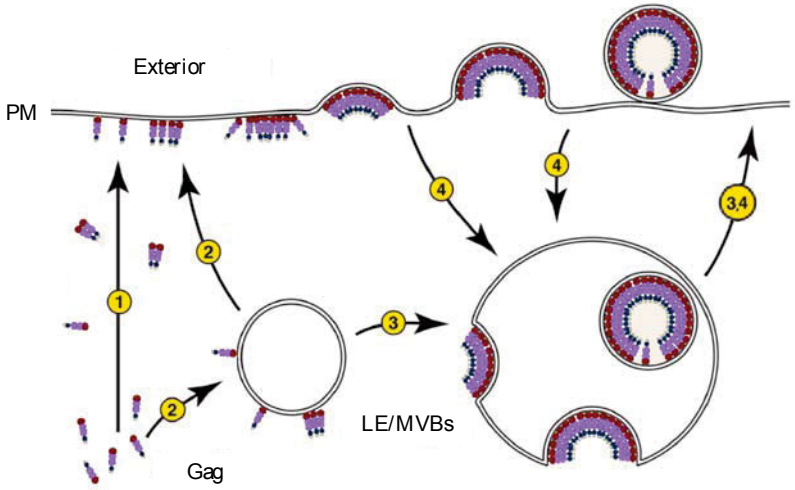

Figure 7. Potential involvement of endosomal trafficking pathways in Gag targeting. Potential Gag trafficking routes. Gag may be either directly targeted to the PM (pathway 1) or transported to the PM through endosomal trafficking routes (pathway 2). Along the latter pathway, Gag may form virus particles inside the endosomal lumen and later get released by fusion of endosomes with the PM (pathway 3). However, the interpretation of Gag localization data is complicated because virus particles accumulated in endosomes may have been formed at the PM and internalized before being released to the extracellular space (pathway 4). Adapted from **[30]**.

This suggests that nascent Gag may be at least in part targeted to endosomal membranes for assembly, and the resultant particles may bud into the lumen of late endosomes/multivesicular bodies from which they exit the cell by usurping cellular processes such as the exosome release pathway [42]. Moreover, as also previously mentioned, it is well established that HIV-1 budding requires the activity of ESCRT proteins, which usually are designate to facilitate the budding of vesicles into the endosomal lumen [33]. Among the many intracellular factors known to facilitate the trafficking of Gag to the assembly site(s), intracellular calcium levels and activation of the phospholipase C (PLC) pathway have been hypothesized to modulate Gag trafficking [43]. In a study on HIV-1 particle production it was demonstrated that induction of a transient rise in the cytosolic calcium concentration results in a dramatic rise in viral particle release, suggesting that calcium might represent a limiting factor in late-stage replication [2,44]. In parallel in another

work, it was demonstrated that activation of PLC and modulation of inositol(1,4,5)-triphosphate receptor (IP3R) function, i.e., recruitment of IP3R to the cell periphery and gating of intracellular calcium stores, influence Gag accumulation at the PM and virus release [1]. Even if the exact role of the activated IP3R and how elevated calcium enhances Gag accumulation at the PM remains to be determined, a preliminary model of functions has been proposed: recruitment of IP3R machinery to the cell periphery and release of calcium may function to increase the portion of PM PIP_2 available for interaction with Gag. Considering that PIP_2 does not have a natural inclination for clustering, due to the energy barrier posed by repulsion of the large polar head groups when they are in proximity, calcium might reduce this barrier and induce PIP_2 clustering in lipid monolayers [45].

Virus-like particles: formation and release

VLPs are replication as well as infection incompetent, since they lack regulatory proteins as well as infectious genetic material. This property has allowed them to be used and studied in different contexts [46,47]. In the context of a mammalian expression vector, VLP formation requires (at least) the presence Gag and specifically of the N-terminal domain of CA (amino acids 133 to 277) for assembly, budding and release in human embryonic kidney 293T (HEK-293T) cells [22,48] (see VLPs formation pathway in Figure 8A-C). Co-expression of Gag and Env results in the formation and release of VLPs bearing also the spike glycoproteins (see VLPs formation pathway in Figure 8F). Besides targeting of membrane binding and virus assembly, MA also influences Env glycoprotein incorporation in the nascent particle. An appealing model invokes, that entrapment of Env into virions is strictly regulated by an interaction between sequences within the long cytoplasmic tail of gp41 and holes present in the lattice-like matrix structure formed upon MA trimerisation [47]. VLPs destined for biochemical and immunological analysis can be easily purified by ultracentrifugation through sucrose gradients resulting in particles with a purity of greater than 80%. Obtained 100–120 nm VLPs include approximately 1500–1800 Gag monomers and resemble morphologically and antigenically native virions [36]. The fact that these VLPs are quite stable and can be manufactured in sufficient quantities makes them an attractive candidate as subunits for a vaccine. Recently, Gag- based VLPs have been used with success as a tool for vaccination against human papillomavirus [49], and, concerning HIV-1, the Gag-based VLP model has been employed to deliver additional antigenic structures, such as specific individual

epitopes or whole proteins, with induction of the immune response [47,50].

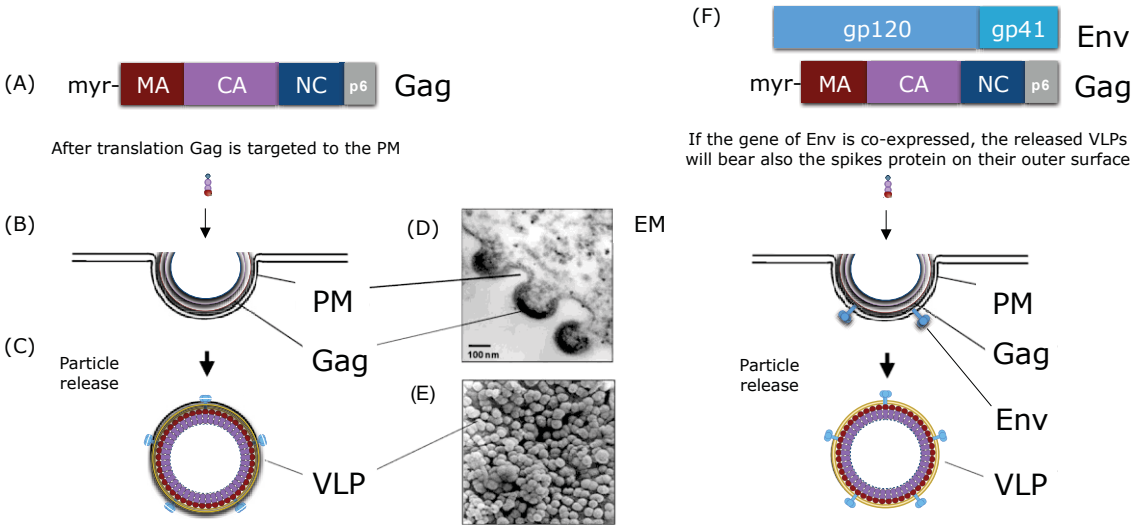

Figure 8. Schematic representation of the HIV Gag polyprotein and particle formation. (A) The Gag polyprotein, consisting of the p17 matrix (MA), the p24 capsid (CA), the p7 nucleocapside (NC) and the p6 linker protein, includes all information to (B) be targeted to the inner leaflet of the membrane of the producer cell and (C) bud in form of enveloped virus-like particles (VLP). (D and E) Electron micrographs of VLPs budding from insect cells after infection with Gag-recombinant baculoviruses. (F) The Env glycoprotein, which consists of the transmembrane domain gp41 and the spike domain gp120, is inserted in the VLP membrane if co-expressed with Gag. Adapted from [47].

1.2 HIV-1 immunopathogenesis

1.2.1 Infection and immune response

Transmission

Most HIV-1 infections occur by sexual exposure through the genital tract or rectal mucosa. It is still uncertain whether HIV-1 is transmitted as a free or a cell-bound virus, but SIV can be transmitted in either form [9]. The exact mechanism by which HIV-1 passes through the genital mucosal epithelium is still not clear. Diffusion of HIV-1 across the vaginal mucosa is slowed by genital mucus. It is presumable that virus crosses the mucosal epithelium barrier by transcytosis or by making direct contact with intraepithelial dendritic cells (DCs). Given that, multiple sexual exposures are usually needed for infection to occur. The crossing of the epithelial cell barrier by the virus is probably a rare event, although it is more common if the genital mucosa is damaged by physical trauma or coexisting genital infections [9].

Phases of infection

A period of about 10 days, following transmission of the virus, is commonly known as the eclipse phase. It corresponds to the period of time before viral RNA becomes detectable in the plasma (Figure 9). It has been suggested that the established infection probably arises from a single focus of infected mucosal $CD4^+$ T-cells [51]. Infectious molecular clones derived from these primary founder viruses, the *quasispecies*[1], could infect $CD4^+$ T-cells with greater efficiency than they could infect macrophages. A second *species* (i.e. "unit") of the virus may arise later in the infection, and can infect equally different immune cell types (e.g. monocytes, macrophages). At the end of the eclipse phase, virus and/or virus**-**infected cells reach the draining lymph node, where they meet activated $CD4^+$ $CCR5^+$ T-cells, which are targets for further infection [9]. The virus can then replicate rapidly and spreads throughout the body to other lymphoid tissues (e.g. gut-associated lymphoid tissue), where a high number of activated $CD4^+$ and $CCR5^+$ memory T-cells are present [52].

[1] A distribution of non-identical but closely related viral genomes. The entire distribution forms an organized cooperative structure, which acts like (*quasi*) a single unit (*species*).

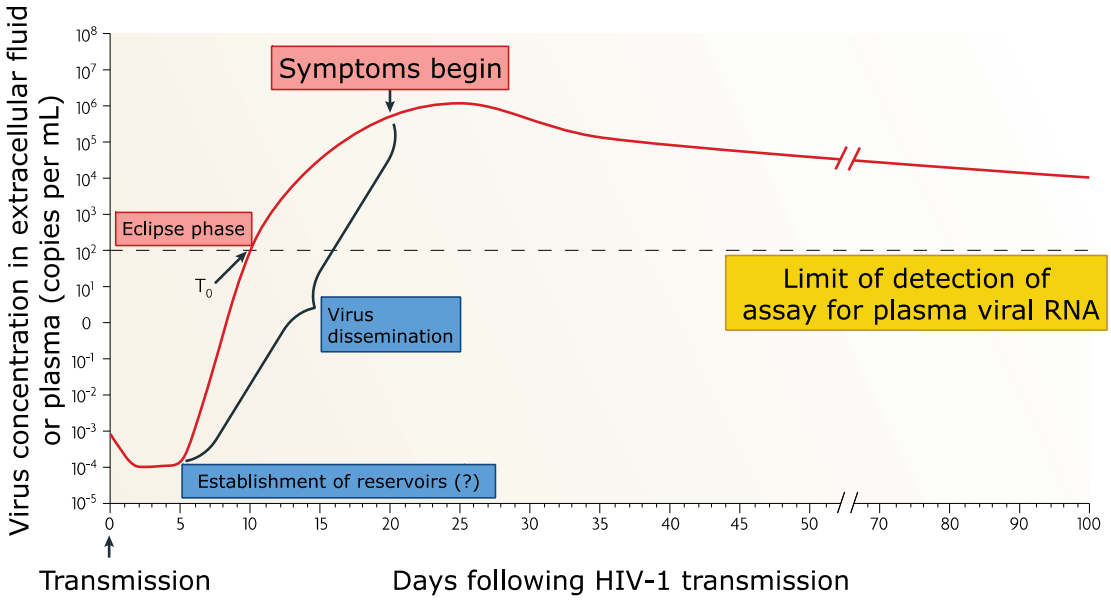

Figure 9. Fundamental events in acute HIV-1 infection. Following HIV-1infection, the virus first replicates locally in the mucosa and is then transported to draining lymphnodes, where further amplification occurs. This initial phase of infection, until systemic viral dissemination starts, constitutes the eclipse phase. The time when virus is first detected in the blood is referred to as t0; after this there is an exponential increase in plasma viraemia to a peak 21–28 days after infection. By this time, significant depletion of mucosal $CD4^+$ T-cells has already occurred. Around the time of peak viraemia, patients may become symptomatic and reservoirs of latent virus are established in cells that have a slower rate of decay than $CD4^+$ T-cells. The 'window of opportunity' between transmission and peak viraemia, prior to massive $CD4^+$ T-cell destruction and the establishment of viral reservoirs, is the narrow but crucial period in which an HIV-1 vaccine must control viral replication, prevent extensive $CD4^+$ T-cell depletion and curb generalized immune activation. Adapted from **[9]**.

At this time point, a large number (about 60%) of uninfected $CD4^+$ T-cells become activated and die by apoptosis, resulting in the release of apoptotic particles that can suppress immune function [53]. Consequently, in the first three weeks of HIV-1 infection about 80% of $CD4^+$ T-cells, located in the gut-associated lymphoid tissues, can be depleted. During viral replication, the plasma *viraemia*[2] increases exponentially to reach a peak (more than a million RNA copies per ml of blood). This corresponds to a strong decrease of the $CD4^+$ T-cell number, which will subsequently return to near normal levels in the blood but not in the gut-associated lymphoid tissues [54]. After the peak viraemia, the viral load decreases over about 20 weeks to reach a more stable level, known as the viral set point (Figure 9). Interestingly,

[2] From the word "virus" together with the old-greek word for blood (haima), *viraemia* is the medical condition, which defines the entry of viruses in the bloodstream and their consequent access to the rest of the body.

during this initial phase, the peak *viraemia*, the amino acid sequence of the virus does not undergo relevant changes. Virus diversification occurs during the period of decrease in viral load [55,56]. Different HIV-1 infected cells can differently respond to infection in terms of half-life: for most infected memory T-cells, the half-life is less than a day [57], while for macrophages, that can maintain latent pools of HIV-1 for months, the rate of decay is much slower [58].

Immune cells activation

Immune activation is associated with early and extensive apoptosis of B- and T-cells, leading to the release of apoptotic microparticles into the blood, and increased expression of tumor necrosis factor (TNF)-related apoptosis-inducing ligands, which kill bystander cells and are immunosuppressive [59]. The causes of HIV-1-associated immune activation established in early infection are not clearly defined [9]. Multiple related events probably contribute to such activation, including direct viral infection of immune cells, pro-inflammatory cytokine production by innate cells (which drives both direct and bystander activation of other immune cells), translocation of microbial products into the blood through damaged intestinal epithelium [60], loss of virally infected regulatory T-cells and chronic mycobacterial and viral co-infections.

1.2.2 Infection of macrophages

Macrophages are terminally differentiated, non-dividing cells, derived from circulating monocytes [61]. They represent a distinct population of phagocytes that are found under different names in various tissues (e.g. microglia in the brain, alveolar macrophages in the lung, or Kupffer cells in the liver) and are involved in various functions (e.g. bone remodeling, muscle regeneration) acting in both innate and adaptive immunity (Figure 10). Macrophages phagocyte cellular debris and pathogens, therefore possess a very active endo-lysosomal system, and almost no intermediate compartments [11]. This suggests that internalized materials are very rapidly targeted to acidic compartments (i.e. LYs). Macrophages also act as professional antigen presenting cells (APC), triggering antibody responses by the presentation of pathogen derived peptides via the major-histocompatibility complex II (MHCII) pathway to $CD4^+$ T-cells and activating $CD8^+$ cytotoxic T-cells (CTL) by

cross-presentation of HIV-1 antigens [11]. Nevertheless, even if macrophages are very resistant to the cytopathic effects of HIV-1 replication (compared to activated $CD4^+$ T-cells) their ability to infiltrate almost all organs (including the brain), and their presence in many different tissues can critically contribute to the spread of HIV-1 within the infected body [62]. In fact, it has been shown that macrophages infection is responsible for many AIDS-associated neuronal disorders [63]. Furthermore, macrophages has been implicated in mother-to child transmission due to breast feeding [62].

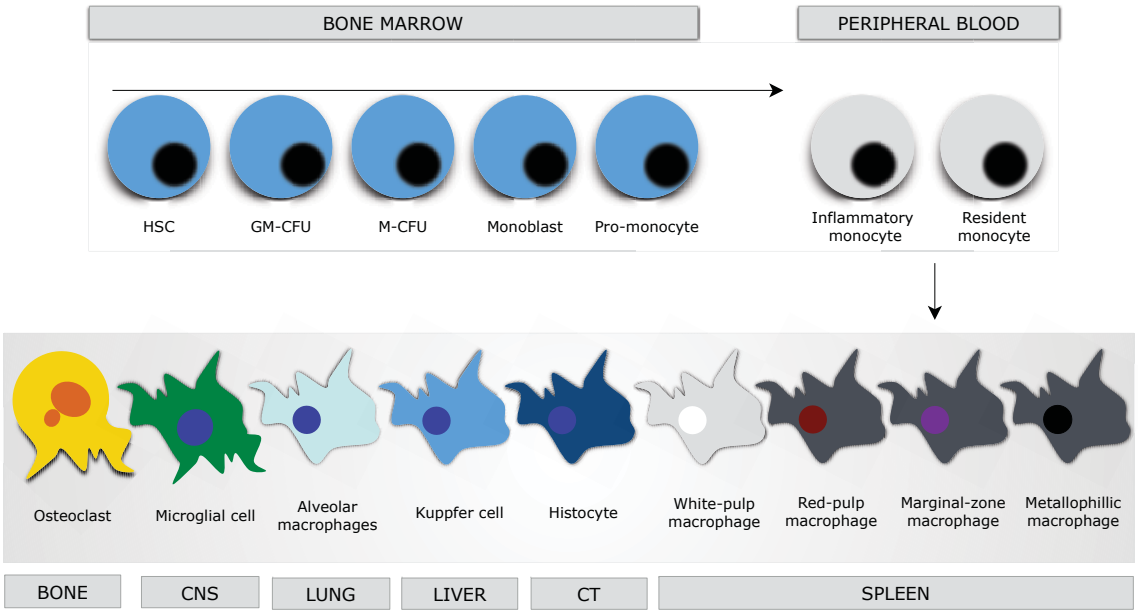

Figure 10. Schematic representation of the macrophages lineage. Monocytes originate in the bone marrow from a common hematopoietic stem cell (HSC). They undergo differentiation steps during which they commit to the myeloid and then to a monocyte lineage. In response to macrophage colony-stimulating factor, they divide and differentiate into monoblasts and then pro-monocytes before becoming monocytes, which exit the bone marrow and enter the blood stream. Human monocytes can also be divided into inflammatory and resident populations. Monocytes migrate to different tissues, where they replenish tissue-specific macrophages. The following abbreviations are used: central nervous system (CNS); granulocyte/macrophage colony-forming unit (GM-CFU); macrophage colony-forming unit (M-CFU); connective tissue (CT). Adapted from [61].

Potential active role of macrophages against HIV-1 infection

Non-infected macrophages can fulfill a potential relevant role against HIV-1 [64]. Macrophages can provide for an efficient and rapid phagocytosis of the virus with consequent presentation of viral-derived peptides via MHCII to $CD4^+$ T-cells. A further cross presentation of antigens via MHCI complexes can optimize an anti-

HIV-1 CTL response [11]. Furthermore, a variety of host-cell factors in macrophages (but also in some other reservoir cells) able to counteract the HIV-1 life cycle at different steps have been described and are now collectively called HIV-1 restriction factors (RFs) [18]. These RFs are usually induced by interferon-α and exert potent antiviral activity in cell culture. However, it must be taken into account that coevolution of virus and host had as a consequence the development of a repertoire of versatile viral accessory proteins able to counteract the activity of many RFs [63]. For example: one well known RF of macrophages is the SAM domain and HD domain-containing protein 1 (SAMHD1)[3], which is a cellular enzyme that exhibits phosphohydrolase activity converting nucleotide triphosphates to a nucleoside and triphosphate. SAMHD1 can deplete the pool of nucleotides available to a reverse transcriptase for viral cDNA synthesis and thus prevents viral replication. Nevertheless, degradation of SAMHD1 induced by Vpx (a virion-associated protein expressed by HIV-2, similar in structure to Vpr) is sufficiently rapid to allow reverse transcription of the viral RNA [65]. On the contrary, Tetherin, another well-known RF, which causes retention of fully formed virions on infected cell surfaces, is not antagonized by any viral protein in infected macrophages. Due to its high expression in macrophages, Tetherin can produce a strong inhibition of viral release in these cells compared to the viral production efficiency in $CD4^+$ T-cells, where the viral protein Vpu counteracts the inhibition activity of Tetherin allowing an efficient viral release from the PM [11].

Impairment of macrophage immune functions upon HIV-1 infection: a focus on Fcγ-receptor-mediated phagocytosis

HIV-1 infection of macrophages results in the impairment of a many of their immune functions (e.g. chemotaxis, phagocytosis, intracellular pathogens killing, cytokine production [66,67]). These defects contribute to the pathogenesis of AIDS by allowing reactivation and development of opportunistic infections [68]. The HIV-1-encoded proteins Nef, Vif, Vpr, and Rev have been shown to affect a number of signaling pathways via interactions with cytoskeletal and cytoplasmic proteins [63]. Specifically, it was shown that the activity of some kinases (e.g. the Src and p21-activated kinases) involved in antibody-mediated phagocytosis processes, such as the Fcγ receptor (FcγR)-mediated phagocytosis, are strongly impaired upon HIV-1 infection [68-70]. This kind of phagocytosis refers to the binding of the FcγR to a

[3] Sterile Alpha Motif (SAM) and Histidine Aspartic (HD) domain-containing protein 1.

part of an antibody known as the Fc[4]–region [71]. Fc receptors are the receptors for the constant region of IgG (FcγRI, FcγRII, and FcγRIII). They bind to antibodies that are attached to infected cells or invading pathogens. Their activity stimulates phagocytic or cytotoxic cells to destroy microbes, or infected cells by antibody-mediated phagocytosis or antibody-dependent cell-mediated cytotoxicity (ADCC) [72]. Those that bind the class of antibody IgG are called Fc-gamma (γ) receptors. Peripheral blood monocytes express mainly the high-affinity FcγRI (CD64) and a low-affinity FcγRII, whereas macrophages also express FcγRIIIA (CD16A). Previous studies have shown that Syk activation in FcγR-mediated phagocytosis is an absolute requirement [73]. Activation of Syk results in cytoskeletal rearrangements needed for phagocytosis of the opsonized particles (Figure 11). A previous study has shown that defective phagocytosis by HIV-1-infected macrophages is due, at least in part, to decreased expression of the FcγR-signaling subunit of the FcγR, which leads to specific signaling defects downstream of FcγRs [68].

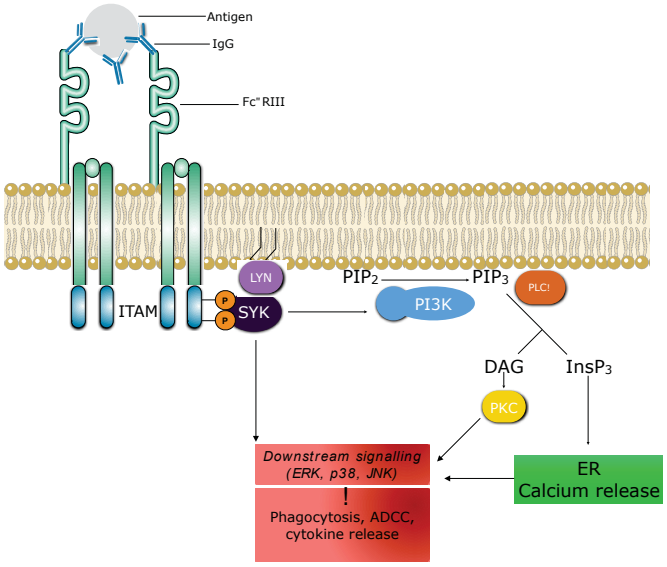

Figure 11. Signaling pathway triggered by activating FcγR. Crosslinking of activating Fc receptors for IgG (FcγRs) by immune complexes induces the phosphorylation of receptor-associated γ-chains by the SRC kinase (not indicated). This generates docking sites for SYK, which in turn activates a number of other signal-transduction molecules such as phosphoinositide 3-kinase (PI3K). The generation of phosphatidylinositol-3,4,5-trisphosphate ($InsP_3$) recruits phospholipase Cγ (PLCγ), which leads to activation of downstream kinases and the release of calcium from the endoplasmic reticulum (ER). Adapted from [71].

[4] (FC) Fragment, crystallizable.

Apoptotic cell phagocytosis by macrophages during HIV-1 infection

Phagocytes, and specifically macrophages, are required to continually sense the extracellular environment [61]. A set of distinct cell surface receptors is required for recognizing and responding to infectious and non-infectious injuries. The FcγR-mediated phagocytosis is only one of the internalization ways active in macrophages [74]. Phagocytic cells, and macrophages in first line, also have the task of sensing the presence of dead entities, binding to specific molecules expressed on the outer surface of apoptotic cells [75]. Phosphatidylserine (PS) (see chemical structure in the Appendix) represents one of the most important apoptotic signals for engulfment of apoptotic cells by macrophages [74,75]. Clearance of apoptotic cells is necessary for tissue development, homeostasis and resolution of inflammation [75,76]. The uptake of apoptotic cells is initiated by an 'eat-me' signal, such as PS, on the cell surface and phagocytes recognize this signal by using specific receptors [76]. Several classes of receptors have been implicated in the recognition of apoptotic cells, by means of direct binding to the exposed PS, including brain-specific angiogenesis inhibitor 1, T-cell immunoglobulin and mucin domains-containing protein 4 and stabilin-2, or indirect binding through bridging molecules (milk fat globule-EGF factor 8 protein, growth arrest-specific 6 [77]). The engagement of the PS receptors initiates signaling events within the phagocytes that lead to activation of specific intracellular signaling which ends to cytoskeletal reorganization of the phagocyte membrane, to allow corpse internalization. PS is a glycerophospholipid present in the membranes of all eukaryotic cells. Like the majority of glycerophospholipids, PS has a glycerol backbone esterified on the sn-1 and sn-2 carbons of the glycerol moiety with 2 fatty acyl chains of variable length and saturation, and a phosphate group on sn-3 (see chemical structure in the Appendix) [78]. The distinguishing feature of PS is the attachment of a serine to the phosphate; the resulting head-group provides PS a net negative charge. While PS is present in all cells, it is a comparatively minor constituent of their membranes, comprising 3–10% of the total lipids [78]. However, this low relative abundance of PS belies its importance within the cell. The best-studied roles of PS involve signaling, not within the intracellular environment, but in an extracellular context such as during apoptosis and during blood clotting. Like most lipids, PS is not evenly distributed throughout all cellular membranes, nor is it always equally distributed between leaflets of a membrane bilayer [75]. In healthy cells PM PS is exclusively on the inner (cytoplasmic) leaflet due to the action of ATP-dependent aminophospho-

lipid flippases [78]. When cells undergo apoptosis (the regulated cell death) PS appears on the outside leaflet, signaling phagocytic cells to engulf the dying cell (Figure 12). The CD91 receptor, also called low density lipoprotein receptor-related protein 1 (LRP1), binds to β2-glycoproteins, which in turn has been reported to directly interact with PS of apoptotic bodies [79]. The LRP1 was shown to be increased on the surface of HIV-1 infected macrophages [80]. This suggests that, although most of immune functions of the macrophages are impaired due to HIV-1 infection, some phagocytic ways, e.g. PS-mediated phagocytosis, might still be active.

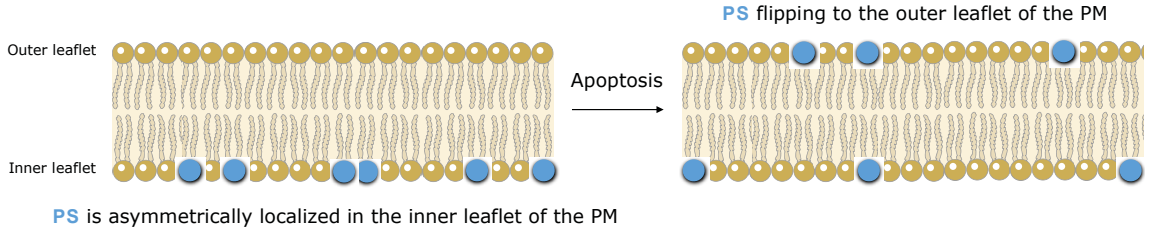

Figure 12. Schematic representation of the re-distribution of PS in the lipid bilayer during apoptosis. PS (blue) is initially asymmetrically localized in the lipid bilayer. During apoptosis, PS re-distributes symmetrically in the lipid bilayer, flipping to the outer leaflet of the PM.

1.2.3 Therapeutic approach against HIV-1

Development of many antiretroviral drugs has made HIV-1 infection a treatable chronic disease [81]. Antiretroviral therapy (ART) includes use of different drug classes, for instance: nucleoside (or non-nucleoside) reverse transcriptase inhibitors; protease inhibitors; integrase inhibitors; fusion and entry inhibitors [82]. Current recommendations for initial therapy for HIV-1 infection include the use of the so-called combined antiretroviral therapy (cART), which corresponds to a combination of three antiretrovirals from at least two drug classes. cART is effective in decreasing HIV-1 RNA level below the limit of detection (50 copies/mL) and has led to significant reductions in HIV-related morbidity and mortality and is a highly cost-effective medical intervention [83]. In general, initiation of cART soon after infection offers near normal quality of life and lifespan: early cART is in fact associated with a reduced latent viral reservoir, reduced viral DNA, and normalization of some immune markers, leading to prevention of the various complications that define AIDS [83]. However, cART does not fully restore health, and lifelong treatment is

necessary to manage patient illness because cART neither eradicates infected cells from reservoirs nor reconstitutes HIV-1-specific immunity that could kill infected cells. Furthermore, findings from studies undertaken in high-income countries show that HIV-1-infected adults who have durable treatment-mediated suppression of HIV replication are at risk for developing several non-AIDS disorders, including cardiovascular disease, cancer, kidney disease, liver disease, osteopenia or osteoporosis, and neurocognitive disease [84]. Beside the compelling need of an HIV-1 vaccine, the request for new and alternative treatment approaches is still increasing [85]. Some suggestions to this end, might come from the research in nanotechnology [86].

Nanotechnology in the treatment of HIV-1

Toward the cure of HIV-1, different nanomedicine classes have been developed with different disease-modifying properties [87]. Application of nanotechnology to the delivery of antiretroviral drugs might represent an important tool in the cure of HIV-1, for example modifying tissue-distribution of drugs that could be targeted to viral reservoirs and by increasing their half-lives. To this aim, copolymer micelles incorporating the non-nucleoside revers transcriptase inhibitor efavirenz into their core were developed [88]. Furthermore, nanomedicine formulation might help in the targeting of antiretroviral drugs to specific cell types (e.g. DCs, Langerhans cells) or organs (e.g. lymphoid organs). Lipid-nanoparticle loaded with the protein kinase C activator, bryostatin-2 [89] and pH-dependent nanoparticle containing the protease inhibitor indinavir [90] were produced to target antiretroviral drugs to DCs and Lymphoid organs, respectively. Some nanomedical formulations were also designed as preventive therapy, as promising strategy to prevent vaginal and rectal HIV-1 transmission (e.g. the vaginal gel containing the nucleoside reverse transcriptase inhibitor tenofovir [91]). Moreover, to increase the epithelial penetration of antiretroviral-based microbicides, specific mucoadhesive and non-mucoadhesive nanomedicine formulations were also investigated [92]. Nanotechnology research was also directed to the development of immunotherapeutic nanocomplexes, multimodular vaccine candidates that may provide high therapeutic effects in comparison to all previous approaches [87]. Many biological phenomena, such as immune recognition and passage across biological barriers, are governed by size considerations. The physical size of nanocomplexes is usually over 50 nm, which is the approximate threshold of immune recognition [86]. Soluble antigens, with a diameter

smaller than 50 nm, are generally not recognized by the immune system and are not immunogenic. In fact, since nature developed an effective and specific immune surveillance against viruses, which takes in consideration also the size of the antigens, immunotherapeutic nanomedicines must correspond to the size range of viruses. Consequently, the body would consider nanomedicine as a harmful virus that needs to be eliminated. DermaVir is the first nanomedicine developed for the treatment of HIV-1 and AIDS that has demonstrated encouraging Phase II clinical safety, immunogenicity, and efficacy results [87]. DermaVir features three elements: the first is the active pharmaceutical ingredient, which is a pDNA that expresses 15 HIV-1 proteins. These proteins self assemble to replication-, reverse transcription- and integration-defective complex VLPs. The creation of such VLPs supports the presentation of the highest number of HIV-1 epitopes and might induce HIV-1 specific T-cell responses. The second is a mannosylated polyethylenimine "envelope", which contains and delivers pDNA to DCs and achieve effective protein expression the pDNA. The third is the formed nanoparticle of 70-300 nm in a buffered solution.

Liposomes as therapeutic tool against HIV-1

Liposomes are lipid vesicles with an aqueous core used to encapsulate hydrophilic drugs whereas hydrophobic and amphiphilic drugs can be solubilized within the phospholipid bilayers. Liposomes and several other nanocarriers are readily opsonized by plasma proteins, phagocytosed by macrophages and localize to cells of the reticuloendothelial system (RES). It has been shown how hydrophilic drugs encapsulated in liposomes can localize in organs rich in macrophages, such as liver, spleen and lungs [93,94]. Specifically, in one study it was shown how liposomes could be used to deliver the nucleoside reverse transcriptase inhibitor azidothymidine (AZT) preferentially to the RES, sparing the bone marrow from this drug and thereby reducing bone marrow toxicity [95]. Furthermore, the surface of liposomes may be modified to increase their targeting specificity: for instance, cells of the RES bear galactose and lectin receptors [96]. Liposomes bearing galactose and mannose residues on their outer surface can specifically target these receptors, and have been used to direct, for example, the nucleoside reverse transcriptase inhibitor stavudine to the RES [86]. Formulation of antibodies-decorated liposomes (i.e. immunoliposomes) have the targeting specificity of antibodies on their surface e.g., anti-HLA-DR monoclonal antibodies which can target follicular dendritic cells, B-cells

and macrophages. Liposomes may also be decorated with recombinant soluble CD4 molecules [97], or antibodies able to target gp120 on HIV-1 infected cells [98].

1.3 Aim of the work

Approximately three decades ago, HIV was found to be the cause of AIDS [99]. Since their discovery, HIV-1 and the less infective HIV-2 are responsible for more than 25 million deaths worldwide, making HIV one of the insurmountable problems of the 21st century [100]. Scientific research on HIV-1 still has to respond to various open questions about the biology of viral assembly and the lack of immune response against the infection [101]. This work will raise both these issues: first (point 1), to study the role of intracellular calcium for the release of viral particles, and second (point 2) the development of a nanotechnological strategy able to elicit clearance of viral particles circumventing the lack of immune response during HIV-1 infection.

1) HIV-1 can follow more than one assembly pathway and partially adapt its own life cycle, exploiting different components of the cellular machinery in regard to the type of infected cell: in macrophages and DCs, HIV-1 assembly takes place mostly in LEs/MVBs where it can remain inactive for several months after infection [18], while in T-cells, HIV-1 buds predominantly from the PM [17].

   The use of different investigation methods and different cell lines as model systems for the study of the biology of HIV-1 assembly and replication has led to sometimes-contradictory observations. Several studies have shown the presence of VLPs in late endosomes and as well in lysosomal compartments [2,23]. Nevertheless, the fate of such late endosomes/lysosomes (LEs/LYs) entrapped VLPs is still a matter of debate. However, increased intracellular calcium concentrations were shown to enhance the release of VLPs [2,44]. This process has been proposed to be caused by fusion events between vesicles of the endo-lysosomal system containing VLPs [2]. This suggests a possible role of the LEs/LYs calcium-mediated fusion machinery and LYs exocytosis, which are common mechanism shared by all cell types [102], in the release of VLPs and their rescue from lysosomal degradation. The aim of the first part of this work was to investigate the role of intracellu-

lar calcium and the LEs/LYs machinery in the release of VLPs.

2) Although the advent of cART, antiretroviral therapy is associated with a high number of disadvantages (e.g. emergence of drug resistant viral strains, serious adverse effects and inability to eradicate HIV-1 from reservoirs [82]). In this scenario, nanotechnology, which can bring together physicochemical and biological properties of different therapeutic approaches, has a vast potential to advance the treatment of HIV/AIDS. In this work, immunoliposomes are presented that can bind Env/Gag virus-like particles (HIV-VLPs) while being specifically phagocytosed by macrophages, thus allowing the co-internalization of HIV-VLPs. These liposomes are decorated with anti-Env antibodies and contain PS. PS mediates liposome internalization by macrophages via a mechanism not impaired by HIV-1. Hence, PS- liposomes mimic apoptotic cells and are internalized into the macrophages due to specific recognition, carrying the previously bound HIV-VLPs.

2 MATERIALS AND METHODS

2.1 Materials

2.1.1 Biological material

Cell lines

Name	Species	Origin	Source
HEK-293T	*Homo sapiens*	Kidney, epithelial	ATCC® CRL-11268
HeLa	*Homo sapiens*	Cervix, epithelial	ATCC® CCL-2
COS-7	*Cercopithecus aethiops*	Kidney, fibroblast	ATCC® CRL-1651
J774A.1	*Mus musculus*	Monocyte, macrophage	Kindly provided by Prof. Dr. Thomas Meyer
MDCK	*Canis familiaris*	Kidney, epithelial	ATCC® CCL-34

Plasmids and siRNA oligonucleotides

Name	Insert	Source
pEGFP	Gag	AIDS Reagents
pEGFP	Rab7	Kindly provided by Prof. Dr. Volker Hauke
pcDNA3.1	p96ZM651gp160-CD5-opt	AIDS Reagents
pYFP	Tau	Kindly provided by Dr. Maik J. Lehmann
pCFP	Syt-VII	Kindly provided by Prof. Dr. T. Südhof
pBAD-His-B	MediumFT/FastFT	Kindly provided by Prof. Dr. V. Verkhusha
Silencer Select SYT7 (ID:s17291)		Life Technology

The Gag-EGFP plasmid was restricted with BamHI and BsrGI in order to substitute EGFP with the following constructs: CFP, mCherry, MediumFT and FastFT.

2.1.2 Lipids and proteins

Molecular structures of the lipids are reported in the Appendix.

Name	**Source**
L-α-phosphatidylcholine (Egg-PC) (Egg, Chicken)	Avanti Polar Lipid
1,2-dipalmitoyl-sn-glycero-3-phosphoethanolamine-N-(cap-biotinyl)(Biotin-cap-PE)	Avanti Polar Lipid
1-palmitoyl-2 (dipyrrometheneborondifluoride) undecanoyl-sn- glycero-3-phosphocholine (TopFluor PC)	Avanti Polar Lipid
1,2-Diacyl-sn-glycero-3- phospho-L-serine	Sigma
Streptavidin	Sigma

2.1.3 Media and solutions

Cell culture media and reagents

Application	**Composition**	**Source**
Cell growth (HeLa, HEK-293T, MDCK, COS-7)	DMEM: 10% fetal calf serum, 200mM L-glutamine, 1% Penicillin/Streptomycin	GE Healthcare
Cell growth (J774A.1)	RPMI: 10% fetal calf serum, 200mM L-glutamine, 1% Penicillin/Streptomycin	GE Healthcare
Cell passaging	PBS: with/without 100 mg/ml Ca^{2+} and Mg^{2+}PBS with 0.5 mg/ml Trypsin, 0.22 mg/ml EDTA	GE Healthcare
Cell freezing medium	70 % DMEM 20 % fetal calf serum 10 % DMSO	GE Healthcare
Transfection	Turbofect	Fermentas
Transfection/RNAi	Lipofectamine 2000	Life Technologies

Buffers

Buffer	Composition
PBS	137 mM NaCl 2.7 mM KCl 10 mM Na_2HPO_4 + 2 H_2O, 1.76 mM KH_2PO_4
TNE Buffer	20 mM Tris-HCl 100 mM NaCl 1 mM EDTA (pH=7.5)
Stacking SDS-gel buffer	1 M Tris/HCl pH 6.8
Separating SDS-gel buffer	1 M Tris/HCl pH 9.0
SDS loading buffer	63 mM Tris/HCl, 10 % glycerol,□2 % SDS, 0.0025 % Bromophenol blue□100 mM -mercaptoethanol
SDS running buffer	25 mM Tris/HCl, 192 mM glycine, 0.1 % SDS

2.1.4 Reagents

Standard chemicals were obtained from Merck, Sigma and Roth.

Chemicals and fluorescent markers

Name	Source
U73122	TOCRIS Bioscience
Mepyramine	TOCRIS Bioscience
Tert-butylhydroquinone	TOCRIS Bioscience
Thapsigargin	ENZO Lifesciences
Cytochalasin D	TOCRIS Bioscience
Dynasore	Sigma Aldrich
Dimethylsulfoxid	Sigma Aldrich
Propidium Iodide	Sigma Aldrich

Name	Source
Lysotracker	Life Technologies
Hoechst 33342	Life Technologies
Mitotracker	Life Technologies
ER-Tracker	Life Technologies
DiI	Life Technologies
Fura2-AM	Life Technologies
Fluo5F-AM	Life Technologies

Antibodies

Name	Source
anti-p24 (mouse)	Millipore
anti-gp120 biotin conjugated (goat)	Abcam
IRDye-680 anti-mouse	LI-COR Bioscience
IRDye-800 anti-goat	LI-COR Bioscience

2.1.5 Kits

Name	Source
Pierce BCA Protein Assay Kit	Thermo Scientific
QIAprep Spin MiniPrep Kit	Quiagen
Plasmid MaxiPrep Kit	Quiagen
Celltiter Blue Cell Viability Assay	Promega

2.1.6 Consumables

Material	Source
Cell culture flasks (T25, T75)	Nunc
Cell culture plates□12-well	Nunc
100 nm polycarbonate filters	Avanti polar Lipid
Cell scraper	Sarstedt
Cryo tubes (1.5 ml)□	Sarstedt
Glass bottom petri dishes	MatTek
Filtropur 0.45 µm	SARSTED

2.1.7 Equipment

Name	Configuration
Olympus FV-1000	IX-81 microscope - 60x/1.2 Water UPlanSApo 405, 560 nm diode lasers 458, 488, 515 nm Argon laser 3 confocal PMTs; Climatization chamber
Olympus FV-1000MPE	IX-81 microscope□- 60x/1.2 Water UPlanSApo□ 405, 440, 560, 635 nm diode lasers (458), 488, 515 nm Argon laser□ 3 confocal PMTs;□Climatization chamber
Olympus IX-81 (Epifluorescence microscope)	HBO lamb□ 100x/1.35 Oil UPlanFL, DIC Oil Zeiss□Filter cube: U-MWU2: BP330-385 BA420 DM400 (DAPI)
BD FACSAria II	375, 488, 405, 633 nm laser line Filters: 515 - 545 nm, 564 - 606 nm, 600 - 620 nm

2.1.8 Software

Name	Supplier
Olympus FV1000 3.1	Olympus
FACS Diva Software	Backton Dickinson
FlowJo	Tree Star, Inc.
ImageJ	US National Institute of Health (NIH)
MetaMorph	Molecular Devices
Matlab	The Mathworks
Prism	GraphPad Software, Inc.
Keynote	Macintosh
Microsoft Office 2011	Microsoft
Papers2	Macintosh

2.2 Methods

Cell culture

The cells were propagated in growth medium in 75 cm^2 culture flasks at 37 °C and 5% CO_2. The cells were passaged every 3 - 5 days before they had reached full confluence. To this end, the cells were washed twice with PBS and detached using trypsin-EDTA at 37 °C for 5 - 15 min. Trypsinization was stopped by addition of growth medium and approximately $1x10^6$ cells were seeded in a new 75 cm^2 culture flask. In the case of J774A.1 macrophages, the cells were scraped off in the presence of 2 ml PBS. For the different assays, cells were seeded into 6-, 12-well plates or petri dishes. For long term storage, the cells from one 75 cm^2 culture flask were detached, pelleted for 5 min at 2000 g and re-suspended in freezing medium. The cells were kept at -80 °C for 24 hours and subsequently stored in liquid nitrogen.

Transfection

Cells were transfected with expression-plasmids using Turbofect according to the manufacturers manual. To this end, cells were seeded in 35 mm glass bottom petri dished and grown until they reached 70 - 90 % confluence. 6 µl Turbofect and 4 µg DNA were diluted in 400 µl serum-free medium and incubated for 20 min at room temperature. The cells were washed in PBS and the DNA/Turbofect mix was added with additional 1.5 ml serum-free medium. After 4 h the medium was changed to growth medium.

RNA interference

For siRNA experiments, cells were always co-transfected with Gag-EGFP and 0.02 µM SYT7-siRNA oligonucleotides (5 pmol in 250 µl transfection volume) according to the manufacturers manual. To this end, cells were seeded and grown until they reached 70 - 90 % confluence. 5 µl Lipofectamine 2000 were diluted in 250 µl serum-free medium, and 4 µg Gag-EGFP together with 0.02 µM siRNA oligonucleotides were diluted separately in 250 µl serum-free medium. After 5 min, the two solutions were mixed together and incubated for 20 min at room temperature. The cells were subsequently washed in PBS and the co-transfection/Lipofectamine

mix was added with additional 1.5 ml serum-free medium. After 4 h the medium was changed to growth medium.

Confocal microscopy live imaging on HeLa and COS-7

The cells were plated in a 2 mm glass-bottom dish two day before analysis. One day after plating, the cells were transfected with the indicated plasmid(s) with the transfection reagent Turbofect, as described before. 24 hours after transfection, the cells were washed with PBS and either stained with intracellular markers (see detailed experiments in the Results section) or directly observed under the confocal microscope. Live-cell imaging of intracellular localization of Gag or co-localization with intracellular compartments or structures was performed always at 37°C, 5% CO_2 with an Olympus FV-1000MPE laser-scanning confocal microscope (Olympus, Shinjuku, Tokyo, Japan). Fluorescence emissions of Lysotracker/mCherry/ER-tracker/Mitotracker, EGFP/Fluo5F, CFP, Hoechst 33342, and YFP were measured at 590 nm, 509 nm, 475 nm, 454 nm and 530 nm, respectively. If indicated, before microscopy, the cells were treated with specific reagents diluted in DMSO (e.g. U73122, Mepyramine, TBHQ) for the indicated time at 37°C, 5% CO_2. The final concentration of DMSO in the cell medium was always equal or below 0,1% of the total volume.

Total Internal Reflection Fluorescence Microscopy

TIRFM was used to study the plasma membrane localization of the expressed protein. An inverted FluoView 1000MPE microscope was modified with a beam expander to allow illumination of the whole field of view using laser excitation sources and a highly sensitive, cooled Hamamatsu Orca ER CCD- camera for epifluorescence observation. The tilting of the angle of the incidenting light beam was achieved by a displacement of the beam, away from the center of the observation objective179 (60x UplanSApo oil objective with a numerical aperture 1.45). In a typical TIRFM experiment, the glass-attached parts of the cells under study were focused and imaged in the epifluorescence mode applying beam expander and CCD-camera. Then, the TIRFM angle was tilted until the out-of-focus light from intracellular structures disappeared and plasma membrane structures dominated the image. As a rule of thumb, if the angle is right, changes of the focus should not change the structures displayed but only the sharpness of the plasma membrane

components. Since only an evanescent field of the excitation light was used to illuminate the fluorophores, high laser intensities of around 50% and image acquisition times of at about 1 second were used.

Intracellular calcium staining with Fluo5F-AM

The cells were plated in a 2 mm glass-bottom dish one or two (in the case of a transfection) day before analysis. The cells were stained with 3 µM Fluo5F-AM for 35 minutes at at 37°C, 5% CO_2. The cells were then washed with PBS and complete culture medium (DMEM) was added. Fluo5F-AM was aliquoted in DMSO. The final concentration of DMSO in the cell medium was always equal or below 0,1% of the total volume.

Confocal live-imaging of Fluorescent Timers

The cells were plated in a 2 mm glass-bottom dish two days before microscopy. 24 hours before microscopy the cells were transfected with either Gag-FastFT or Gag-MediumFT. Live-cell imaging of the transfected cells was performed at the Olympus FV-1000MPE microscope. The During the FT maturation, the fluorescence of the blue forms increased to its maximum value, and after that decreased to zero (Table 1).

Fluorophore		Ex Peak (nm)	Em Peak (nm)	Characteristic time at 37°C (hours)
FastFT	Blue form	403	466	0.25
	Red form	583	606	7.1
MediumFT	Blue form	401	464	1.2
	Red form	579	600	3.9

Table 1. Properties of the blue and red forms of the FTs at 37°C. The indicated characteristic times correspond to fluorescence maxima for the blue forms, and to maturation half times for the red forms.

The fluorescence of the red forms increased with time with some delay and then reached a plateau. At 37°C the maxima of the blue fluorescence intensities are observed at 0.25 and 1.2 for the fastFT and the mediumFT, respectively. The half-

maxima of the red fluorescence intensities were reached at 7.1 and 3.9, respectively, which corresponds to the half-times of the maturation for the red FT forms. Fluorescence emissions of the blue and the red form were measured at 454 nm and 590 nm, respectively.

Confocal microscopy live imaging on macrophages

Macrophages were plated in a 2 mm glass-bottom dish one day before analysis. Acidic compartments were marked using Lysotracker as described in the product's guidelines. The cells were then washed and treated with αEnv-PS-LUVs and HIV-VLPs as described above. Live-cell imaging of intracellular co-localization of αEnv-PS-LUVs and HIV-VLPs in acidic compartments was performed in an environmental chamber at 37°C, 5% CO_2 with an Olympus FV-1000MPE laser-scanning confocal microscope (Olympus, Shinjuku, Tokio, Japan). Fluorescence emissions of Lysotracker, EGFP and DiI were measured at 590 nm, 509 nm and 564 nm, respectively. Percentage of HIV-VLPs/ acidic compartments co-localization was obtained calculating the areas (i.e. number of pixels) of dots corresponding to the fluorescent signal of EGFP (HIV-VLPs) overlapping with pixels corresponding to the signal of Lysotracker (acidic compartments). The co-localization was calculated as a ratio of overlapping area and total pixel area occupied by HIV- VLPs, expressed as a percentage, and averaged over ten different confocal micrographs using CellProfiler (Broad Institute, Cambridge, MA). In order to identify the HIV-VLPs and distinguish them from the autofluorescence signal, a user-defined threshold was selected.

Calcium-release in macrophages

Macrophages were seeded into MatTek dishes a day before analysis. Subsequently, cells were stained with 3 einther incubated with 3 μM Fura2-AM for 35 minutes at at 37°C, 5% CO_2. The cells were then washed with PBS and complete culture medium (RPMI) was added. Fluo5F-AM was aliquoted in DMSO. The final concentration of DMSO in the cell medium was always equal or below 0,1% of the total volume. After calcium staining, the cells were observed at the Olympus IX-81 epifluorescence microscope. The release of intracellular calcium was measured live, upon addition of either αEnv-PS-LUVs or αEnv-LUVs. The emission was detected at 420 nm. For preliminar ER-calcium depletion, the cells were treated with 10 μM Thapsigargin for 1 hour at 37°C, 5% CO_2 before adding the immunoliposomes.

Correlative Light and Electron Microscopy

HeLa, COS-7 or J774A.1 macrophages were seeded into a 35-mm gridded MatTek dish. Subsequently, cells were either transfected with the indicated construct or, one day after seeding, incubated for 1 hour with HIV-VLPs and αEnv-PS-LUVs as described in the Results section and fixed for 20 minutes at room temperature with 2.5% (v/v) glutaraldehyde and 2% (w/v) paraformaldehyde in PBS. For fluorescence microscopy, the cells were imaged with an Olympus FV- 1000MPE laser-scanning confocal microscope. For subsequent electron microscopy, cells were rinsed three times for 5 minutes with 100 mM cacodylate buffer (pH=7,4), post-fixed for 1 hour in 1% (v/v) osmium tetroxide, rinsed three times with distilled water, en bloc stained with 0.5% (w/v) uranyl acetate, dehydrated through a graded ethanol series and finally embedded using EMBed 812 (EMS). Cells within a region previously identified by confocal microscopy were cut en face and 70-90 nm sections were collected. Sections were counterstained with 4% (w/v) uranyl acetate followed by lead citrate. All samples were imaged on a Zeiss EM 900 transmission electron microscope equipped with a wide-angle CCD camera (TRS-System, Moorenweis, Germany). Correlation of fluorescence images and electron micrographs was accomplished through alignment of cell surface structures.

Preparation of liposomes

The lipids were dissolved in chloroform to 5-10 mM stock concentration. To prepare 100 nm diameter LUVs, lipids were mixed and dried under nitrogen followed by high vacuum for at least 30 minutes. The amounts of lipids in the mixtures were: 1) sample "LUVs", 99.95mol% Egg-PC, 0.05 mol% TopFluorPC: 2) sample "PS-LUVs", 30mol% PS, 69.95mol% Egg-PC, 0.05mol% TopFluorPC; 3) samples "αEnv-PS-LUVs and αEnv-LUVs": 30% (or 0 mol% for αEnv-LUVs) PS, 68.95% (or 98.95% for αEnv-LUVs) Egg-PC, 1 mol% Biotin-cap-PE, 0.05 mol% DiI; 4) "αEnv-PS-LUVs and αEnv-LUVs" samples used in the toxicity tests: 30 mol% (or 0 mol% for αEnv-LUVs) PS, 69 mol% (or 99 mol% for αEnv-LUVs) Egg-PC, 1 mol% Biotin-cap-PE. The lipid mixtures described above were then re-suspended in PBS without Ca^{2+} and Mg^{2+}, vortexed and passed through 100 nm polycarbonate filters 11 times using a Mini-Extruder (Avanti Polar Lipids) in order to obtain LUVs of uniform size. All LUV samples were extruded directly at 300 μM and subsequently diluted to the desired concentration. To obtain antibody-decorated liposomes (αEnv-PS-LUVs and αEnv-LUVs), 2.5 μL (1 mg/mL) of streptavidin and 4 μL (50 μg/mL) of

αEnv-Abs (polyclonal anti-HIV-1 gp120-biotin conjugated) were pre-mixed for 30 minutes at 4°C, then added liposomes with or without PS (total volume 100 µl, lipid concentration 300 µM) and further incubated for 1 hour at room temperature. In the text, both αEnv-PS-LUVs and αEnv-LUVs are sometimes referred to as "immunoliposomes".

HIV-VLPs uptake by macrophages

The mouse macrophage cell line J774A.1 was used to study the uptake of HIV-VLPs in the presence of immunoliposomes. Cells were grown to 70% confluency in 12 mL cell-flasks in the presence of RPMI, 10% FBS, 1% penicillin-streptomycin, and 2 mM L-glutamine. Then, cells were gently scraped off, plated in a 12-well plate and incubated at 37°C in 5% CO_2 for 24 hours. 100 µL (300 µM) of αEnv-PS- LUVs (or αEnv-LUVs) and 20 µL (from a 0.81 mg/mL stock solution) HIV-VLPs were mixed together for 1 hour at room temperature. The cells were washed with PBS and treated with the liposomes/HIV-VLPs mix for 1 hour in RPMI medium (up to 1 mL total volume) at 37°C with 5% CO_2. Then, the medium was removed, the cells were washed with PBS and gently scraped off in the presence of PBS for flow cytometry measurements.

Production and purification of HIV-VLPs

HEK-293T cells were grown in the presence of DMEM, 10% FBS, 1% penicillin-streptomycin, and 2 mM L-glutamine and plated in a 100x 20 mm tissue-culture dish. Once the cells reached 90% confluence (usually after 24 hours), they were co-transfected either with pGag-EGFP alone or together with p96ZM651gp160-CD5-opt using the transfection reagent Turbofect. Transfection medium was replaced 3-4 hours after transfection and collected 48 hours later for HIV-VLPs purification. HIV-VLPs were purified as previously described [18]. Briefly, medium from transfected cells was filtered through a 0.45 µm pore-size filter (Filtropur S 0.45). The filtrate was layered on top of a 20% sucrose cushion and centrifuged at 4°C for 2 hours at 28000 rpm in a SW40Ti rotor. Finally, the HIV-VLPs pellet was re- suspended in 200 µl TNE buffer. Purified HIV- VLPs were analyzed by western blot.

Western blot and protein quantification in HIV-VLPs

The presence of Gag-EGFP and/or Env in the HIV-VLPs was determined by western blot with mouse anti-p24 and goat anti-gp120-biotin conjugated antibodies. HIV-VLPs were separated by electrophoresis through 10% SDS-polyacrylamide gels and electroblotted onto nitrocellulose membrane. Following incubation with appropriate primary and secondary antibodies, proteins were visualized using an infrared-based imaging system (Odyssey; LiCor Biosciences, Lincoln, NE, USA). To quantify the protein content of the purified HIV-VLPs containing solution, different amounts of HIV-VLPs were subjected to reducing SDS-PAGE (10%, pH=7.5). The same was done for concentration series of a BSA reference. The obtained coomassie-stained polyacrylamide gel (not shown) was imaged using a LI-COR Odyssey Scanner and the band intensities were analyzed with the ImageJ Software. By comparison between the resulting band intensities from the HIV-VLPs samples with the concentration series of BSA standard, it was possible to estimate the protein content of purified HIV-VLPs stock solution.

Flow cytometry measurements and fluorescence intensity quantifications

Macrophages were analyzed in PBS using a BD FACS Aria II Flow Cytometer (BD Biosciences, San Jose, CA, USA) with a 100 µm nozzle and 2.0 ND filter. A total of 10,000 events were counted and the fluorescence values of HIV-VLPs and αEnv-PS-LUVs or PS-LUVs/LUVs alone were measured. The presence of internalized EGFP-tagged HIV-VLPs was quantified by exciting at 488 nm and detecting with a 530/30 band-pass filter. The presence of internalized DiI-labeled liposomes was quantified by exciting at 561 nm and detecting with a 616/23 band-pass filter. The presence of internalized Top- Fluor-PC-labeled liposomes was quantified using the same settings for HIV-VLPs. Quantification of fluorescence intensities was performed using the software FlowJo.

Toxicity test

Toxicity of the treatment with HIV-VLPs in the presence of immunoliposomes on the mouse macrophage cell line J774A.1 was tested. Cells were grown to 70% confluency in 12 mL cell-flasks in the presence of RPMI, 10% FBS, 1% penicillin-streptomycin, and 2 mM L-glutamine. Then, cells were gently scraped off, plated in

a 96-well plate and incubated at 37°C in 5% CO_2 for 24 hours. αEnv-PS- LUVs HIV-VLPs were mixed together for 1 hour at room temperature. The cells were washed with PBS and treated with the liposomes/HIV-VLPs or 10% DMSO, and incubated for 1, 48 or 72 hours at at 37°C with 5% CO_2in RPMI medium (up to 200 µl total volume per well). Subsequently, the cells were washed and the CellTiter-Blue test was performed according to the manufacturers manual. The fluorescence emission of the fluorescent dye was measured at a plate-reader. For the test with propidium iodide, the cells were re-suspended in PBS, stained with 1 µl PI (from a 10 µg/mL in PBS stock solution) and the fluorescence of PI was measured with FACS by exciting at 561 nm and detecting with a 616/23 band-pass filter.

Statistical analysis

In order to compare different datasets and verify whether they were significantly different, we performed Student's t-tests.

The associated probabilities were calculated using the Matlab function *ttest2* (Matlab, The Mathworks Inc., Natick MA). Two datasets were considered significantly different if the calculated probability *p* was lower than 0.

3 RESULTS AND DISCUSSION

3.1 Intracellular distribution and dynamics of HIV-1 Gag, and calcium-dependent release of virus-like particles

The first aim of this work was to study the intracellular distribution and dynamics of HIV-1 Gag and to unravel calcium-dependent mechanisms able to mediate the release of VLPs from the host cell. To these aims, experiments were conducted with a combination of confocal and total internal reflection fluorescence microscopy, and correlative-light and electron microscopy.

The study of VLPs release in permissive (COS-7, HEK-293T) and non-permissive (HeLa) cell lines, and chemical modulation of intracellular pathways, allowed the identification of an alternative mechanism for VLPs release.

3.1.1 Intracellular distribution of HIV-1 Gag

Expression in appropriate mammalian cell lines (e.g. HeLa, COS-7, HEK-293T) of a fluorophore-tagged version of Gag (e.g. Gag-EGFP[5], Gag-CFP[6], Gag-mCherry) allows studying, e.g. by confocal fluorescence microscopy, the intracellular localization of the Gag protein in a way that highly resembles the distribution of the wild-type Gag in the context of a HIV-1 infection [2,103]. In Figure 13 a HeLa cell 24 hours after transfection with a Gag-EGFP plasmid is shown. As it can seen in the merged panel with the DIC– images and by the shape and the size of the nuclear staining, Figure 13A and 13B show the same cell in two different confocal planes: in the middle of the cell and at the bottom, respectively. In these images, Gag-EGFP can be found intracellularly in two different distribution patterns: I) associated to the PM and II) in a dot-like form in the perinuclear and cytosol area. Depending on the expression level and the timing after protein expression, Gag can also be ob-

[5] (EGFP) Enhanced green fluorescent protein

[6] (CFP) Cyan fluorescent protein

served in a third distribution pattern, as shown in Figure 16 and 19: III) homogeneously distributed in the cytosol. Total internal reflection fluorescence microscopy (TIRFM) imaging is a technique for the identification of fluorescent molecules specifically localized at the basal PM - very near to the support (see Material and Method section for further details). Visualization of a Gag-EGFP transfected cell in TIRFM-modus (Figure 13C) allows therefore the visualization of the Gag distribution at the basal PM.

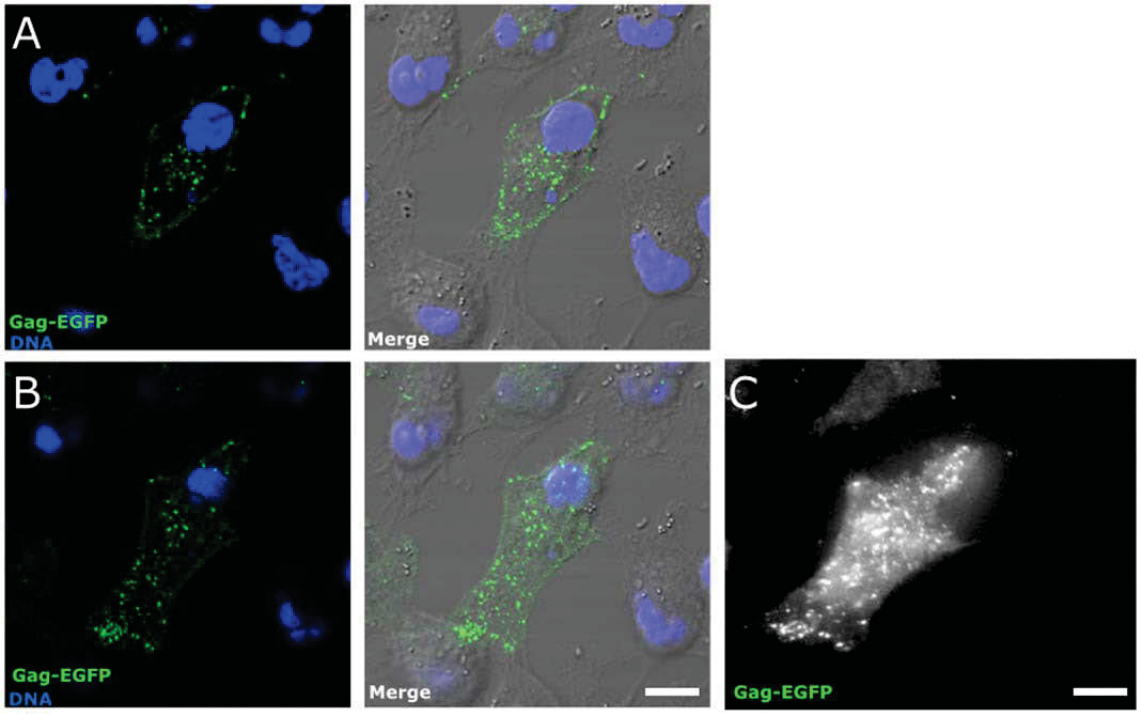

Figure 13. Live cell confocal microscopy of Gag-EGFP transfected HeLa cells. The focal plane was positioned approximately at the middle of cell height (A) or at the bottom of the sample (B). Gag-EGFP (green channel) is localized in two distribution patterns: I) associated to the PM and II) in a dots-like form in the perinuclear and cytosol area. DNA staining (blue channel) indicates the location of the nucleus and helps to identify the position of the confocal plane. (C) TIRFM modus of the image shown in (B). Gag-EGFP is shown here in the white channel. Scale bar is 5 µm. Images were collected 24 hours after transfection at 37°C, 5% CO_2.

3.1.2 Activation of both G_q-protein and receptor-protein tyrosine kinase - dependent phospholipase C is required for Gag transport to the PM

Many host factors are believed to play an important role supporting different steps of HIV-1 assembly and release. A previous study has shown that activation of phospholipase C (PLC) in COS cells is required for efficient release of VLPs from host cell [1,43]. The reason why the PLC might play an important role regulating the release of VLPs remains to be understood. Nevertheless, inhibition of PLC in COS cells was shown to keep Gag in an aggregate conformation in the perinuclear area [1]. In this work, the use of TIRFM on HeLa cells transfected with Gag-EGFP enabled to confirm the previously obtained results and to further characterize the effects on PLC inhibition on Gag trafficking to the PM. Analysis of VLPs-release in HEK-293T upon modulation of the PLC pathway added new information on the role of the PLC signaling pathway.

Figure 14 shows how upon inhibition of PLC (with 10 μM of the PLC inhibitor U73122), besides a decrease in Gag protein expression, a strong reduction of the presence of Gag at the PM, compared to untreated cells (Figure 13) and aggregation in the perinuclear area can be observed. The inhibitor U73122 is able to block the activation of both γ and β isoforms of the PLC in many different cell types [104,105]. The enzymatic activity of these two isoforms of PLC is triggered by two different pathways: the γ isoform is activated by the tyrosine-kinase receptor (TKR) and the β isoform by the G-protein coupled receptor (GPCR) [106]. Specific inhibition of the "q" isoform (G_q) of the G-protein with 10 μM of the G_q-protein inhibitor mepyramine [107], caused aggregation of Gag in the perinuclear area (Figure 15A) and resulted in a reduced release of VLPs (from HEK-293T cells) (Figure 15B).

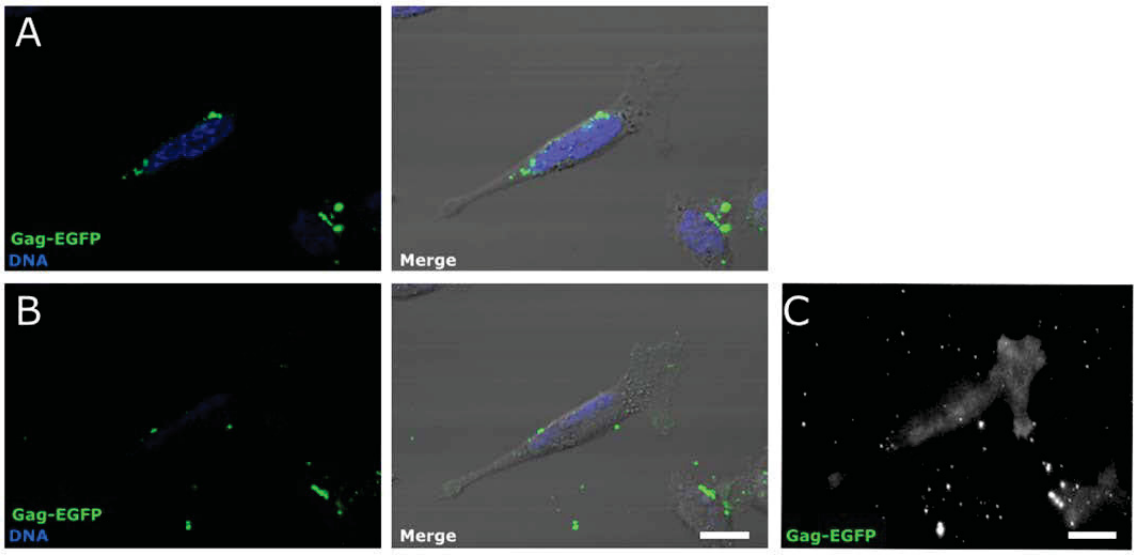

Figure 14. Inhibition of PLC activity blocks Gag in aggregates and strongly decreases Gag localization at the PM. The focal plane was positioned approximately at the middle of cell height (A) or at the bottom of the sample (B). Gag-EGFP (green channel) is localized in aggregates in the perinuclear area. DNA staining (blue channel) indicates the location of the nucleus and helps to identify the position of the confocal plane. (C) TIRFM modus of the image shown in (B). Gag-EGFP is shown here in the white channel. Scale bar is 5 µm. Images were collected 24 hours after transfection at 37°C, 5% CO_2

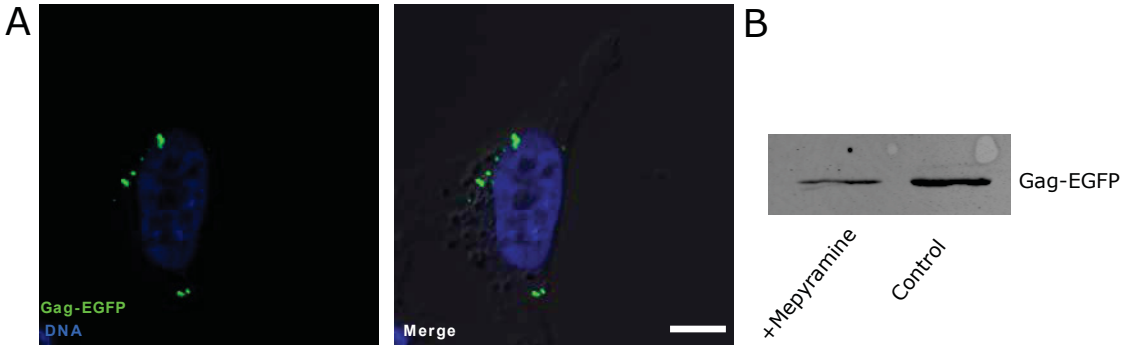

Figure 15. Inhibition of G_q-protein activity blocks Gag in aggregates in the cytosol and reduces VLPs release. (A) The focal plane was positioned approximately at the middle of cell height. Gag-EGFP (green channel) is localized in aggregates in the perinuclear area. DNA staining (blue channel) indicates the location of the nucleus and helps to identify the position of the confocal plane. Scale bar is 6 µm. Images were collected 24 hours after transfection at 37°C, 5% CO_2. (B) Western blot of purified VLPs from untreated (control) and Mepyramine-treated (+Mepyramine) HEK-293T cells, visualized after staining with an anti-p24 antibody.

3.1.3 Gag, assembled in VLPs, is entrapped into vesicles of the endo-lysosomal system

While the Gag population at the PM (previously mentioned as distribution-pattern I) most probably corresponds to monomeric/polymeric PM-bound Gag or nascent VLPs, and the cytosolic spread state (distribution-pattern III) represents freely distributed Gag proteins into the cytosol [2], the nature of the observed intracellular dots might need further characterization. The distribution pattern of Gag in a dot-like form, in the cytosol and the perinuclear area (previously mentioned distribution-pattern II), mostly resembles the distribution of vesicles of the endo-lysosomal system [108]. Endosomal and lysosomal vesicles can be distinguished by different parameters (e.g. associated GTPases, specific membrane receptors, proton content) [102,108]. However, one characteristic is common to all of these vesicles: a high intralumenal calcium concentration [109]. Staining with the low-affinity calcium fluorophore Fluo5F, which is known to localize in intracellular high-calcium containing compartments (e.g. ER in renal cells [110]), was applied. Interestingly, in HeLa cells Fluo5F detects the presence of calcium in an intracellular dot-like distribution pattern, which mostly co-localizes with the Gag-CFP dots (Figure 16).

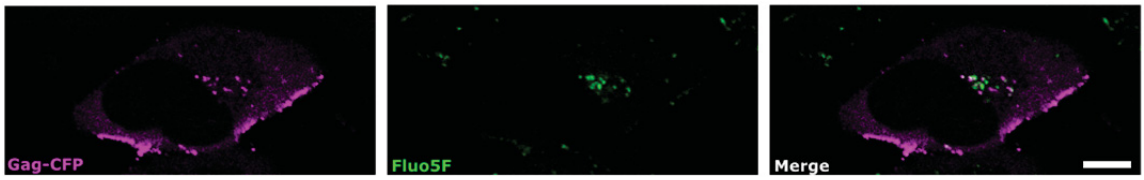

Figure 16. Gag-CFP intracellular dots co-localize with Fluo5F. The focal plane was positioned approximately at the middle of cell height. Intracellular dots of Gag-CFP (magenta channel) co-localize with Fluo5F dots (green channel) in the perinuclear area. Scale bar is 5 µm. Images were collected 24 hours after transfection at 37°C, 5% CO_2.

Furthermore, live-cell imaging of Gag-CFP transfected cells stained with Fluo5F showed that the Gag/Fluo5F co-stained vesicles move in the intracellular space following straight trajectories, moving from and to the PM (data not shown).

In order to further characterize the intracellular co-localization of Gag-CFP and Fluo5F with high spatial resolution, a correlative fluorescence and electron microscopy imaging approach was used. Figure 17 shows that Gag-CFP/Fluo5F-positive

compartments are membrane-delimited vesicles containing Gag assembled in VLPs. Vesicles of the endo-lysosomal system are not the only calcium-containing compartments in mammalian cells. Co-localization with other calcium-containing compartments (e.g. mitochondria, ER, nucleus) must be investigated. To this aim, co-staining with Fluo5F, a DNA-, a mitochondrial-, and an ER-marker was performed (Figure 17 and Figure 18). As shown by the images, Fluo5F stained vesicles do not co-localized either with the nucleus, the mitochondria or the ER. Subsequently, Gag-CFP transfected HeLa cells, stained with Fluo5F, were either co-stained with the lysosomal marker Lysotracker or co-transfected with a fluorophore-tagged version of the Rab7 protein (i.e. Rab7-GFP) as marker for LE. As shown in Figure 19, indicated by the arrows, Fluo5F stains at least two different kind of vesicles of the endo-lysosomal system: LEs and LYs. Gag is contained in both compartments (Figure 19A and B).

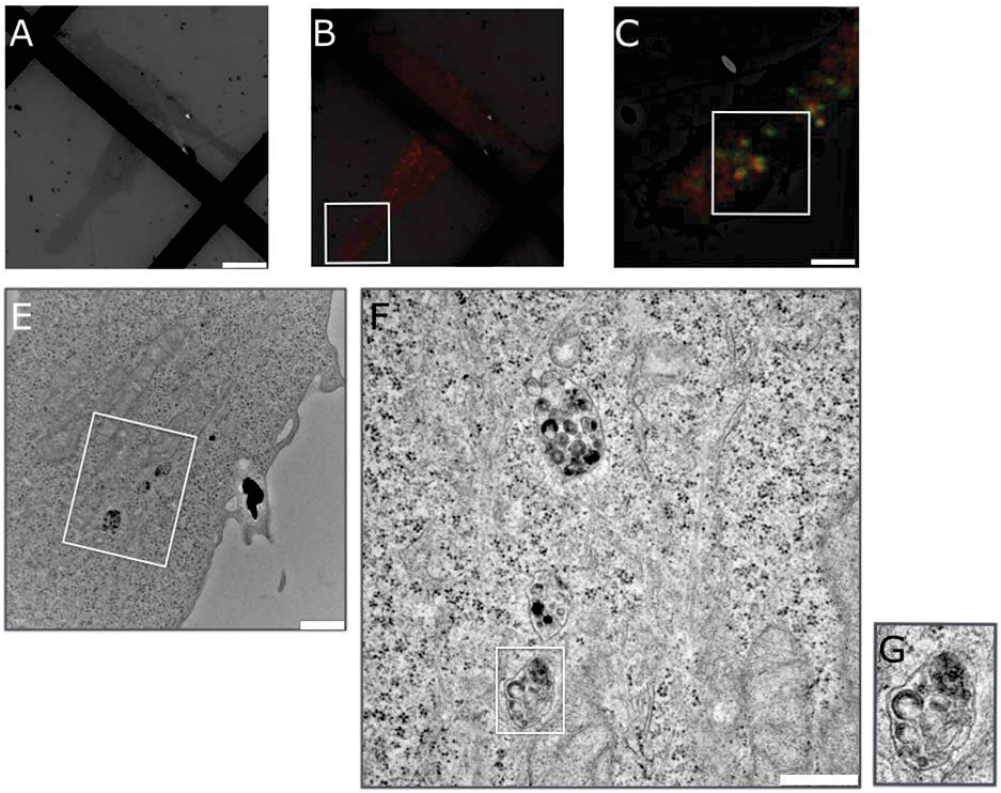

Figure 17. Co-localized Gag/Fluo5F dots correspond to VLPs-containing intracellular compartments. (B-C) Gag-CFP (red channel) and Fluo5F (green channel) were visualized by confocal laser scanning microscopy 24 hours after transfection, and correspond to endosome-like structures containing VLPs imaged by transmission electron microscopy (E-G). (A, E-G) electron micrographs, (B-C) correlation of fluorescence images with electron micrograph by alignment of cellular surface structures. Indicated squares represent the area of magnification in the subsequent panel. Scale bars: 5 µm (A-B), 2 µm (C), 1 µm (E), 500 nm (F).

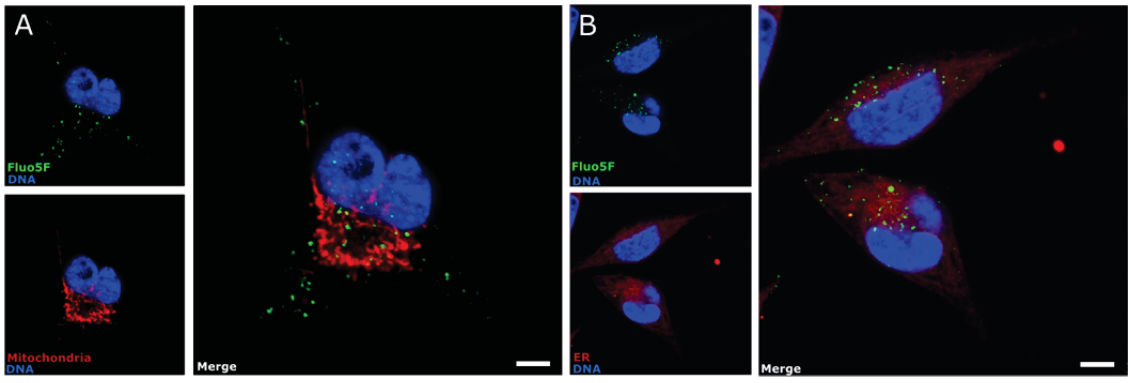

Figure 18. Fluo5F does not co-localize with mitochondria or ER. The focal plane was positioned approximately at the middle of cell height. Intracellular dots of Fluo5F (green channel) do not co-localize with (A) mitochondria (red channel) or (B) ER (red channel). DNA staining (blue channel) indicates the location of the nucleus. Scale bar is 4 µm. Images were collected at 37°C, 5% CO_2.

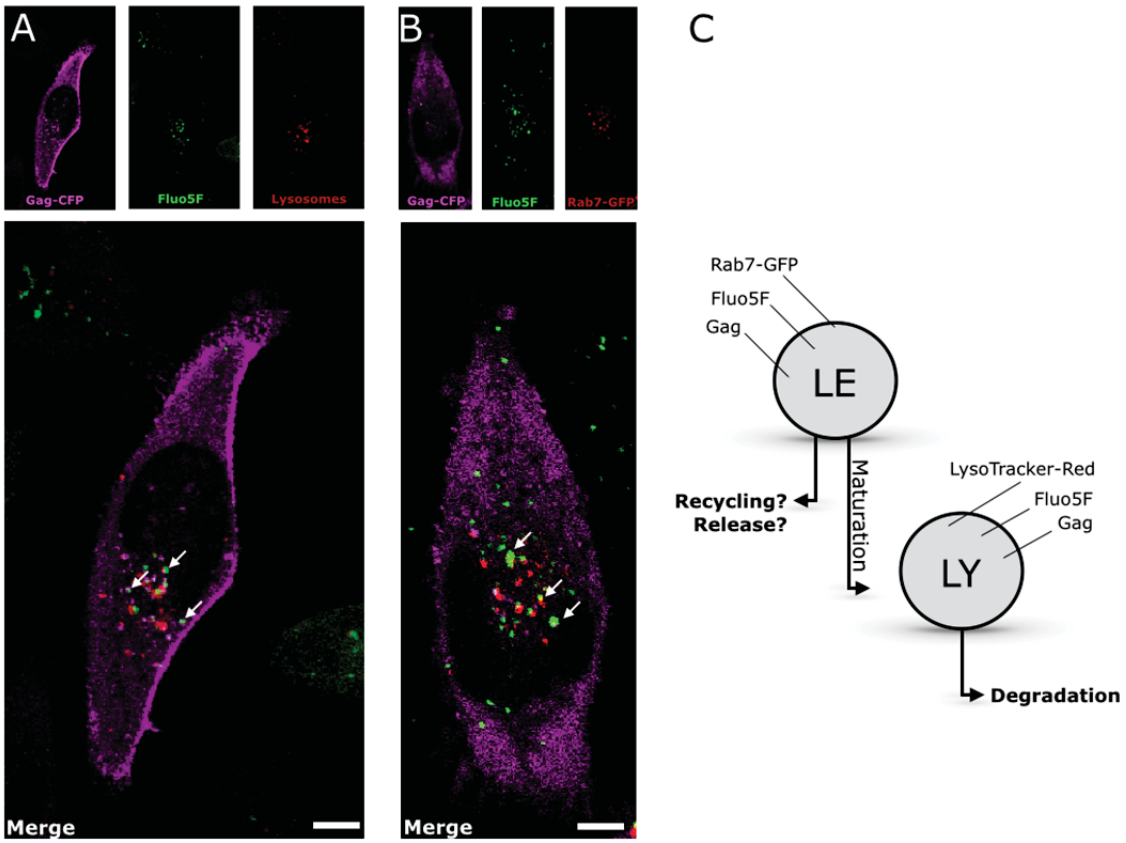

Figure 19. Intracellular Gag dots partially co-localize with Fluo5F and LY/LE. The focal plane was positioned approximately at the middle of cell height. Intracellular dots of Gag-CFP (magenta channel) co-localize with Fluo5F dots (green channel) in the perinuclear area. In the merged image in (A), shown by the arrows, Gag-CFP and Fluo5F co-localize with Lysosomes (red channel). In the merged image in (B), shown by the arrows, Gag-CFP and Fluo5F co-localize with Rab7-GFP (red channel) Scale bar is 2 µm. Images were collected 24 hours after transfection at 37°C, 5% CO_2. (C) Schematic representation of the maturation pathway of LEs to LYs and the possible fates of the two different compartments.

Clearly, Gag assembled in VLPs exists intracellularly in calcium-containing, membrane-delimited intracellular vesicles that belong to the endo-lysosomal system. These compartments can be specifically identified as LEs and LYs. The fate of the entrapped VLPs is unclear and needs further investigations. Figure 19C shows a schematic representation of the maturation pathway of LEs to LYs and the possible fates of the two different compartments.

3.1.4 Lysosomal calcium leakage induces release of VLPs from HeLa cells

Previous studies have shown that induction of a transient rise in cytoplasmic calcium increased the amounts of VLPs in LEs/MVBs/LYs, and resulted in a dramatic enhancement of VLPs release [2,44]. However, although cellular factors have been already proposed as mediators of calcium provision (e.g. ER [1]), how calcium can promote the release of VLPs remains to be determined. In order to further investigate the role of intracellular calcium in VLPs release, it is intriguing to investigate whether the calcium of lysosomal origin might also play a role affecting the release of VLPs. In fact, calcium release from LYs is known to be specifically activated in the case of membrane injuries [111]. More in detail, the calcium released from LYs can then trigger fusion between lysosomal and late-endosomal vesicles, causing the formation of hybrid LY/LE organelles inducing therefore a intralumenal content mixing [112,113] (for a schematic representation, see Figure 35). Furthermore, generally, elevation of cytosolic calcium triggers fusion of LYs with the PM and release of lysosomal content into the extracellular space [102]. More specifically, wounding the PM by scratching induces the surface exposure of the major lysosomal membrane glycoprotein Lamp-1 at the wound site as a consequence of intracellular calcium release [114]. This mechanism has been described as LY-mediated PM-repair [112]. VLPs contained in LYs and/or LEs might be not completely destined to degradation, but rather indirectly "recycled" from such PM-repair mechanism, which involves release of calcium from LYs and subsequently multiple fusion processes.

Gag-CFP transfected HeLa cells, stained with Fluo5F, were treated for 3 hours with the SERCA[7]3-ATPase inhibitor t-Butylhydroquinone (TBHQ), and then observed at the confocal microscope. TBHQ inhibits the re-captation of calcium into LYs, blocking the activity of the SERCA3-ATPase [115], and inducing therefore a leakage of calcium from lysosomal compartments that express the SERCA3-ATPase on their surface (see schematic representation in Figure 20B). Surprisingly, induced calcium-leakage from LY, instead of causing a loss of Fluo5F fluorescence from those compartments, resulted in a dramatic enlargement of Fluo5F-positive vesicles (i.e. endo-lysosomes), and their spread distribution among the cytosol (Figure 20A). Furthermore, treatment with TBHQ for 3 hours, 48 hours after transfection with

[7] (SERCA) Sarcoplasmic/endoplasmic reticulum calcium ATPase

Gag-CFP, resulted in release of a small amount of VLPs (Figure 20C). HeLa cells are known to be unable to allow the release of VLPs, because of the constitutively expression of Tetherin, whose inhibitory activity on VLPs release can be counteracted only by the presence of the HIV-1 protein Vpu [116,117]. Collection of VLPs from Gag-transfected HeLa cells, after treatment with TBHQ, suggests that there might be some other mechanism, correlated with the leakage of calcium from LYs, which might enable the release of VLPs from HeLa cells.

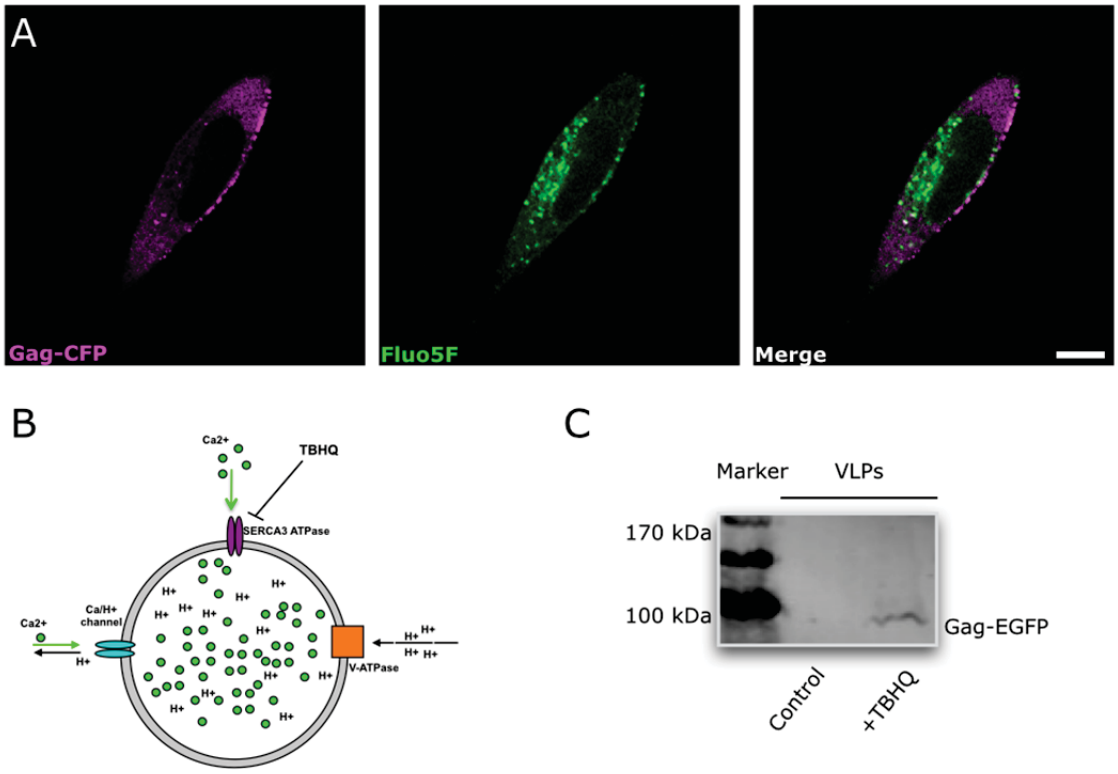

Figure 20. Lysosomal calcium leakage induces enlargement of endo-lysosomal compartments and causes release of VLPs from HeLa cells. (A) Gag-CFP transfected cells, stained with 3 μM Fluo5F and treated for 3 hours with 1 μM TBHQ. The focal plane was positioned approximately at the middle of cell height. Intracellular dots of Gag-CFP (magenta channel) partially co-localize with enlarged Fluo5F dots (green channel). Scale bar is 5 μm. Images were collected 24 hours after transfection at 37°C, 5% CO_2. (B) Schematic representation of the inhibitory activity of TBHQ on LE/LY. Calcium ions and calcium fluxes are colored in green; the SERCA3-ATPase is shown in purple, the V-ATPase in orange, and the calcium/proton channel in light blue. Protons and protons fluxes are also indicated. The inhibition activity of TBHQ is indicated with an interrupted arrow. (C) Western blot of purified VLPs from untreated (control) and TBHQ treated (+TBHQ) HeLa cells, visualized after staining with an anti-p24 antibody.

In order to confirm the results obtained in HeLa cells, specifically regarding the relevance of lysosomal-calcium leakage in the release of VLPs, it is necessary to express Gag in a different cell-type, which is permissive for VLPs release in absence of Vpu protein expression (e.g. COS-7, HEK-293T). In the following paragraphs, the intracellular distribution and dynamics of Gag and the release of VLPs will be investigated in COS-7 cells. COS-7 are also larger than HeLa cells and posses a wide microtubule net. These conditions make them appropriate for the study of Gag intracellular dynamics and for the further investigation of the reasons behind the release of VLPs upon TBHQ treatment.

3.1.5 Characterization of Gag intracellular distribution, dynamics and VLPs release in COS-7 cells

Transfection of an appropriate cell line, which in contrast to HeLa cells does not express Tetherin (e.g. COS-7, HEK-293T cells), with only a Gag-EGFP plasmid, is sufficient for the production and the release of VLPs.

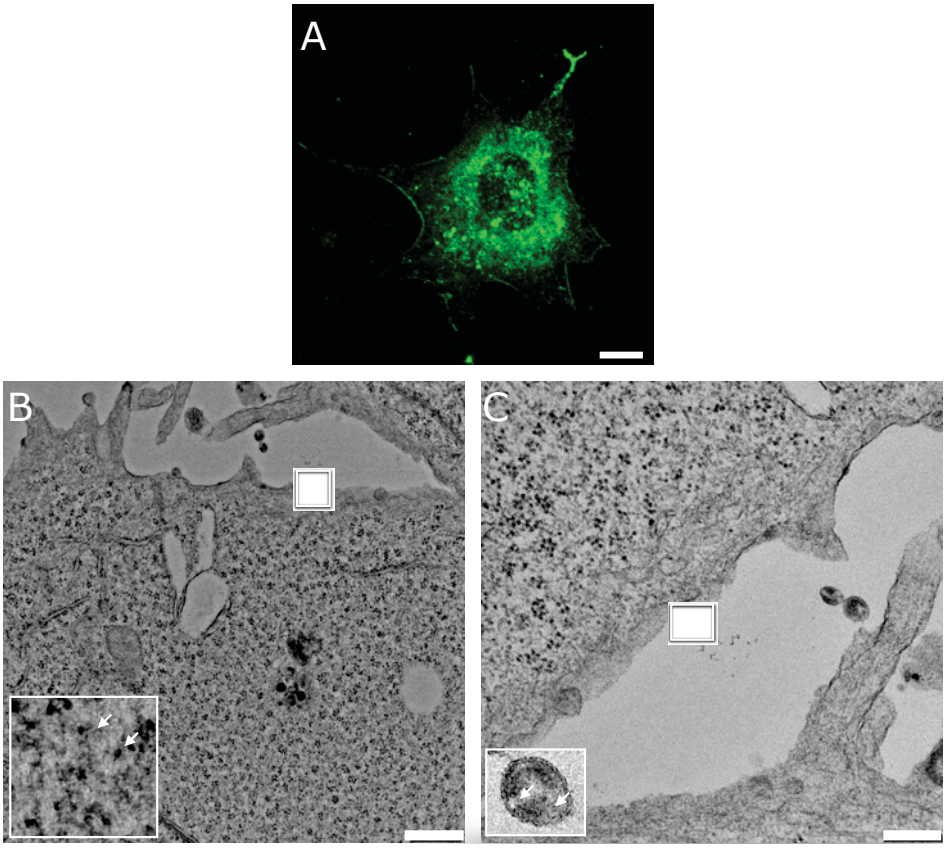

Figure 21. Intracellular distribution of Gag-EGFP in COS-7 cells and release of VLPs. (A) COS-7 transfected with Gag-EGFP (green channel). Image was collected 24 hours after transfection at 37°C, 5% CO_2. (B-C) Released VLPs and budding events in COS-7 cells 48 hours after transfection with Gag-EGFP imaged by transmission electron microscopy. Indicated squares represent the area of magnification. White arrows indicate the points of discontinuity in the Gag shell. Scale bars: 6 µm (A), 500 nm (B), 300 nm (C).

Budding of VLPs from the PM of Gag-EGFP transfected COS-7 or HEK-293T cells results in the release of particles with a discontinuous Gag shell (Figure 21B and 21C - zoomed sections), in contrast to the evenly distributed ring of Gag density

that is normally observed beneath the membranes of immature HIV-1 virions and Gag VLPs [118]. However, the intracellular distribution of Gag-EGFP in COS-7 cells (Figure 21A) can be compared to the previously suggested distribution patterns, observed in HeLa cells (see Figure 13 and Figure 16). In order to identify whether the different populations of Gag form at specific time points after protein synthesis, the EGFP gene in C-terminal of Gag was substituted with two different genes of mCherry-derived monomeric variants, called fluorescent timers (FTs), that change their fluorescence from blue to red over time [119] (see Material and Method section for the cloning procedures).

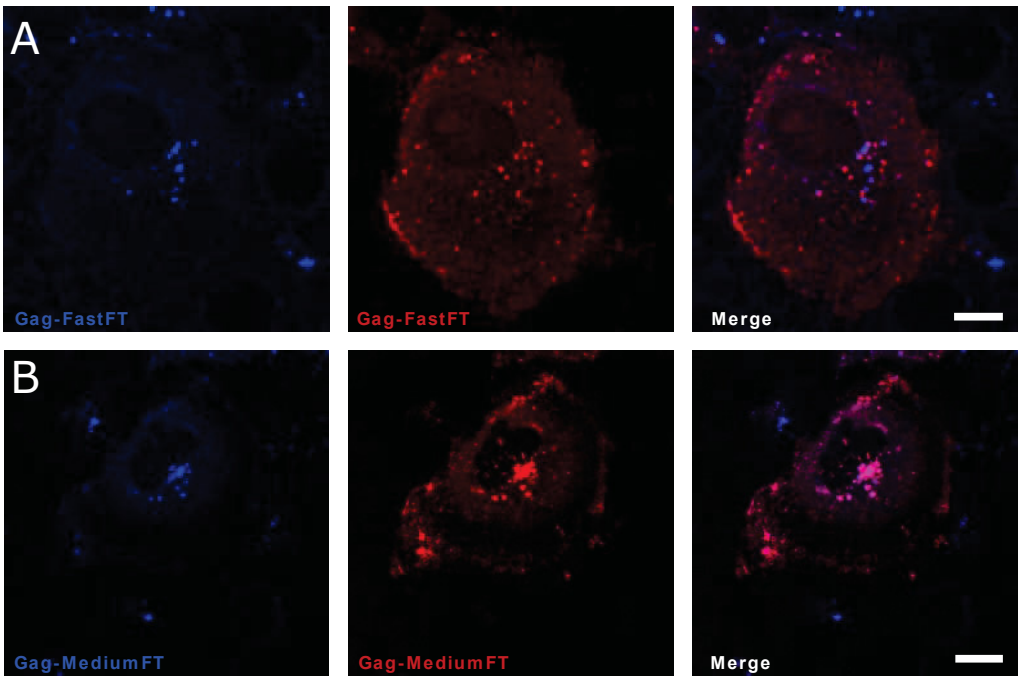

Figure 22. Intracellular distribution of Gag-FastFT and Gag-MediumFT. (A) COS7-cells transfected with Gag-FastFT. Early fluorescent form of the FastFT (blue channel) and late fluorescent form of the FastFT (red channel) are shown. (B) COS7-cells transfected with Gag-MediumFT. Early fluorescent form of the MediumFT (blue channel) and late fluorescent form of the MediumFT (red channel) are shown. Overlays of the two channels are shown in magenta. Scale bar is 4 µm. Images were collected 24 hours after transfection at 37°C, 5% CO_2.

FTs can be used as molecular genetically encoded tools to study trafficking of different cellular proteins and to provide accurate insight into the timing of intracellular processes [119]. The two FTs used in this work are called FastFT and MediumFT, in regard to the timing of blue-to-red switch after protein synthesis. The fluores-

cence switching times of the two FTs are indicated in Table 1 in the Material and Method section. Briefly, during the FT maturation the fluorescence of the blue forms increase to its maximum value, and after that decrease to zero. The fluorescence of the red forms increase with time with some delay and then reach a plateau. At 37°C the maxima of the blue fluorescence intensities were observed at 0.25 and 1.2 hours for the FastFT and the MediumFT, respectively. The half-maxima of the red fluorescence intensities were reached at 7.1 and 3.9 hours, respectively [119]. COS-7 cells transfected with Gag-FastFT (Figure 22A) showed a blue Gag population mostly aggregated in dot-like form in the perinuclear area, while the red variant was found to be poorly concentrated in dots in the perinuclear region but rather both spread in the cytosol and near to- or associated to the PM. COS-7 cells transfected with Gag-MediumFT (Figure 22B) mostly resembled the Gag-FastFT transfected cells with the exception of the higher amount of red population of perinuclear dots. The convergence of dots in the perinuclear area, particularly notable in a later phase after Gag translation (see distribution of the blue and the red forms of Gag-MediumFT in Figure 22B), together with the previous results obtained in HeLa cells (i.e. co-localization in endo-lysosomal compartments), suggest that Gag may move exploiting microtubular structures. LEs and LYs are transported on microtubules in a bidirectional manner, by the help of both kinesin and dynein motor proteins [120]. These motor proteins use ATP to move either from the point of convergence of the microtubules (microtubules organization center - abbreviated: MTOC) to the PM (kinesins), or *vice versa*, toward the perinuclear area (dyneins). Maturation of LEs to LYs corresponds to a vesicle movement toward the MTOC, where most of the LYs localize [108]. On the contrary, vesicles (e.g. LEs and/or LYs) that move from the MTOC to the PM are most probably destined to exocytosis or secretion from the PM. Live cell confocal microscopy of COS-7 co-transfected with Gag-mCherry and Tau-YFP (a YFP-tagged version of the microtubule-stabilizing protein Tau) was performed.

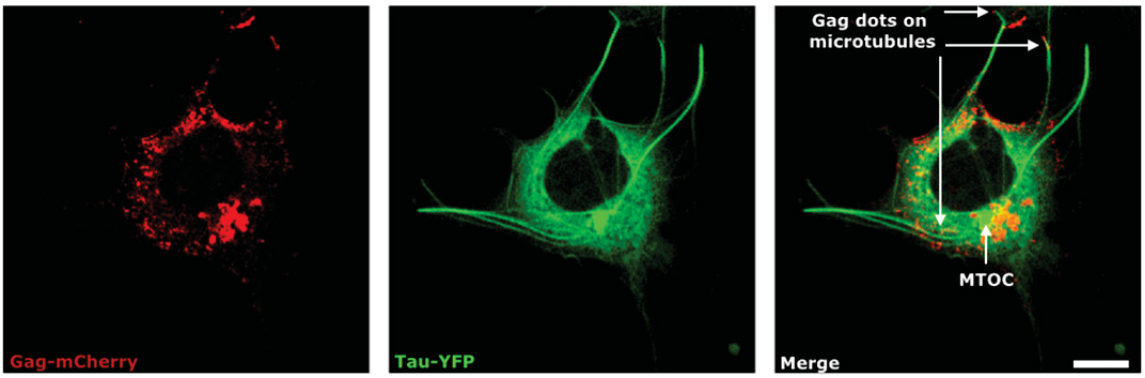

Figure 23. Distribution of Gag on the microtubular filaments. COS-7 cell co-transfected with Gag-mCherry (red channel) and Tau-YFP (green channel). The arrows indicate the MTOC and Gag dots apparently associated to microtubular filaments. Scale bar is 4 μm. Images were collected 24 hours after transfection at 37°C, 5% CO_2.

In Figure 23, microtubular ramifications and MTOC are clearly shown (see arrows in Figure 23). In Figure 23, the point of convergence of the perinuclear Gag dots, located on the MTOC and the concomitant Gag association to the microtubular filaments in different intracellular areas can be identified (see arrows in Figure 23). However, since the movement direction of the endo-lysosomal vesicles is one of the parameters that can identify the fate of a LE or LY, a time scanning imaging of a COS-7 cell co-transfected with Gag-mCherry and Tau-YFP was performed (Figure 24). In the different time frames reported in this figure, it is possible to identify two Gag dots that, following a trajectory on the microtubular filaments, move away from the MTOC, suggesting that such vesicles might be associated to kinesin motor proteins.

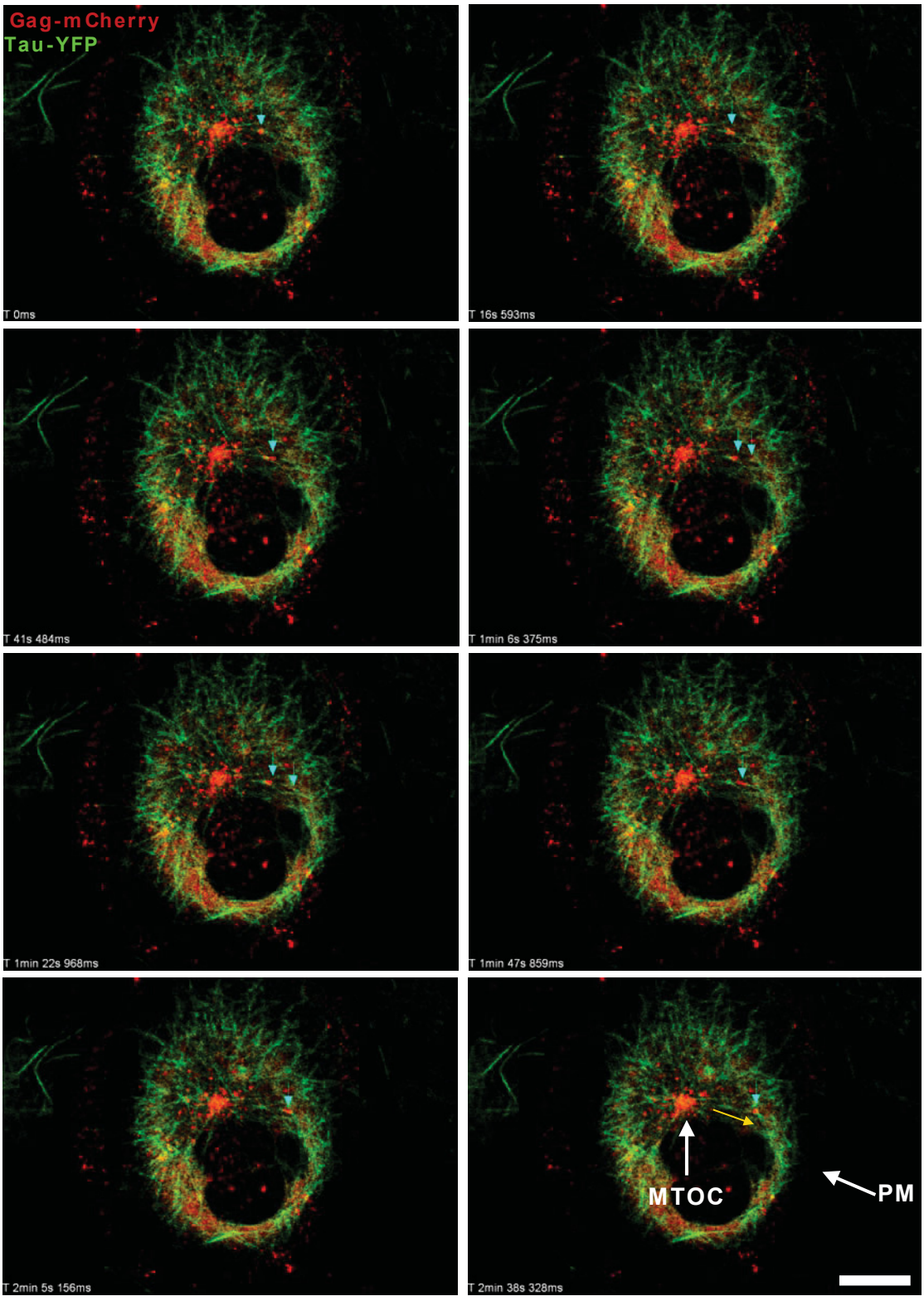

Figure 24. Gag dots move on the microtubular filaments. COS-7 cell co-transfected with Gag-mCherry (red channel) and Tau-YFP (green channel). The light blue arrows follow the movement of two Gag dots on the microtubular filaments. Frame times are indicated. Scale bar is 6 μm. Images were collected 24 hours after transfection at 37°C, 5% CO_2.

3.1.6 TBHQ-induced lysosomal calcium leakage causes fusion between Fluo5F containing compartments and enhanced release of VLPs

The previously observed enlargement in Fluo5F-positive compartments after induced calcium-leakage with TBHQ (Figure 20), which *de facto* in HeLa cells corresponded to an increased fluorescence intensity of the Fluo5F-positive vesicles and therefore to an increased lumenal calcium concentration, seems to be contradictory. However, enlargement of endo-lyososmal compartments after calcium release from the lysosomal lumen is a well-known consequence of a mechanism that involves fusion between LEs and LYs [112]. This mechanism can be physiologically activated by the binding of Nicotinic acid adenine dinucleotide phosphate (NAADP) to the lysosomal two-pore channel (TPC), which in turn allows release of calcium from the LYs [121,122]. The fusion process between LEs and LYs is a calcium-mediated process and a highly regulated mechanism that requires the co-operation of proteins of the SNAREs[8]–complex machinery [102], and might take place in response to very specific intracellular stimuli [121,122]. This fusion process usually entails mixing of the LEs/LYs content, which in this case may be in part represented by completely of partially formed VLPs. Besides such fusion processes, enhanced calcium concentrations can activate exocytosis of LYs, that can fuse with the PM in a Synaptotagmin VII (Syt-VII) mediated manner [102,123]. Syt-VII is a protein localized on the membrane of LYs, able to mediate lipid-bilayer fusion if activated upon binding by calcium ions. Figure 25 shows a COS-7 cell transfected with Gag-CFP, stained with Fluo5F and Lysotracker and treated for 3 hours with TBHQ. As already shown in HeLa cells, an enlargement of the endo-lysosomal compartments (i.e. Fluo5F and Lysotracker positive vesicles) takes place (Figure 25A merged image). Specifically, considered that Lysotracker staining is specific only for LYs and Fluo5F most probably unspecifically stains LEs and LYs, events that mostly resemble pre- and post-fusions between endo-lysosomal vesicles can be observed (see zoomed sections and schematic representations in Figure 25B). The presence of Gag into the fused vesicles can be deduced by the CFP signal overlapping with the signal of Lysotracker and Fluo5F (zoomed section "2" in Figure 25B).

[8] (SNARE) Soluble N-ethylmaleimide-sensitive factor- attachment protein receptor.

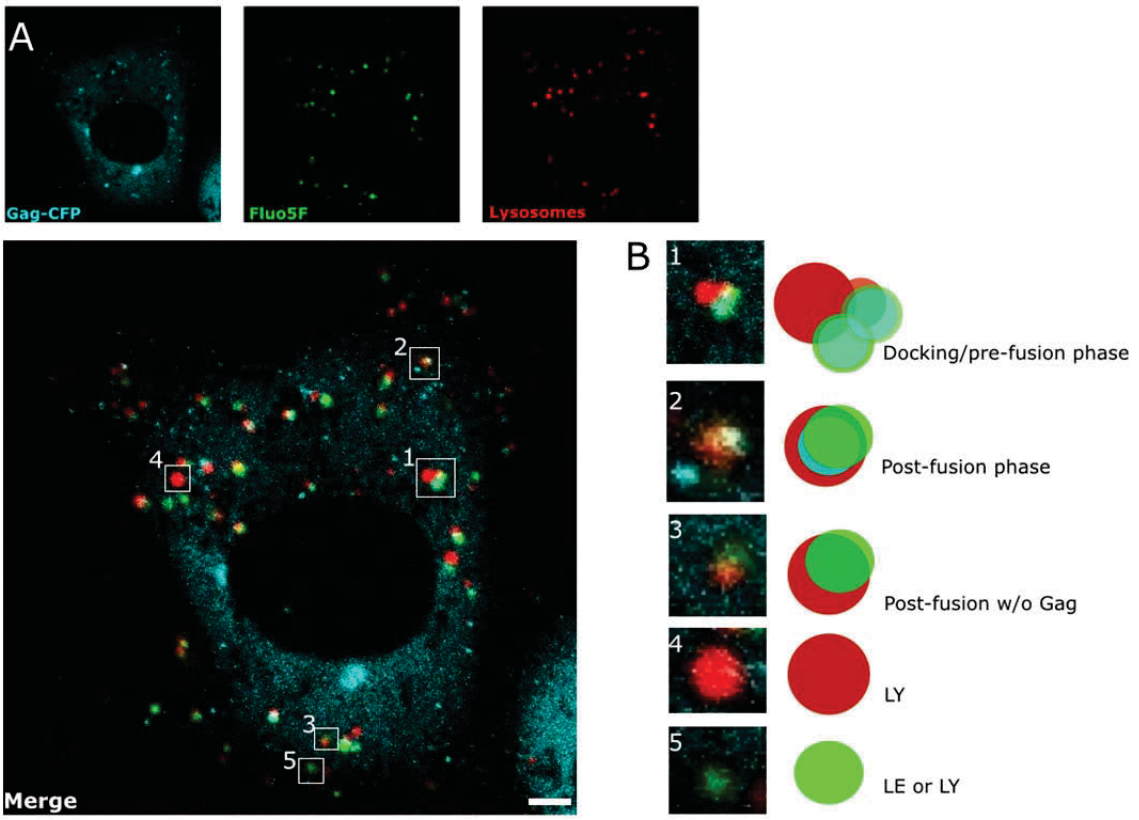

Figure 25. TBHQ treatment induces fusion between LE and LY. (A) COS-7 cell transfected with Gag-CFP (light blue channel) and stained with 3 μM Fluo5F (green channel) and Lysotracker (red channel). 24 hours after transfection the cells were treated with TBHQ for 3 hours. The squares in the merged image indicate regions reported enlarged in (B). (B) Enlargements of 5 different sections of the merged image in (A); schematic representations of the visualized vesicles are also shown: the color-code used in the schematic representation is the same of the fluorescent channels. Scale bar is 5 μm. Images were collected 24 hours after transfection at 37°C, 5% CO_2.

Notably, by comparing untreated and TBHQ-treated cells (Figure 26) the intracellular distribution of the enlarged Fluo5F compartments is changed upon lysosomal calcium leakage. Fluo5F vesicles are, upon TBHQ treatment, not anymore concentrated only in the perinuclear area, but rather more spread in the cytosol and localized in perimembrane areas. The re-distribution of LYs upon TBHQ-treatment can be observed in Figure 27, where COS-7 cells transfected with a CFP-tagged version of the lysosomal protein Syt-VII are shown. Increased cytosolic concentration partially re-localize Syt-VII-positive vesicles (i.e. LYs) from the perinuclear area to the proximity of the PM.

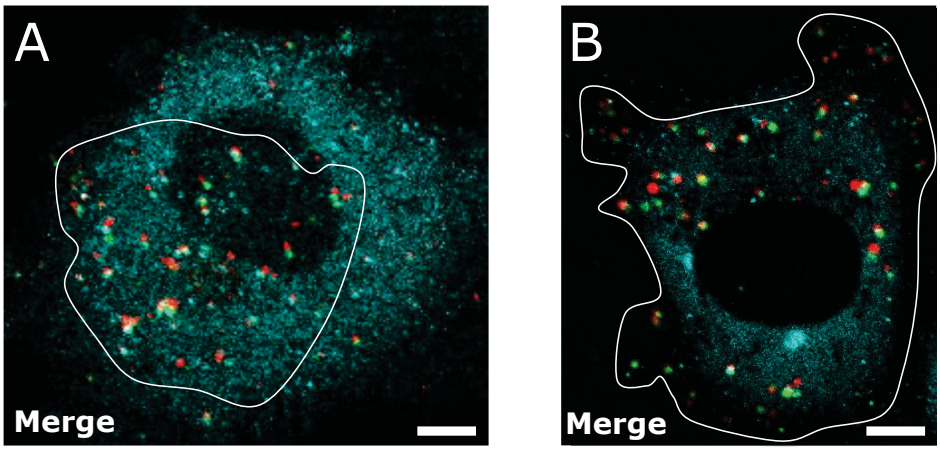

Figure 26. TBHQ treatment induces intracellular re-distribution of Fluo5F/Lysotracker positive compartments. COS-7 cells transfected with Gag-CFP (light blue channel) and stained with 3 μM Fluo5F (green channel) and 50 μM Lysotracker (red channel). 24 hours after transfection, the cells were (A) untreated or (B) treated with TBHQ for 3 hours. The area covered by the Fluo5F/Lysotracker-positive compartments is indicated by white boundaries. Scale bar is 5 μm. Images were collected at 37°C, 5% CO_2.

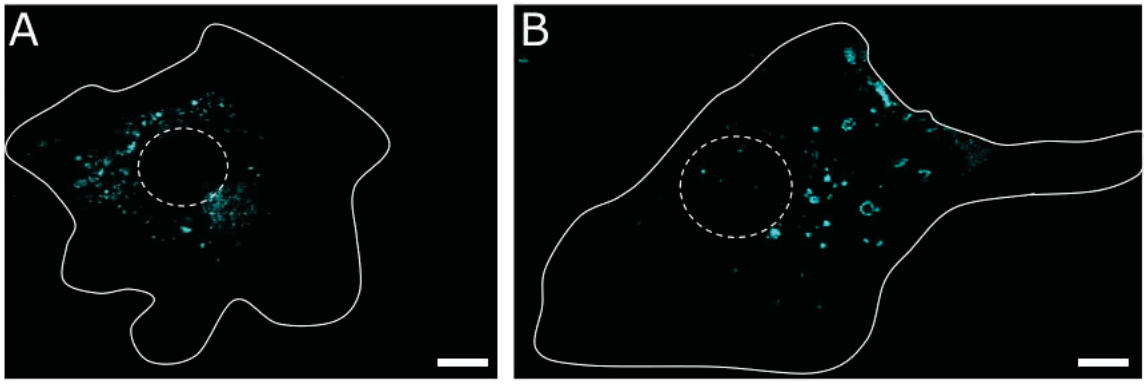

Figure 27. LYs (Syt-VII-CFP-positive compartments) re-locate in the proximity of the PM upon TBHQ treatment. COS-7 cell transfected with Syt-VII-CFP (light blue channel). 24 hours after transfection the cells were (A) untreated or (B) treated with TBHQ for 3 hours. Cell boundaries are shown in white, cell nuclei are marked with dotted circles. Scale bar is 5 μm. Images were at 37°C, 5% CO_2.

In addition, in Figure 28 a COS-7 transfected with Syt-VII and stained with Lysotracker and Fluo5F upon TBHQ treatment is shown. Fusion processes of LYs with LEs can be again visualized by the overlap of the red with the green signals and the concomitant enlargement of such compartments. Furthermore, due to the lysosomal size increase, Syt-VII can be visualized as a ring-like structure, thereby

identifying the lysosomal membrane (square sections in Figure 28). In the same image, the arrow indicates a group of LYs localized at the very proximity of the PM.

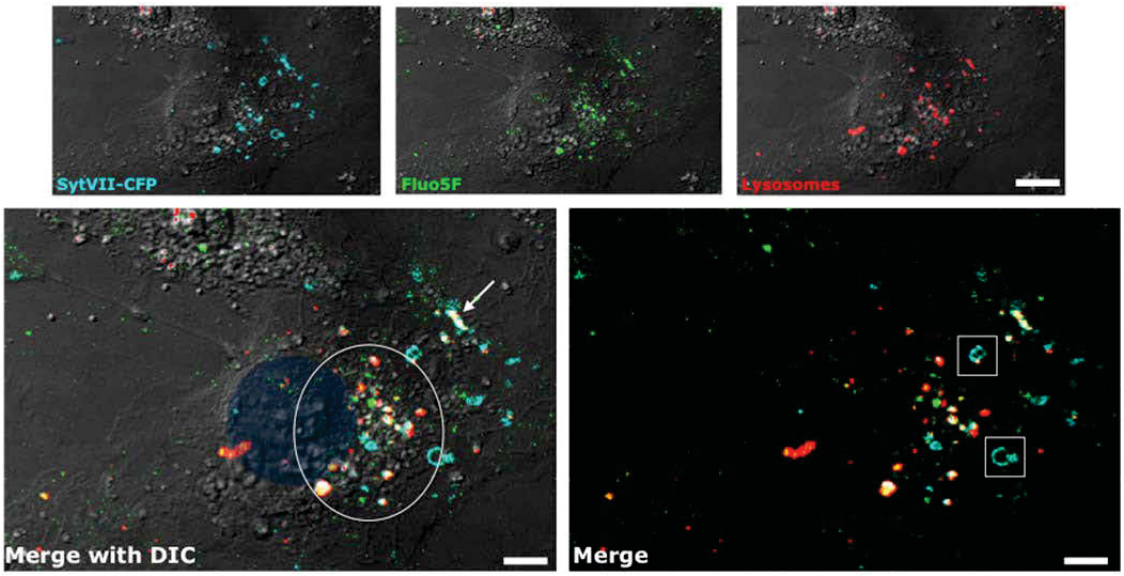

Figure 28. Upon TBHQ treatment, LYs increase their size and migrate to the PM. COS-7 cell transfected with Syt-VII-CFP (light blue channel) and stained with 3 μM Fluo5F (green channel) and Lysotracker (red channel). 24 hours after transfection the cells were treated with TBHQ for 3 hours. The circle indicates the MTOC region where the LEs/LYs fusion events occur; the arrow indicates LYs docked at the PM; squares in the merged image visualize the typical ring-like structures of enlarged LYs. Scale bar is 5 μm. Images were collected at 37°C, 5% CO_2.

Furthermore, treatment of COS-7 with TBHQ for 3 hours, 48 hours after transfection with Gag-EGFP, resulted in an enhanced release of VLPs (Figure 29A), while knocking-down of the Syt-VII gene with siRNAs resulted in a decreased release (Figure 29C).

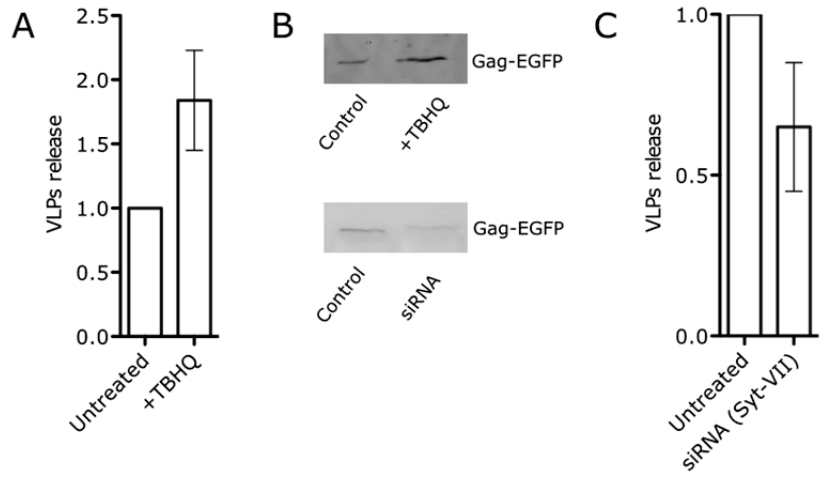

Figure 29. TBHQ treatment enhances release of VLPs, while Syt-VII siRNA diminishes it. (A) Quantification of VLPs release from COS-7 cells 48 hours after transfection with Gag-EGFP and treated or not for 3 hours with TBHQ. Error bars represent standard deviations of 3 independent replicates. (B) Western blot of purified VLPs from untreated (control) and TBHQ treated (+TBHQ) COS-7 cells, visualized after staining with an anti-p24 antibody.

3.1.7 Summary and conclusion

This section described how Gag is distributed in the intracellular environment revealing a similar pattern in the two different cell types analyzed (i.e. HeLa and COS-7 cells). Gag is found at the PM, in a dot-like form in the perinuclear area, and can be also observed in a diffuse distribution in the cytosol (Figure 13, Figure 16 and Figure 21). It was shown that the intracellular dots are membrane-delimited compartments (i.e. vesicles) that belong to the endo-lysosomal system (Figure 19), enriched in intralumenal calcium and containing VLPs (Figure 17). Analysis of Gag's intracellular localization in dependence of time in COS-7 cells (Figure 22) revealed that Gag can reach its endo-lysosomal localization in the perinuclear area very soon after its synthesis (considering the timing of blue-to-red switch of the FastFT, within the first 25 minutes), and the amount of Gag in this form as well its presence at the PM increase with time.

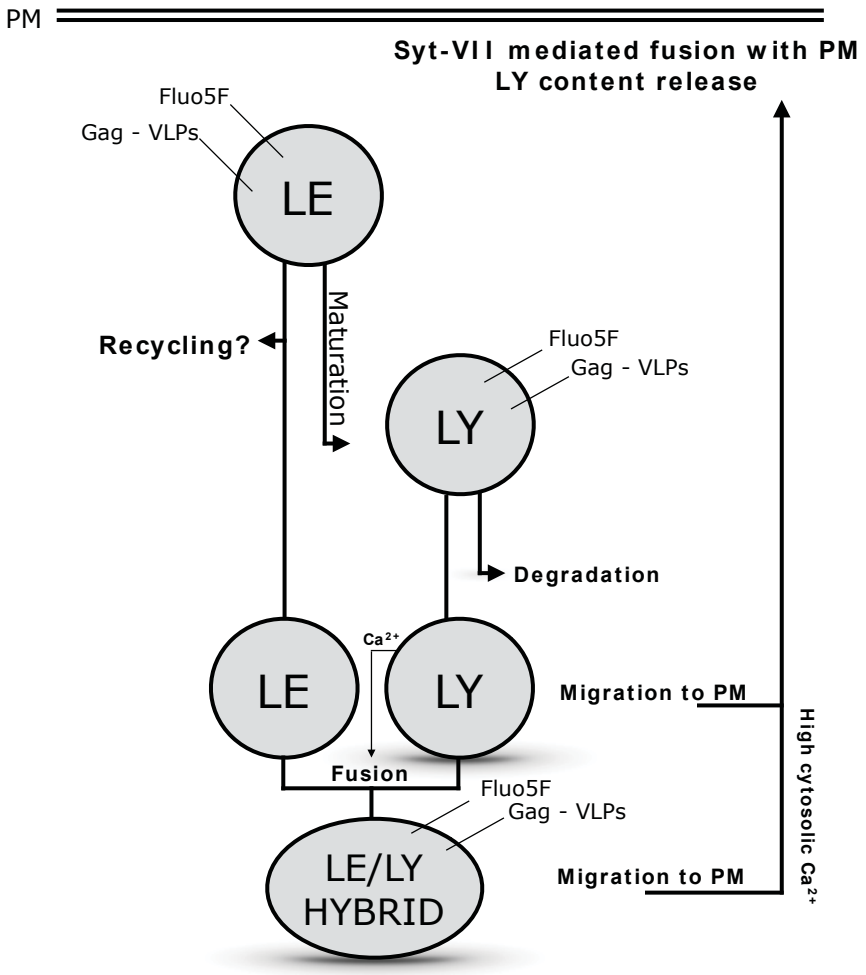

Figure 30. Schematic representation of the possible fates of the endo-lysosomal entrapped VLPs. Late endosomes (LEs) and lysosomes (LYs) that contain VLPs undergo different destinies (e.g. maturation and degradation, recycling). Upon release of calcium from LYs, LEs/LYs might fuse and LYs-exocytosis occurs, allowing extracellular release of VLPs contained in such compartment.

Calcium depletion from the lysosomal lumen resulted in an enhanced release of VLPs in COS-7 (Figure 29A) and in an unexpected release of VLPs in non-permissive HeLa cells (Figure 20), while Syt-VII knockdown resulted in a decreased release (Figure 29C). These observations can be converted into a model for the possible fates of the endo-lysosomal entrapped VLPs, reported in Figure 30: release of calcium from the lysosomal lumen, a process which physiologically takes place in response to specific stimuli [121], induces fusion between LEs and LYs and, due to the increase of the cytosolic calcium level, exocytosis of LYs from the PM in a Syt-VII mediated manner. Considering that VLPs are effectively contained in vesicles of the endo-lysosomal system, the model presented here suggests that LEs/LYs con-

tent mixing and LYs fusion with the PM might represent a rescue mechanism of endo-lysosomal localized VLPs that were initially destined to degradation by the cellular machinery. In Table 2, the results and their respective interpretations presented in the sections 3.1.4 and 3.1.6, that allowed the identification of the suggested model (Figure 30), are summarized.

Experimental approach	Expected biochemical/ biological consequence	Experimental observation	Figures showing the result	Interpretation and conclusion	Physiological context
Staining with Lysotracker and Fluo5F	-Staining with Lysotracker targets highly acidic compartments (e.g. LYs) -Staining with Fluo5F interests highly calcium containing compartments (e.g. ER, mitochondria, LEs, LYs)	Lysotracker and Fluo5F stain intracellular vesicles mostly localized in the perinuclear area. Sometimes the two stainings co-localize in the same vesicle	Fig. 18,19	-Lysotracker exclusively stains LYs, due to their highly acidic pH -Fluo5F is able to stain both LYs and LEs, since both are have a high calcium content	While the pH of LYs is different from that of LEs, the intralumenal calcium content of these compartments is much similar. For these reasons, Fluo5F can mark indistinguishably LEs and LYs, while Lysotracker is specific for LYs only
Electron microscopy of Gag-transfected cells treated with Fluo5F	—	Gag is assembled as VLPs in Fluo5F positive compartments (i.e. LYs and LEs)	Fig. 17	VLPs are either assembled directly into LEs/LYs, like in macrophages, or most probably endocytosed from the PM while the budding process is still occurring	Re-endocytosis of VLPs that are assembling at the PM might represent a cellular mechanism to decrease viral production
TBHQ treatment on HeLa	-Lysosomal-calcium leakage/exit of calcium from LYs -Increased cytosolic calcium	-Enlargement of Fluo5F positive compartments -Partially PM localization of LEs/ LYs	Fig. 20	Increased intracellular calcium concentration induces release of VLPs from HeLa despite the high expression of Tetherin. This suggests the presence of an alternative mechanism for VLPs release, which does not involve the mere pinching off of the VLPs from the PM	Increased intracellular calcium concentration can trigger fusion of LEs with LYs and LYs exocytosis
		VLPs release			
TBHQ treatment on COS-7	-Lysosomal-calcium leakage/exit of calcium from LYs -Increased cytosolic calcium	-Enlargement of LEs and LYs -Fusion between LEs and LYs	Fig. 25	Calcium exit from LYs trigger fusion and content mixing (VLPs) between LEs and LYs	Release of calcium from the lumen of LYs is a highly regulated mechanism, which involves the binding of NAADP to the TPC proteins on the lysosomal membrane. This process represents the activation of a specific intracellular signalling, which might physiologically take place in all cell types
		Partially PM localization of LEs/ LYs	Fig. 26,27,28	LYs de-localize from the perinuclear area and migrate to the PM in response to the elevated calcium	
		Enhanced VLPs release	Fig. 29	Elevated cytosolic calcium triggers LEs/LYs content mixing (VLPs) and LYs exocytosis	
Syt-VII knock-down	Inhibited Syt-VII production	Reduced VLPs release	Fig. 29	VLPs-entrapping LYs can not fuse anymore with the PM, releasing their content in the extracellular space	Syt-VII usually mediates fusion of LYs with the PM in response to increased cellular calcium concentrations

Table 2. Summary of the results and conclusion from the sections 3.1.4 and 3.1.6. In green are highlighted the results concerning the characterization of the organelles involved in the suggested mechanism (see Figure 30). In blue and orange are highlighted the results related to TBHQ treatment and the Syt-VII knockdown, respectively.

3.1.8 DISCUSSION: intracellular routes of Gag and release of VLPs via calcium-mediated fusion between LEs/LYs and LYs exocytosis

3.1.8.1 Gag's intracellular routes to VLPs release: one mechanism for all cell-types?

HIV-1 Gag, as other retroviral Gag proteins, is an N-myristylated membrane-bound polyprotein, necessary and sufficient for production and release of VLPs. After its synthesis in the free ribosomes in the cytosol, Gag traffics through the cell and reaches the site of particle production. Possible destinations of Gag have been suggested to include not only the PM, but also some membrane-limited intracellular compartments (e.g. LE/MVBs) [2,23]. However, the routes followed by Gag from its synthesis to the site of viral assembly still have to be completely characterized. Clearly, assembly at the PM may ensure efficient virus release and dissemination. On the other hand, the fact that the different viral components have to travel through the extremely compartmentalized cytoplasmic space to target the PM may represent an obstacle for a successful viral production. Free Gag and Gag assembled as VLPs, or in form of immature virions, have been observed in intracellular compartments enriched in late-endosomal markers [2,23,30]. Furthermore, in previous study, Gag was shown first diffusely distributed in the cytosol, accumulates in perinuclear cluster, pass transiently through a MVB-like compartment, and then travel to the PM. Sequential passage of Gag through these temporal intermediates was confirmed by live cell imaging [2]. These observations suggested that Gag might be targeted also to endosomal membranes for assembly and budding into the lumen of LE/MVBs and subsequently exit the cell via an exosome release pathway. Furthermore, Gag's use of proteins belonging to the ESCRT machinery, which facilitates budding of vesicles into the endosomal lumen, has been exhaustive demonstrated [124,125].

Nevertheless, perturbing LE/MVBs trafficking was shown to affect neither Gag association with the PM nor virus release. Moreover, in a study on HeLa cells, with the help of TIRFM to monitor the dynamics of single HIV-1 assembly events at the PM, it was shown that the Gag population that effectively participates on HIV-1 production and budding is recruited directly from the cytosol and is of non-endosomal

origin, whereas those Gag assemblies that are not destined to be released as cell-free virus are associated with LE markers and appeared to have been internalized via endocytosis [126]. Such controversial observations appear to further confuse the already unclear understanding of Gag's trafficking and assembly processes. However, it has to be mentioned, that many of the studies that until now have focused on the understanding of Gag's trafficking attempted to address this issue using non-authentic Gag derivatives, codon-optimized for higher expression in mammalian cells, and tagged with fluorescent proteins exhibiting slow maturation kinetics and non-physiological tissue culture cell lines (e.g. HeLa, COS, and HEK-293T) [6]. Such experimental set-up (in particular concerning the use of the mentioned cell lines), on the other hand, allows easy transfection procedures and is particularly suitable for confocal microscopy. Not surprisingly, the use of different cell types (physiological and non-physiological) and different Gag expression systems in some cases led to contradictory results [6]. Nevertheless, many previous works on Gag trafficking and VLPs assembly conducted on HeLa, COS and HEK-293T cells have demonstrated the validity and the relevance of such cell lines as models for the study of the cell-biology of Gag and other HIV-1 proteins [1,2,23,103,127]. Furthermore, the direct visualization of genetically unmodified HIV-1 proteins still remains elusive [103]. Only the recent development of fluorescent intracellular single domain nanobodies (i.e. chromobodies), the use of which was not applied in this study, offers a general approach for dynamic detection and visualization of virtually any natural and genetically unmodified factor in living cells [103,128].

HIV-1 assembly site(s) in physiologically relevant cell types like macrophages and T-cells have also produced contradicting observations: although HIV-1 assembly and release in T-cells is now generally accepted as being PM-associated, in a recent study it was shown that LE/MVBs compartments in both T-cells and macrophages can support productive HIV-1 assembly; specifically, a MVB-targeted Gag mutant was released efficiently in these two cell types [23]. In macrophages it was shown that a significant proportion of HIV-1 assembly took place in intracellular compartments with LE/MVBs markers [18], which in turn were shown to be present in the membranes of the released viruses. Interestingly, such intracellular compartments, marked with LE/MVBs proteins, are connected to the PM via micro-channels with a diameter of ca. 20 nm and therefore are actually deep invaginations of the macrophage PM [129]. It seems to be difficult to find a common mechanism for Gag's trafficking in different cell types. Nevertheless, taking together the already men-

tioned observations and considering the results from previous studies, Gag's localization and release in physiologically relevant cell can be summarized as follows: Gag is primarily localized at the PM at steady state in T-cells [17]. In these cells, Gag is targeted to the PM with no prior interaction with MVBs. Subsequently, specific Gag's interactions recruit the ESCRT machinery to the PM. On the contrary, in macrophages and DCs, multivesicular late endosome-derived compartments are the sites for Gag localization and particle production. In some cases, a regulated exocytosis of the virus located in LE/MVBs takes place [6,62].

In conclusion, Gag's routes to VLPs assembly and release are different for different cell-types. Gag targeting to PM and VLPs assembly (upon transfection or viral infection) involve, in different cell-lines, trafficking through specific host-cell compartment and the association to diverse host-cell structures.

3.1.8.2 VLPs in intracellular compartments probably originate from the PM

In this work, the distribution of Gag in the intracellular environment in two different cell types (e.g. HeLa and COS-7 cells) was studied. 24 hours after transfection, Gag was found in three different localization patterns: I) at the PM, II) in a dots-form in the perinuclear area, and III) in a diffuse state in the cytosol (Figure 13, Figure 16 and Figure 21). Live cell confocal microscopy was applied to study the timing of intracellular Gag localization in COS-7 cells transfected with Gag tagged with FTs, that change their fluorescence from blue to red over time (Figure 22). These fluorophores allow identifying the intracellular localization of Gag populations that are present at different time points after Gag's synthesis. For example, the maximum fluorescence emission of the blue form of Gag-FastFT is reached 0.25 hour (see Table 1 in Material and Methods section) after protein synthesis and subsequently loses its fluorescence intensity, while the red form turns up. Therefore, the blue signal visualized by this fluorophore identifies Gag proteins that are at most 15 minutes "old". For the blue form of the MediumFT, the maximum fluorescence emission is reached after 1.2 hour. Both red forms of the two fluorophores are maintaining their fluorescence intensities for longer time, allowing the identification of Gag populations that are present at least since 7.1 and 3.9 hours after synthesis, for the FastFT and the MediumFT, respectively.

COS-7 cells transfected with Gag-FastFT (Figure 22A) showed a blue Gag population mostly enriched in dots in the perinuclear area and rarely localized at the PM, while the red form was found to be equally distributed in dots in the perinuclear region, homogeneously distributed in the cytosol and near to- or associated to the PM. Cells transfected with Gag-MediumFT (Figure 22B) mostly resembled the Gag-FastFT transfected cells with the exception of the higher amount of red population of perinuclear dots. These results are summarized in Figure 31.

A

Fluorophore	Amount of Gag in intracellular dots	Amount of Gag at the PM
FastFT Blue form (0.25 hour post synthesis)	Low	Very low
FastFT Red form (7.1 hours post synthesis)	High	High
MediumFT Blue form (1.2 hour post synthesis)	High	Low
MediumFT Red form (3.9 hours post synthesis)	High	Very high

B

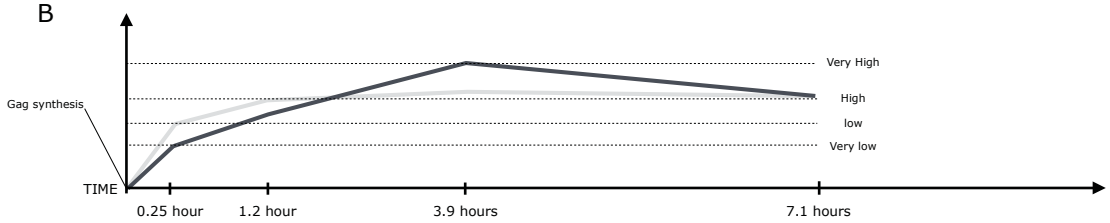

Figure 31. Gag's presence at both the PM and in intracellular dots increases with time, reaching equilibrium. Summary of the results shown in fig. 22. (A) Approximate amount of Gag at the PM or in the dots-form at different time points. The quantity of Gag at these sites is arbitrary indicated as "very low", "low", "high" and "very high". (B) On the basis of such classification, the amount of Gag at the PM (dark grey) and in intracellular dots (light grey) are depicted in function of the time after Gag's synthesis.

In particular, it can be noted that I) presence of Gag at the PM increases with time after protein synthesis and II) the earliest intracellular localization observed (blue form of Gag-FastFT) is the dot-like distribution in the perinuclear area, suggesting that Gag might be immediately targeted to intracellular compartments after synthesis. However, Gag has been observed to bind membrane within 5–10 minutes post-synthesis [37]. Specifically, it has been shown that Gag reaches the PM already 7

minutes after its synthesis, and can complete a budding within 20 minutes (see schematic representation in Figure 32).

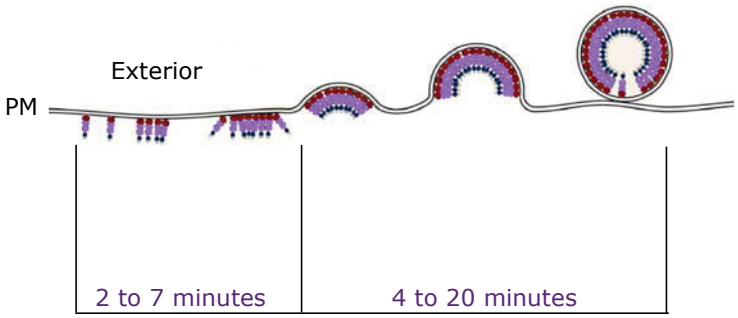

Figure 32. Schematic representation of the sequential steps in the assembly of HIV-1 at the PM. Gag assembly at the PM is shown divided in different assembly steps. In purple are indicated the times of the relative steps according to **[37]**.

Hence, identification of virus assembly sites must account for the events that occur within this narrow window of time. Therefore, taking into account that the peak of maximum excitation for the blue form of the FasFT is reached 15 minutes after protein folding (0.25 hour), the blue dots of Gag-FastFT found in the perinuclear area can not be exclusively considered as the first localization site reached by Gag in COS-7 cells.

In conclusion, most probably, also accordingly to previous observations [130], the population of Gag observed in such intracellular and perinuclear compartments is the result of a re-endocytosis of budding VLPs at the PM. The presence of completely or partially formed VLPs in intracellular compartments was confirmed by electron microscopy on HeLa cells (Figure 17) and on COS-7 (data not shown).

3.1.8.3 Characterization of VLPs-containing intracellular compartments

The intracellular distribution of Gag in perinuclear dots mostly resembles the localization of LEs and LYs. Specifically, with confocal and electron microscopy, it was shown that the intracellular dots are actually membrane-delimited compartments that belong to the endo-lysosomal system (Figure 19). In addition, they co-localized with either the lysosomal marker Lysotracker, or with the late endosomal protein Rab7 (i.e. Rab7-GFP), which was co-transfected together with Gag-CFP. Fur-

thermore, such Gag-containing intracellular vesicles move on the filaments of the microtubular system following trajectories advancing from the MTOC to the PM (Figure 23 and Figure 24). The host cell cytoskeleton, comprised of microtubules and actin filaments, has long been suggested of being involved in targeting viral proteins to particle assembly sites [131,132]. Microtubules mediate long-range cargo transport and therefore are potentially suited for delivering viral proteins to assembly sites like the PM, where actin filaments, which transport cargo across short distances, may play a role in virus budding and release. Recent findings suggest that inhibition of actin and tubulin remodeling in T-cells disrupts Gag and Env enrichment at polarized raft-like membrane domains, Env incorporation into viruses, Gag release, viral infectivity, and cell-cell spread [6,133]. Conversely, Gag expression has been reported to remodel the actin cytoskeleton at the site of particle budding [17]. Two types of microtubule-based proteins with opposing motor activities exist; kinesins facilitate cargo transport toward the cell periphery, whereas dyneins promote cargo transport toward the perinuclear MTOC. Previous observations showed that the kinesin superfamily member KIF4 binds HIV-1 Gag [134], promotes Gag trafficking to the PM, and perturbing KIF4 function reportedly diminishes virus production.

In this work, the use of the low-affinity calcium fluorophore Fluo5F on Gag-transfected cells resulted in the staining of intracellular compartments, which mostly co-localized with Gag-CFP (Figure 16). In fact, endosomal and lysosomal vesicles share the common characteristic to posses a high intralumenal calcium concentration, estimated to be between 500 and 600 μM [102,108,135]. LEs and LYs have also a high intralumenal concentration of other ions (e.g. chlorine and potassium) (see schematic representation in Figure 33) [136]. The presence of Fluo5F in other calcium-containing compartments (e.g. ER, mitochondria) could be excluded by confocal microscopy (Figure 18). Within the endo-lysosomal system, calcium is important for maintaining normal trafficking, recycling and vesicular fusion events [109]. Specifically concerning LYs, which are organelles primarily involved in degradation and recycling processes, the remarkable presence of intralumenal calcium is related to the role of LYs in many cellular processes, not directly referred to the degradation processes of cellular components, but rather e.g. to calcium-mediated fusion between intracellular membranes and amplification of calcium signaling [109]. For instance, LYs are the target of one of the most potent intracellular calcium releasing second messengers: NAADP. This molecule directly interacts with lysosomal TPC proteins and causes release of calcium from the lysosomal lumen,

contributing to the regulation of crucial cellular signaling processes important for diverse cellular functions (e.g. vesicles exocytosis, fertilization, cell death [115,121,137]). Endocytosis of calcium has been shown to contribute for only ca. 50 μM to the total content of lysosomal calcium [138]. To reach higher intralumenal calcium concentrations, LYs use the activity of both a calcium transporter (i.e. a SERCA-ATPase), and a calcium/proton channel, which exploits the proton gradient across the LY membrane to import calcium ions into the lumen (Figure 20B).

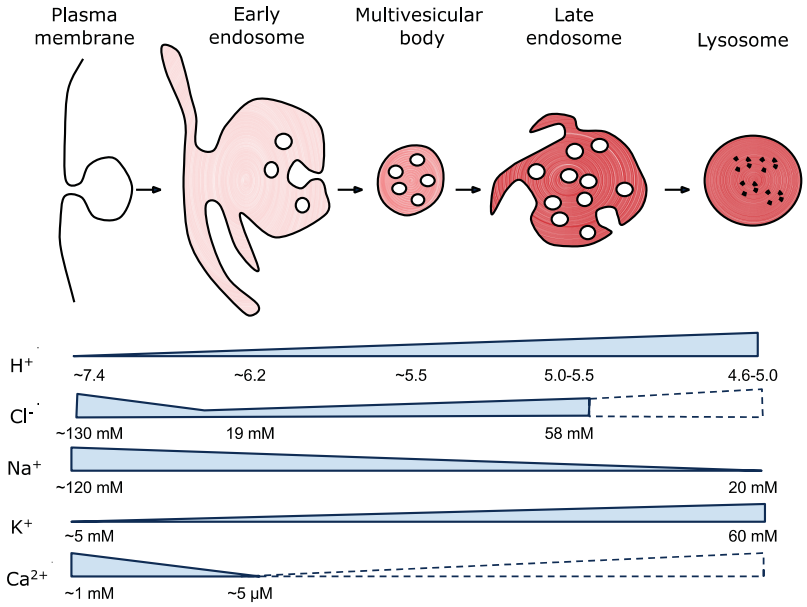

Figure 33. Schematic representation of the concentrations of ions inside the vesicles of the endo-lysosomal system during their maturation process. Concentrations of different intralumenal ions are reported in correspondence to the maturation state of the vesicles. Adapted from [136].

The passage of endocytosed material and membrane-bound proteins through the endocytic pathway of mammalian cells to LYs occurs via early endosomes (EEs) and LEs [102,138]. Direct fusion events between LEs and LYs represent *de facto* the main cargo-delivery mechanism to LYs. This content mixing can be a result of kiss-and-run events [112] and/or direct fusion between the two organelles [113]. The luminal ionic composition of vesicles of the endocytic machinery is of considerable importance both in the trafficking of endocytosed ligands and in the membrane fusion processes. In mammalian cells, the organelles of the late endosomal pathway have been shown to interact with each other and to be in dynamic equilibrium both *in vivo* and *in vitro* [102,108,139]. LYs are also involved in a secretory pathway

known as lysosomal exocytosis, which requires two sequential steps: I) recruitment of LY to the close proximity of the PM, II) fusion of the pool of pre-docked LYs with the PM in response to calcium elevation [113]. Lysosomal exocytosis plays a major role in several physiological processes such as cellular immune response, bone resorption, and PM repair. Calcium-dependent lysosomal exocytosis was considered to be limited to specialized secretory cells; however, recent studies indicate that this process occurs many different cell types [102,113,137].

HIV-1 VLPs (or HIV-1 virions) are found in LEs and LYs in almost all cell types and at different time points after infection or transfection with a Gag plasmid. Given the degradative nature of the LYs, the presence of VLPs in such compartments has been considered by previous studies not relevant for virus release, but rather connected to unproductive pathways, that more probably are destined to degradation [126]. Nevertheless, increased intracellular calcium concentration, similar to those reached during activation of calcium release upon specific physiological stimuli, was shown to enhance VLPs release in different cell types. It therefore was postulated that LE/MVBs-entrapped VLPs might be released due to a calcium-mediated vesicles/vesicles and vesicles/PM fusion process.

3.1.8.4 PLCβ as host factor needed for efficient Gag targeting to PM

The sources of intracellular calcium that are needed for the functionality of the various signaling pathways and for calcium-mediated mechanisms, as in the case of LYs-exocytosis, might be different (e.g. ER, mitochondria, LEs/LYs). Generally, viruses have evolved the capability to hijack the host cell machinery in order to achieve their own purposes. Calcium, in particular, was identified to play a role in almost every step in virus replication cycles [140]. Specifically in the case of HIV-1, the Tat protein has been shown to up-regulate viral gene expression and replication [141,142], allowing HIV-1 to replicate in inactivated T-cells [140]. Furthermore, Tat-induced disregulation of intracellular calcium levels leads to neurotoxicity and contributes to HIV-related dementia and further stimulates production of the pro-inflammation cytokine TNF-α, which plays a major role in progression to AIDS.

One of the most relevant calcium stores in the cell is the ER. Activation of calcium release from this organelle usually is triggered by specific signals [109,143]. The signal cascade starts typically at a PM, upon activation of GPCR or TKR. The direct

consequence of this reaction, which represents the activation of specific cell signaling response, is the activation of a PLC enzyme, which results in the generation of two second messengers: inositol 1,4,5-trisphosphate ($InsP_3$), a universal calcium-mobilizing second messenger, and diacylglycerol (DAG), an activator of several types of effector proteins, including protein kinase C (PKC) isoforms [106]. PLC enzymes comprise a group of proteins mostly localized in the cytosol, that upon stimulation migrate to the PM and cleave the polar head group from PIP_2 [104]. These second messengers provide a common link between highly specific receptors for hormones, neurotransmitters, antigens, components of the extracellular matrix and growth factors to downstream, intracellular targets. Thirteen PLC isozymes have been identified and categorized into six classes, the β (1–4), γ (1,2), δ (1,3,4), ε, ζ, and η (1,2) types, on the basis of structure and regulatory activation mechanisms. Previous study has shown that activation of PLC is requested for proper Gag localization at the PM and VLPs release and that chelation of intracellular calcium resulted in a decreased release of VLPs [1]. In the mentioned previous study, the general PLC inhibitor U73122, which is able to block the activity of both PLCγ and PLCβ (see schematic representation in Figure 34), was applied.

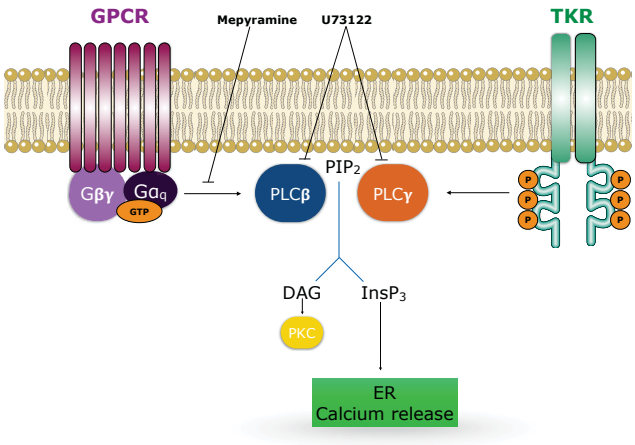

Figure 34. Inhibition of PLCβ and PLCγ upon Mepyramine and U73122 treatment. G-protein coupled receptor (GPCR) and tyrosine-kinase receptor (TKR) are shown. Stimulation of GPCR and TKR trigger activation of PLCβ and γ, respectively. Both PLCs induce formation of inositol 1,4,5-trisphosphate ($InsP_3$) and diacylglycerol (DAG), and result in the activation of downstream signaling (e.g. PKC and ER calcium release).

Use of U73122 on Gag-transfected cells resulted in an altered intracellular localization of Gag (i.e. in aggregates in the cell interior) and in a dramatically reduced

release of VLPs. In this work, it was shown how an analog intracellular mislocalization of Gag was obtained blocking the activity of only the G_q-protein-stimulated PLCβ, with the use of the G_q-protein inhibitor Mepyramine (see schematic representation in Figure 34). These data suggest that a proper function of PLCβ signaling pathway is essential for Gag targeting to PM and VLPs release. The reasons for this still have to be determined.

3.1.8.5 LY/LE-entrapped VLPs can be rescued from lysosomal degradation through release from the host cell via calcium-mediated fusion between LYs and LEs and lysosomal exocytosis

Restoration of PM integrity after injury is essential for the survival of animal cells. As already mentioned, in many cell types LYs can fuse with the PM in response to an increase in the concentration of cytosolic calcium. Such LYs provide the extra lipid bilayer for PM wound repair [111]. Calcium-regulated exocytosis of LYs and direct fusion with the PM require the activity of the ubiquitously expressed calcium-sensor, member of the synaptotagmin family, Syt-VII. When calcium is released from the lumen of LYs (e.g. upon stimulation via NAADP), a LEs/LYs fusion process might occur. Much of such fusions occur in the perinuclear region of the cell, since LEs and LYs are mostly concentrated near the MTOC. In common with other fusion events in the secretory and endocytic pathways, the fusion of LEs with LYs requires the presence of *N*-ethylmaleimide sensitive factor (NSF), soluble NSF attachment proteins (SNAPs) and a small GTPase of the Rab family, probably Rab7 [102]. Similar to other fusion events, the fusion process between LYs and LEs can be divided into three fundamental steps: I) tethering, II) formation of a *trans*-SNARE complex that bridges across the two organelles and III) membrane fusion [112,113] (see schematic representation in Figure 35).

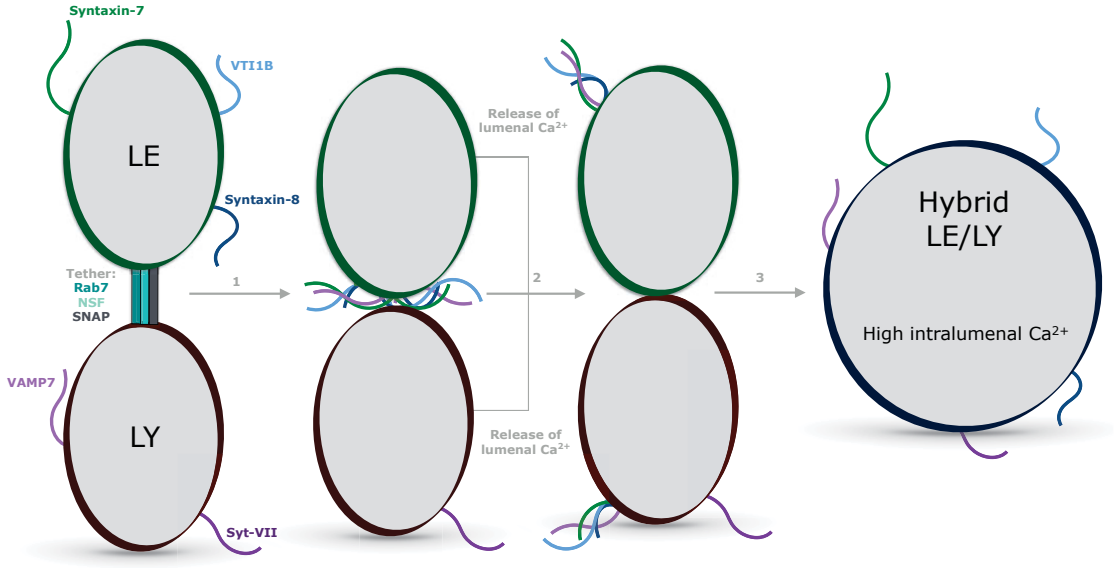

Figure 35. Schematic representation of calcium-mediated LEs/LYs fusion process. 1) Rab7 first tethers LEs and LYs. The fusion of LEs with LYs requires N-ethylmaleimide sensitive factor (NSF) and soluble NSF attachment proteins (SNAPs). 2) trans-SNARE (SNAP receptor) complex formation requires syntaxin-7, VTI1B (Vps10 tail interactor-1B) and syntaxin-8 3) The release of lumenal calcium leads to phospholipid bilayer fusion. Adapted from [102].

The formation of *trans*-SNARE complex requires the participation of four components: the SNARE proteins syntaxin-7, VTI1B–, syntaxin-8 and the R-SNARE vesicle-associated membrane protein-7 (VAMP7). These proteins are subsequently all required for the effective LYs/LEs fusion event. Finally, LE/LY-Hybrid organelle fusion with the PM is regulated by the calcium sensor Syt-VII, which seems to be required for both temporal and geometric control of the fusion pore that is formed at the cell surface [114,123]. Staining of LYs and LEs in Gag-transfected COS-7 cells upon treatment with TBHQ (Figure 25), an inhibitor of calcium re-uptake in LYs, revealed that such organelles I) increase in size and in intralumenal concentration of calcium, which might be the consequence of LEs/LYs content mixing, II) show different co-localization patterns (typical pre- ad post-fusion states of LYs and LEs as already described elsewhere [139]), and III) often contain Gag, as shown by the presence of a CFP signal inside such compartments. Western blot analysis of VLPs release after TBHQ treatment revealed an enhancement in particle release compared to the untreated control (Figure 29), while siRNA knock down of Syt-VII, which regulates the last step of lysosomal exocytosis, resulted in a diminished re-

lease of VLPs from the host cells. The model reported in Figure 36 shows how LEs/LYs-entrapped VLPs might be rescued from lysosomal degradation if a calcium-mediated fusion between LEs and LYs occurs. PM-repair and more generally activation of lysosomal calcium release via NAADP are processes common to all cell types that may be activated in many different situations, upon a *plethora* of different stimuli [111-113,123]. Specifically in the case of HIV-1 infection, the constant budding of the virus from the PM might injure the lipid bilayer causing activation of PM-repair mechanisms that involve fusion between endo-lysosomal vesicles that eventually contain VLPs or HIV-1 virions.

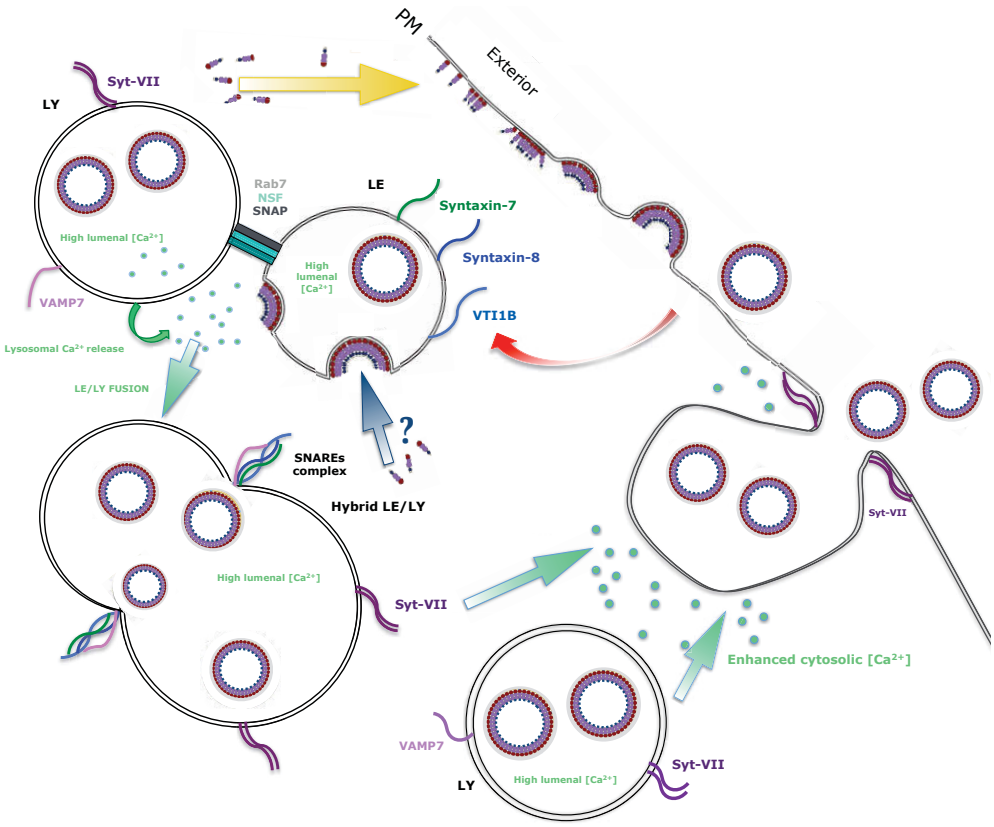

Figure 36. Schematic representation of calcium-mediated LEs/LYs fusion process. Gag migrates at the PM, where assembly takes place (yellow arrow). In some cases, VLPs that are pinching off from the PM can be re-endocytosed and directed into vesicles of the endo-lysosomal system (red arrow). In some cell types (e.g. macrophages, DCs) Gag can bud directly into the lumen of LEs/MVBs; if this is also the case for other cell-types, remains to be determined (blue arrow). Activation of intracellular stimuli may trigger release of calcium from LYs and subsequent docking and fusion between LEs and LYs (green arrows) that may contain re-endocytosed VLPs. General increase in cytosolic calcium (e.g. due to LYs calcium release, ER calcium release) may lead to the exocytosis of LYs and hybrid organelles (green arrows). Proteins of the endo-lysosomal system involved in this mechanism are shown. Calcium ions are indicated as green dots.

3.2 HIV-VLPs phagocytosis in macrophages via αEnv-PS-LUVs

The aim of the second part of the work was to develop a nanotechnological system able to induce phagocytosis of Gag/Env-VLPs (in the following part called HIV-VLPs) in macrophages. An immunoliposomal system based on PS-containing liposomes (αEnv-PS-LUVs) is here presented. Confocal microscopy imaging on live macrophages, electron microscopy and flow cytometry were applied to study the validity of the system (see schematic representation in Figure 37).

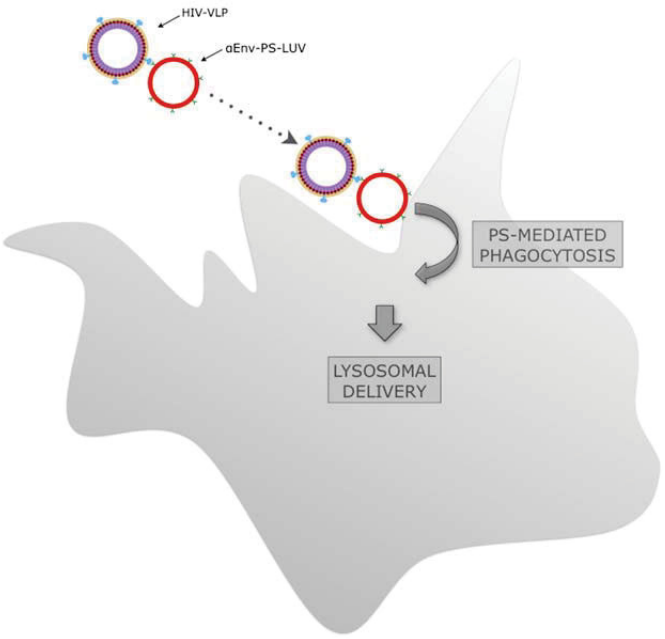

Figure 37. Schematic representation of HIV-VLPs phagocytosed in the presence of αEnv-PS-LUVs. αEnv-PS-LUVs bind to HIV-VLPs, are phagocytosed into macrophages (shown in grey) via a PS-dependent mechanism and finally delivered to lysosomes.

3.2.1 αEnv-PS-LUVs trigger efficient phagocytosis of HIV-VLPs by macrophages

The efficiency of phagocytosis of HIV-VLPs by macrophages in different conditions was investigated. To this end, HIV-VLPs were produced co-expressing in HEK-293T cells HIV-1 Gag-EGFP and Env, as already described elsewhere [47,144]. Purified HIV-VLPs were loaded on an SDS-Page and blotted to verify the presence of both Gag and Env proteins (Figure 38). As already mentioned before, it is known that the polyprotein Gag precursor, even in the absence of other viral proteins and the viral genome, is sufficient to drive the formation and the release of non-infectious VLPs when expressed in an appropriate cell line. Furthermore, the presence of EGFP at the C-terminus of Gag, even if it decreases the yield of produced VLPs, affects neither the assembly nor the release process of VLPs [145] and represents a simple tracking strategy to monitor and quantify the presence of VLPs (e.g. when internalized by macrophages).

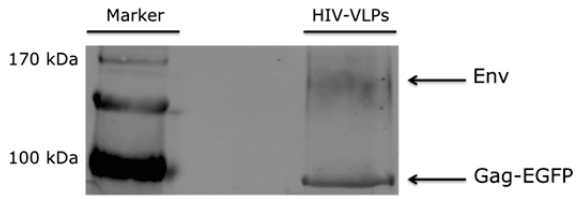

Figure 38. Western blot of purified HIV-VLPs. HIV-VLPs were separated by electrophoresis through 10% SDS-polyacrylamide gels and electroblotted onto nitrocellulose membrane. The presence of Gag-EGFP and Env in the HIV-VLPs was determined with mouse anti-p24 (CA domain) and goat anti-gp120-biotin conjugated antibodies.

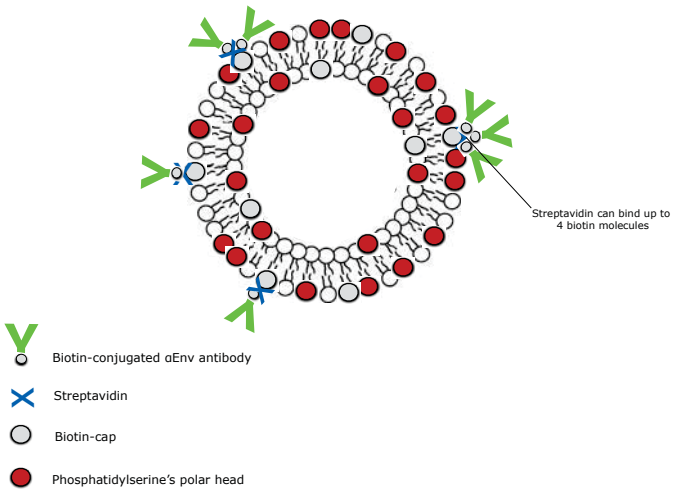

Figure 39. Schematic representation of a αEnv-PS-LUV. The LUVs included in their bilayer phosphatidylserine (Phosphatidylserine polar head shown in red), biotinylated lipids (Biotin-cap of the lipid shown in grey) used to decorate the LUVs with biotin-conjugated αEnv-Abs (shown in green) via streptavidin (shown in blue) binding, and thus obtained PS-containing LUVs bound to αEnv-Abs.

100 nm radius PS-containing LUVs were produced. These LUVs included in their bilayer a biotinylated lipid used to decorate the LUVs with biotin-conjugated αEnv-Abs via streptavidin binding, and thus obtaining PS-containing LUVs bound to αEnv-Abs (αEnv-PS-LUVs) (see schematic representation in Figure 39). It was expected that the αEnv-PS-LUVs would effectively recognize and bind the Env proteins on the HIV-VLPs and, due to the presence of PS, would be phagocytosed by macrophages together with the bound HIV-VLPs (see schematic representation in Figure 37). For internalization measurements, HIV-VLPs were first mixed either with I) αEnv-PS-LUVs, II) αEnv-LUVs (without PS), III) αEnv-Abs (i.e. antibodies without liposomes) or IV) PS-LUVs (i.e. PS-containing liposomes without antibodies). In the following step, they were administrated to macrophages and incubated by gentle agitation for 1 hour at 37°C. The intracellular fluorescence signal of phagocytosed HIV-VLPs was quantified with flow cytometry. In the live cell confocal fluorescence microscopy images reported in Figure 40 it is possible to visualize the internalization of HIV-VLPs/αEnv-PS-LUVs complexes in macrophages.

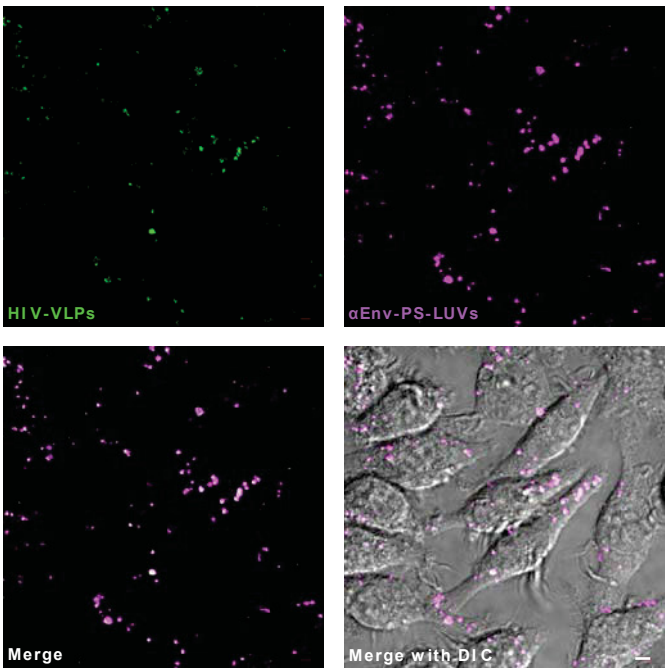

Figure 40. HIV-VLPs are most efficiently internalized in the presence of αEnv-PS-LUVs. Live cell confocal microscopy images of living macrophages incubated with HIV-VLPs together with αEnv-PS-LUVs. The focal plane was positioned approximately at the middle of cell height. HIV-VLPs (green channel) co-localize with αEnv-PS-LUVs (magenta channel) in the intracellular environment. Scale bar is 2 μm. Images were collected at 37°C.

The fluorescence images merged with the DIC channel in confocal-geometry give additional information about the localization of the HIV-VLPs/αEnv-PS-LUVs complexes into the cells: visualization of part of the nuclear membrane, observable in the DIC channel, suggests that the internalized complexes are not localized on the cell surface, but rather in the inner part of the cells. Figure 41 further confirms that incorporation of PS into αEnv-LUVs resulted in the most effective phagocytosis of HIV-VLPs into macrophages. αEnv-LUVs or αEnv-Abs alone caused less internalization of HIV-VLPs and the lowest internalization values were observed when viral particles were incubated by themselves or in the presence PS-LUVs without antibodies. It appears clear that the internalization of the HIV-VLP/immunoliposome complex is determined primarily by the presence of the antibody-decorated liposomes (PS-LUVs in particular), since HIV-VLPs are not internalized by themselves. For this reason, the attention was next focused on the mechanism of liposome uptake by macrophages. Furthermore, since the presence of antibodies does not increase the uptake efficiency induced by LUVs or PS-LUVs (data not shown), it was decided to use PS-LUVs and LUVs without αEnv-Abs for the following test.

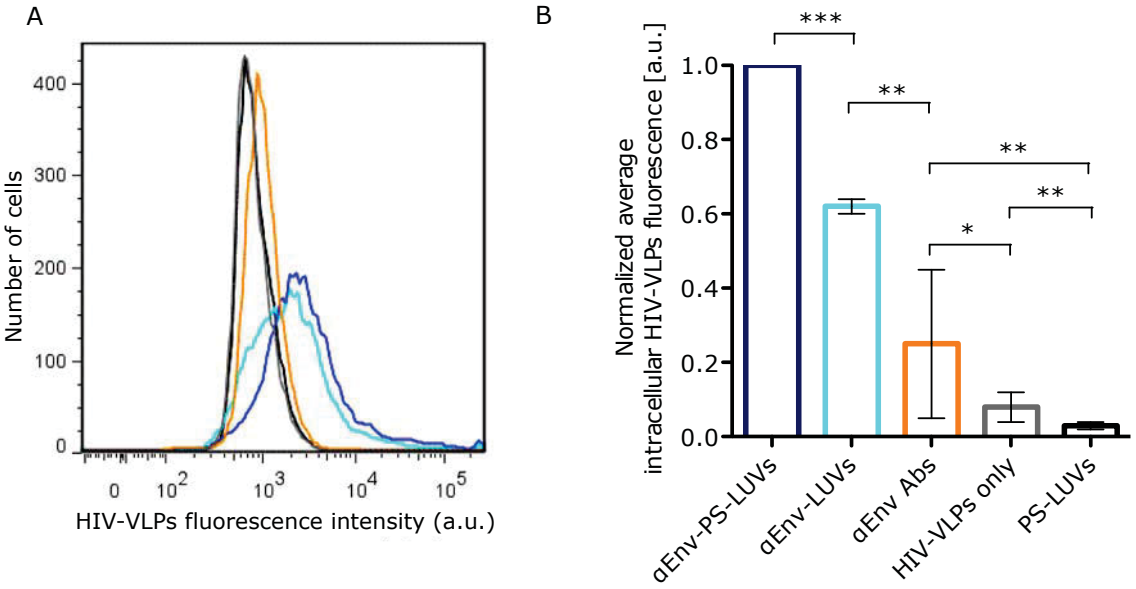

Figure 41. Flow cytometry analysis show how αEnv-PS-LUVs trigger efficient internalization of HIV-VLPs. Macrophages were incubated for 1 hour at 37°C in gentle agitation with HIV-VLPs exclusively or together with αEnv-PS-LUVs, αEnv-LUVs, αEnv antibodies, or with PS-LUVs. (A) Representative flow cytometry histograms for all the examined samples. Each curve refers to a single independent measurement for one treatment condition and represents the number of cells as a function of the fluorescence intensity of internalized HIV-VLPs. The color-code used for the histograms is the same used in panel B. (B) The fluorescence signal of internalized HIV-VLPs was quantified with flow cytometry and normalized to the value measured for the αEnv-PS-LUVs sample, averaged over a 10000-cell population. Error bars represent standard deviations of 6 independent replicates. The average fluorescence signal of αEnv-PS-LUV samples was normalized to 100%. "*" corresponds to datasets that cannot be statistically distinguished (i.e. two-sample t-test probability $p>0.05$). "**" and "***" denote significantly different datasets with two-sample t-test associated probability $p<0.05$ and $p<0.01$, respectively.

The internalization efficiency of the liposomes under inhibition of actin polymerization, which is known to be required for phagocytosis [146], was measured. Cytochalasin D is a potent inhibitor of actin polymerization and a highly toxic compound for animal cells. To avoid an excessive toxicity of Cytochalasin D on macrophages, a concentration 10-fold lower than that usually needed to have 90% inhibition of phagocytosis was used [147]. Notwithstanding the very low amount of Cytochalasin D, these cells showed already ~30% less internalization of PS-LUVs (Figure 42A). Inhibition of dynamin-dependent processes (e.g. endocytosis) with the dynamin inhibitor Dynasore did not affect the internalization of the PS-LUVs (Figure 42B).

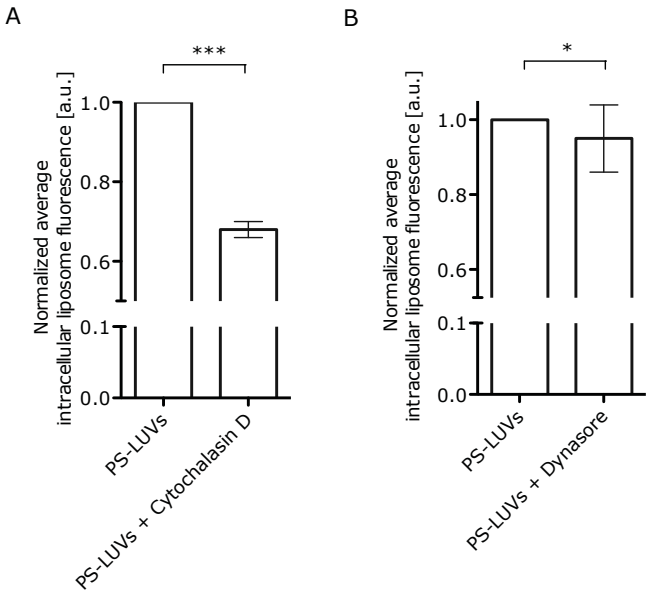

Figure 42. Inhibition of actin polymerization, and not of dynamin, decreases uptake of PS-LUVs. Macrophages were incubated for 1 hour at 37°C with PS-LUVs or LUVs in the presence or in the absence of (A) 1 μM Cytochalasin D or of (B) 1 μM Dynasore. The fluorescence signal of internalized fluorescently labeled liposomes was quantified with flow cytometry and normalized to the value measured for the PS-LUVs sample, averaged over a 10000-cell population. Error bars represent standard deviations of 3 independent replicates. The respective value of αEnv-PS-LUVs was normalized to 100% in each experiment. "*" corresponds to datasets that cannot be statistically distinguished (i.e. two-sample t-test probability $p>0.05$). "***" denotes significantly different datasets with two-sample t-test associated probability $p<0.05$ and $p<0.01$, respectively.

These results suggest that actin-mediated internalization pathways might play a prevalent role in the uptake of liposomes. Engulfment of external bodies through the phagocytosis process requires not only the polymerization of actin, but also the activation of a specific intracellular signaling [148]. Concerning phagocytosis of apoptotic cells, it was shown that an acute and sustained calcium flux from the ER into the cytosol of phagocytic cells represents a direct and specific consequence of the recognition of apoptotic bodies by macrophages [148]. In order to show whether the treatment of macrophages with the αEnv-PS-LUVs (but also with PS-LUVs - not shown) is able to trigger this specific intracellular response, the cells were loaded with the membrane-permeable calcium fluorophore Fura2, a fluorescent dye which binds to free intracellular calcium, and treated either with I) αEnv-PS-LUVs, II) αEnv-LUVs, or III) pretreated with Thapsigargin (Thaps) and then with αEnv-PS-LUVs. Fura2 fluorescence can show an acute increase or decrease in its fluorescence intensity reflecting a change in the cytosolic calcium concentration. In Figure

43 the intracellular Fura2 fluorescence was visualized in a pseudo color mode and monitored live at an epifluorescence microscope. The addition of αEnv-PS-LUVs to macrophages resulted in a strong and fast increase of the intracellular Fura2 fluorescence, while the addition of αEnv-LUVs did not. Furthermore, pre-treatment with Thaps, which causes the depletion of calcium from ER, and subsequent addition of αEnv-PS-LUVs did not result in an increase of the Fura2 fluorescence, suggesting that the intracellular source of calcium needed upon binding between macrophages and αEnv-PS-LUVs is the ER.

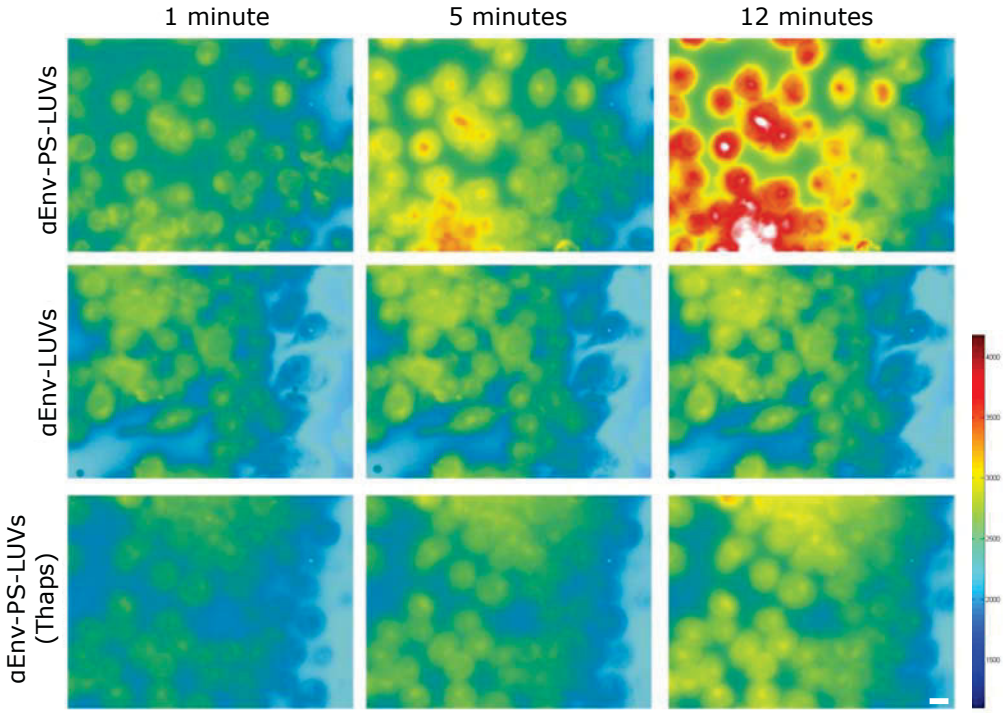

Figure 43. Addition of αEnv-PS-LUVs to macrophages results in release of calcium from endoplasmic reticulum. Macrophages were incubated for 30 minutes at 37°C with Fura2-AM in calcium-free medium, then washed with PBS and, when indicated, treated with 2 μM Thapsigargin (Thaps) for 1 hour at 37°C. Addition of either αEnv-PS-LUVs or αEnv-LUVs was performed live at an epifluorescence microscope. The pseudo color scale was the same for all the samples. Scale bar is 8 μm.

3.2.2 Internalization of PS-LUVs is specific for macrophages

It was shown that cell type plays a prominent role in intracellular uptake of nanoparticles with different physical characteristics [149,150]. In the context of our studies, it would be important to show that immunoliposomes are preferentially internalized by macrophages, rather than unspecifically interacting with the PM of also other cell types. To this end, the internalization of PS-LUVs in macrophages was compared with the internalization in epithelial non-phagocytic cells (e.g. Madin-Darby canine kidney cells (MDCK)). The results shown in Figure 44 indicate that the uptake efficiency of PS- LUVs in this cell type is much lower (ca. 60% decrease) than in macrophages. This result is in agreement with previous studies showing increased internalization of negatively charged particles specifically to phagocytic cells [150].

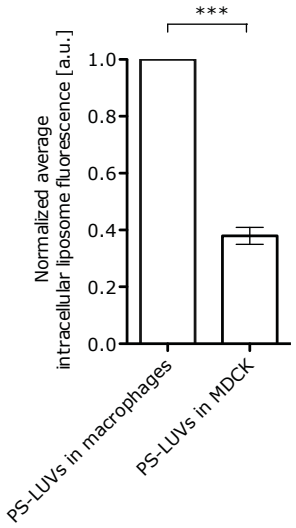

Figure 44. Comparison of internalization efficiencies of PS-LUVs or LUVs in macrophages and MDCK cells. Macrophages or MDCK cells were incubated with PS-LUVs or LUVs for 1 hour at 37°C. The fluorescence signal of internalized fluorescently labeled liposomes was quantified with FACS and normalized to the value measured for the PS-LUVs sample in macrophages, averaged over a 10000-cell population. Error bars represent standard deviations of 3 independent replicates. The respective value of αEnv-PS-LUVs was set to 100% in each experiment. "***" denotes significantly different datasets with two-sample t-test (probability $p<0.01$).

3.2.3 The amount of PS in LUVs influences phagocytosis efficiency of both LUVs and HIV-VLPs

Next, the effect of increasing PS concentration on the HIV-VLPs internalization efficiency was investigated. The internalization of liposomes and HIV-VLPs is strongly correlated to the amount of PS incorporated in the liposome bilayer. As shown in Figure 45, this dependence is more pronounced for the liposomes (almost 10 fold increase in the internalization of αEnv-50mol%PS-LUVs compared to αEnv-0mol%PS-LUVs) than for the HIV-VLPs. The highest internalization was observed for the HIV-VLPs sample incubated with αEnv-50mol%PS-LUVs. A lower but non-negligible uptake of HIV-VLPs incubated with αEnv-0mol%PS-LUVs was also observed, in agreement with the results reported in Figure 41. According to the results shown in Figure 45B, already 30mol% PS concentration in the αEnv-PS-LUVs is sufficient to induce significant HIV-VLPs internalization. Therefore, in all further experiments 30mol% PS concentration was used. In order to investigate the possible presence of multiple populations in our samples (e.g. cells that massively internalized liposomes coexisting with cells showing negligible internalization), the forward scatter/fluorescence intensity dot-plot was analyzed. These 2-d histograms shown in Figure 45C-D report the cell distribution of two different samples of macrophages as a function of cell-size and fluorescence intensity of internalized αEnv-30mol%PS-LUVs. The dot-plots of untreated cells and cells incubated with αEnv-30mol%PS-LUVs are shown in Figure 45C, respectively. First, the background fluorescence of macrophages in an untreated sample was identified (population 1 -P1, rectangle in Figure 45C), i.e. the cells that did not internalize any liposome. Only few outliers were observed, and they were not included. The plot in Figure 45D refers to cells that were incubated with αEnv-30mol%PS-LUVs. The vast majority of these cells can be grouped together as a single population (population 2 -P2, rectangle in Figure 45D). Only a negligible amount of the total cell population shows a fluorescence signal compatible with the parameters identified in Figure 45C for P1. In other words, almost all of the macrophages incubated with αEnv-30mol%PS-LUVs do internalize liposomes and the data here presented do not support the presence of heterogeneity in the examined samples.

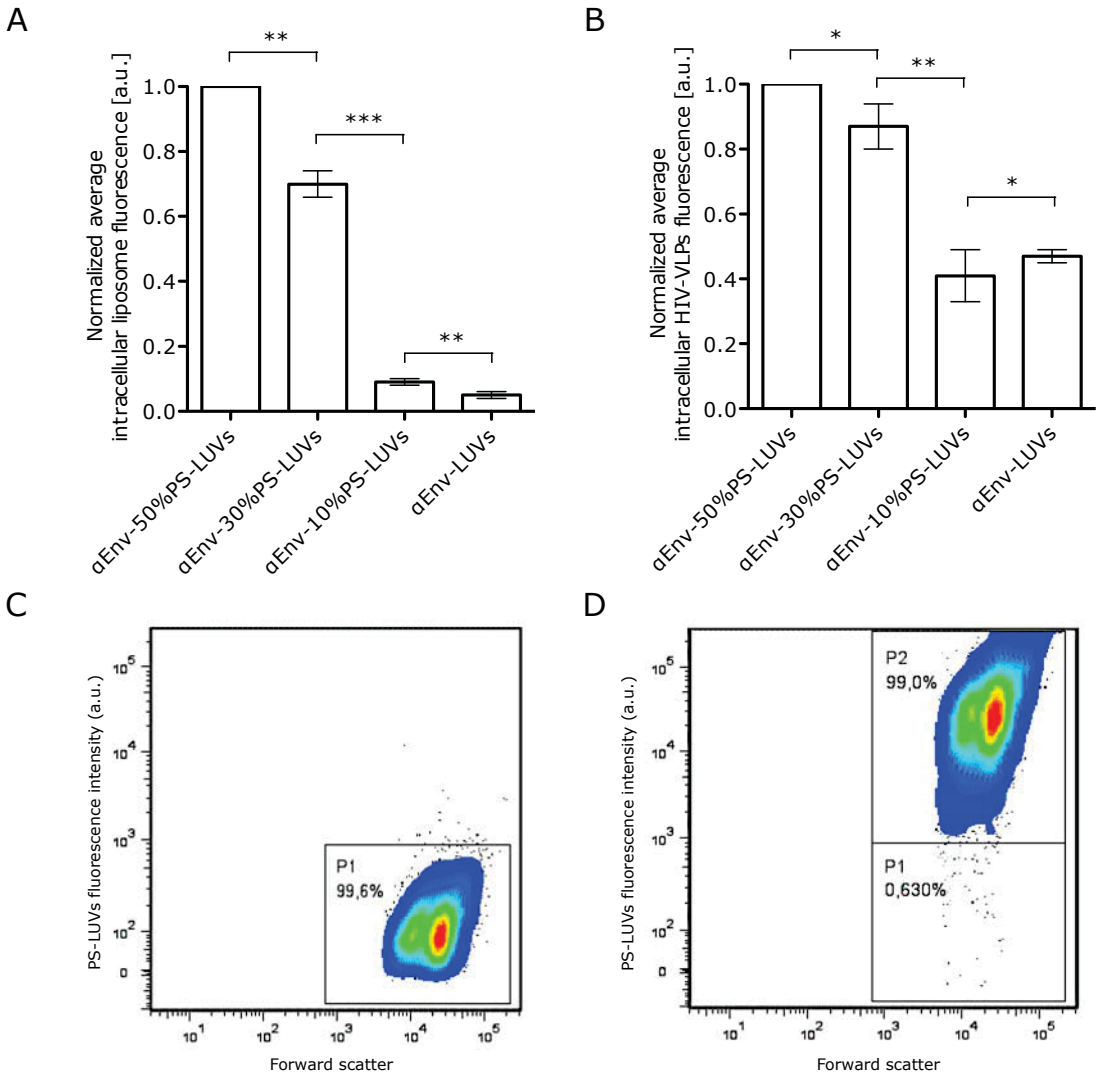

Figure 45. Internalization efficiency of LUVs and HIV-VLPs is related to PS concentration. Macrophages were incubated for 1 hour at 37°C in gentle agitation with αEnv-PS-LUVs containing different PS mol% concentration and HIV-VLPs. The fluorescence signal of internalized fluorescently labeled liposomes (A) and HIV-VLPs (B) were quantified with flow cytometry and normalized to the value measured for αEnv-50mol%PS-LUVs, averaged over a 10000-cell population. Error bars represent standard deviations of 3 independent replicates. "*" corresponds to datasets that cannot be statistically distinguished (i.e. two-sample t-test probability $p>0.05$). "**" and "***" denote significantly different datasets with two-sample t-test associated probability $p<0.05$ and $p<0.01$, respectively. (C-D) Representative dot-plots of two independent flow cytometry-measurements of 10000-cells populations. The two dot-plots report the distribution of the cells in relationship to their size (forward scatter) and fluorescence intensity of internalized αEnv-30mol%PS-LUVs. Panel C shows untreated cells identified as population 1 (P1), and panel D shows cells incubated with αEnv-30mol%PS-LUVs and identified as population 2 (P2). The previously determined P1 position in the graph is also shown in panel D. The cells distribution is reported as intensity profile of the number of cells (red= high, blue=low); outlier cells are indicated as single points.

3.2.4 αEnv-PS-LUVs deliver co-internalized HIV-VLPs to acidic compartments

Once the αEnv-PS-LUVs-mediated phagocytosis of HIV-VLPs has been triggered, it is of paramount importance that the internalized pathological agents are properly degraded. In order to investigate the exact intracellular fate of αEnv-PS-LUVs and HIV-VLPs, confocal microscopy imaging of live macrophages incubated with αEnv-PS-LUVs and HIV-VLPs and stained with a marker for acidic compartments was performed. The images in Figure 46A show that HIV-VLPs together with αEnv-PS-LUVs accumulate in lysosomes, while HIV-VLPs administrated alone to the macrophages (Figure 46B) do not localize therein. It is worth noting that, in the latter case, we observed a much lower internalization of HIV-VLPs, in line with the results shown in Figure 41. A statistical analysis of the intracellular localization of HIV-VLPs in 30 images of the three samples is shown in Figure 46C (see Material and Method section). This analysis revealed that more than 70% of the HIV-VLPs co-localize with LYs if they were together with αEnv-PS-LUVs. If the particles were administrated alone, the localization into LYs was estimated below ca. 14%. In the presence of αEnv-LUVs, the co-localization of HIV-VLPs into LYs was on average intermediate between the two above-mentioned cases. Also, although the αEnv-LUV samples were not statistically distinguishable from the αEnv-PS-LUV samples, they exhibited much larger sample-to-sample variation (see standard deviations in Figure 46C). In order to further characterize the intracellular localization of HIV-VLPs and immunoliposomes with high spatial resolution, a correlative fluorescence and electron microscopy imaging approach was used. Figure 47 shows that HIV-VLPs co-localize with αEnv-PS-LUVs in membrane-delimited intracellular compartments. These sub-cellular structures are vesicular in shape and well separated from the PM.

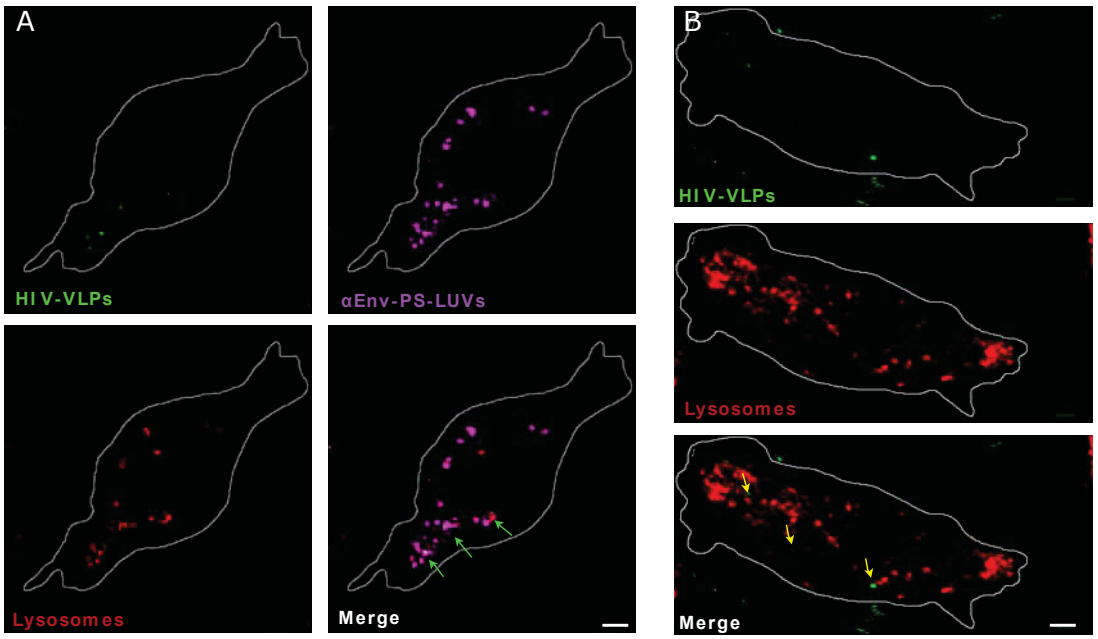

C

Co-localization between HIV-VLPs and LYs

Treatment	Average of HIV-VLPs co-localizing with LYs	SD	t-test probability
αEnv-PS-LUVs	72%	± 9	N/A
αEnv-LUVs	52%	± 32	0.09
w/o immunoliposomes	14%	± 12	<0.01

Figure 46. HIV-VLPs together with αEnv-PS-LUVs accumulate in LYs. Representative confocal images of living macrophages at 37°C stained with Lysotracker and treated with (A) HIV-VLPs together with the αEnv-PS-LUVs (green arrows indicate HIV-VLPs co-localized with αEnv-PS-LUVs into acidic compartments) or (B) HIV-VLPs alone for 1 hour at 37°C (yellow arrows indicate the HIV-VLPs outside acidic compartments). The fluorescence signals of internalized HIV-VLPs, αEnv-PS-LUVs and LYs marked with Lysotracker are shown. Cell boundaries are shown in white. White bars represent 2 μm. (C) Percentages of HIV-VLPs/LYs co-localization with or without co-administration of αEnv-PS-LUVs, or αEnv-LUVs. The co-localization was calculated as ratio between overlapping areas (i.e. pixels occupied both by HIV-VLPs and Lysotracker) and total pixel areas occupied by HIV-VLPs, expressed in percentage and averaged over ten different confocal micrographs. Standard deviation (SD) and two-sample t-test probability (comparison to αEnv-PS-LUV sample) are also shown.

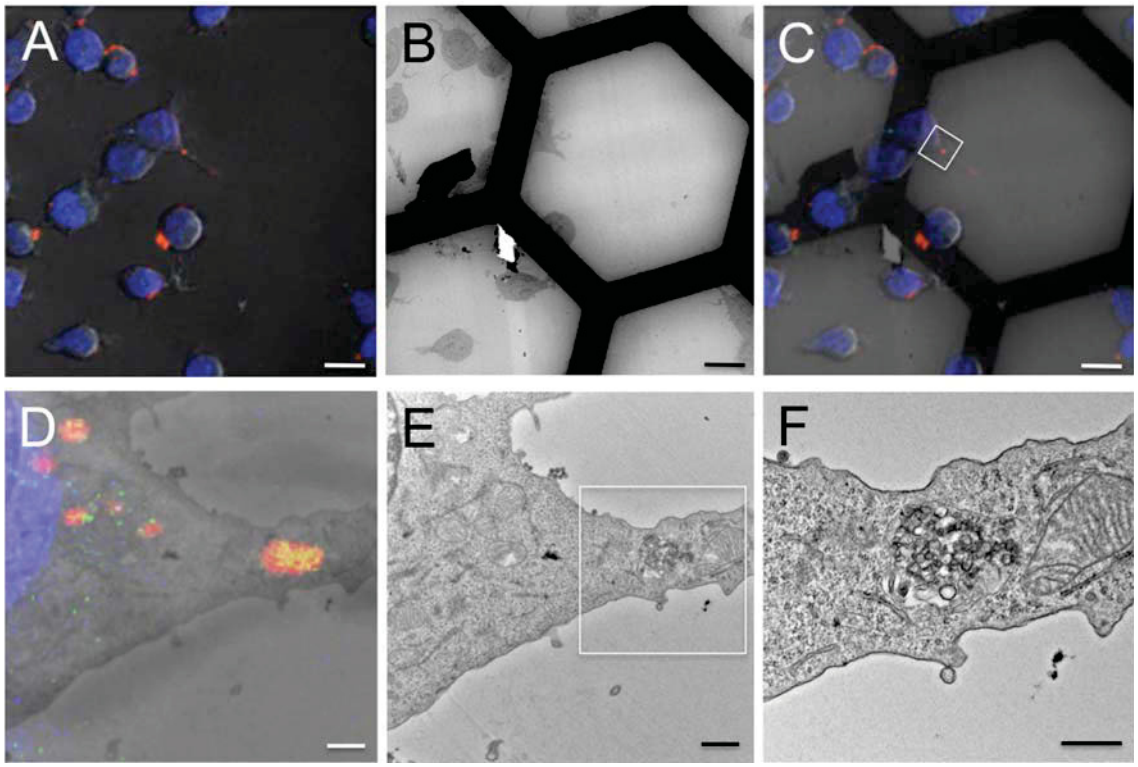

Figure 47. HIV-VLPs together with αEnv-PS-LUVs accumulate in phagosome-like compartments. Correlative fluorescence and electron microscopy. (A-E) HIV-VLPs (green) and αEnv-PS-LUVs (red) were visualized by confocal laser scanning microscopy and correspond to a membranous, phagosome-like structure imaged by transmission electron microscopy (F). (A) Fluorescence confocal image, (B, E, F) electron micrographs, (C, D) correlation of fluorescence images with electron micrograph by alignment of cellular surface structures. Indicated squares represent the area of magnification in the subsequent panel. Scale bars: 5 µm (A-C), 1 µm (D,E), 500 nm (F).

3.2.5 Treatment with HIV-VLPs and αEnv-PS-LUVs does not affect viability of macrophages

Finally, the effects of HIV-VLPs/αEnv-PS-LUVs treatment on the viability of macrophages was tested. The cells were treated with HIV-VLPs/αEnv-PS-LUVs or 10% dimethylsulfoxid (DMSO), and incubated for 1, 48 or 72 hours at 37°C. Subsequently, two different tests were performed in parallel. The results of the first test are shown in Figure 48A, which reports the values of responsiveness of the cells to the CellTiter-Blue test. This test measures the metabolic activity of the cells upon addition of the non- fluorescent dye resazurin. During the incubation period, cells

convert resazurin to the fluorescent resorufin product. The conversion of resazurin to fluorescent resorufin, measured at a plate-reader, is proportional to the number of metabolically active and viable cells. As shown in Figure 48A the viability of the cells treated with HIV-VLPs/αEnv-PS-LUVs is not affected. Moreover, after 72 hours the curves of treated and untreated cells both increase, indicating that the cells are actively dividing. As expected, the metabolic activity of the DMSO (positive control) treated cells decreases monotonously over the observation time.

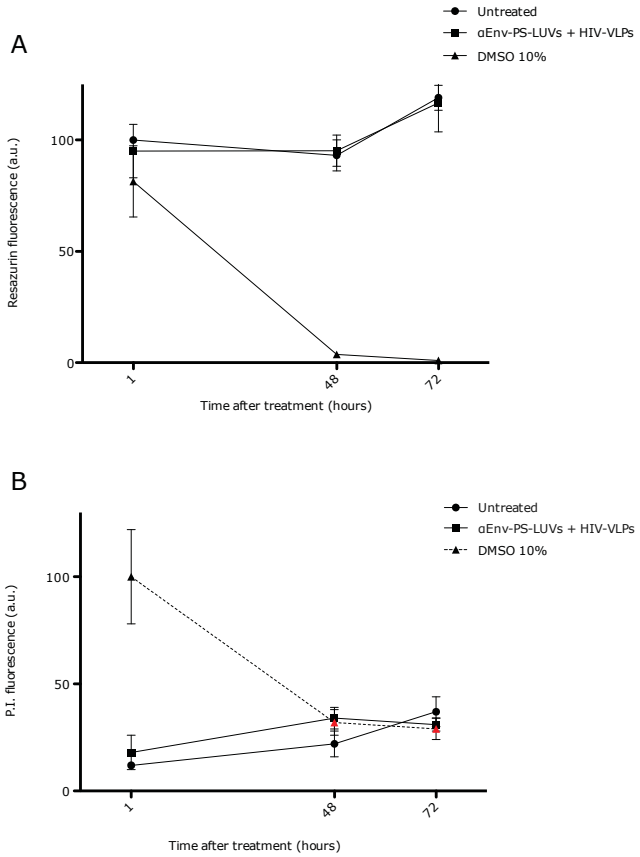

Figure 48. Treatment with HIV-VLPs and αEnv-PS-LUVs does not affect viability of macrophages. (A) Macrophages were plated in 96-well plates and incubated with HIV-VLPs/αEnv-PS-LUVs or 10%DMSO or with medium only, for the indicated times. The fluorescence signal of the converted resofurin product for each sample was quantified with a plate reader and normalized to the value measured for the "untreated cells 1 hour after treatment" sample. Error bars represent standard deviations of 24 independent replicates. (B) Macrophages were plated in 12-well plates and incubated with HIV-VLPs/αEnv-PS-LUVs or 10%DMSO or with medium only, for the indicated times. The fluorescence signal of propidium iodide for each sample was quantified with FACS analysis and normalized to the value measured for the "10% DMSO-treated cells 1 hour after treatment" sample. Error bars represent standard deviations of 3 independent replicates.

The second test performed was the propidium iodide (PI) test. PI is a fluorescent and intercalating agent, which shows an increase up to 30 fold of its fluorescence upon binding to nucleic acids. PI is membrane impermeable and generally excluded from viable cells. The fluorescence of PI was measured with FACS. As shown in Figure 48B, cells treated with HIV-VLPs/αEnv-PS-LUVs maintain low values of PI fluorescence over 72 hours after addition of the particles/liposomes. For the positive control, a strong decrease of membrane impermeability is observed in the first hour. Concerning the results of the DMSO control on a longer time range (see 48-hours and 72-hours points, marked in red), two aspects must be considered: first, treatment with 10% DMSO is known to produce almost 90% cell death after 1 hour treatment [151]. Second, the FACS measurements must be performed in PBS, which implicates that the dead cells detached and present in the culture medium were excluded from the FACS analysis. Therefore, the DMSO-treated cells after 48 and 72 hours, which show low level of PI fluorescence, most probably are representative only of the 10% of the survived cells after the first hour.

3.2.6 Summary and conclusion

The results shown in the previous section demonstrated the efficacy of αEnv-PS-LUVs in triggering efficient internalization of HIV-VLPs in macrophages, without affecting cell viability. The efficient internalization of HIV-VLPs into macrophages was shown to be primarily dependent by I) the presence of PS into the LUVs and II) the decoration of the LUVs with αEnv-Abs (Figure 41). The mechanism of internalization of the HIV-VLPs/immunoliposomes complex was identified as phagocytosis. In fact, inhibition experiments demonstrated the need of actin polymerization for successful internalization of HIV-VLPs in macrophages. Furthermore, the release of calcium from the ER in macrophages, which is necessary (and specific) for a successful cargo-phagocytosis [148], occurred exclusively after addition of PS-LUVs and was not observable after depletion of the ER-calcium stores (Figure 43). Increasing amount of PS in the immunoliposomes correlated with higher internalization of both liposomes and HIV-VLPs. Fluorescence confocal and electron microscopy of macrophages treated with HIV-VLPs and αEnv-PS-LUVs showed that HIV-VLPs are localized in membrane-delimited vesicles and that, specifically αEnv-PS-LUVs,

and not αEnv-LUVs, are able to deliver the viral particles to membrane-delimited phago-lysosomal compartments (see schematic representation in Figure 49).

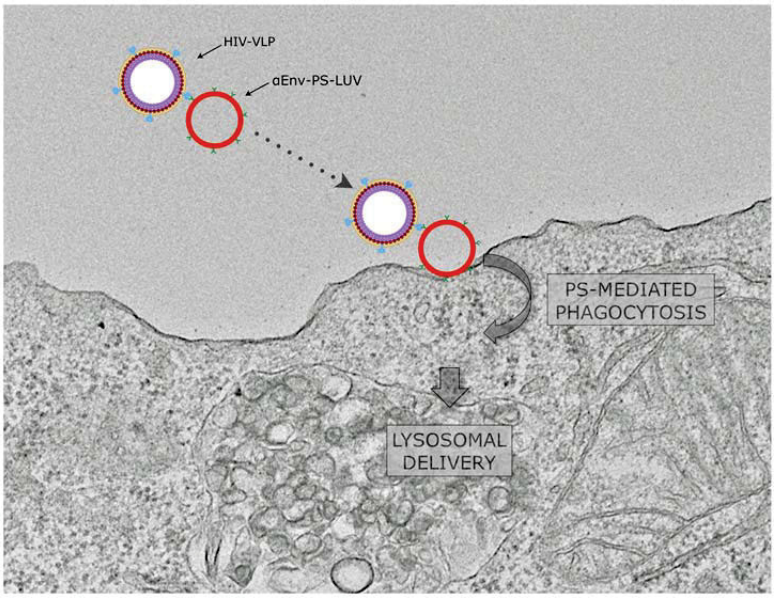

Figure 49. Representation of HIV-VLPs phagocytosed by a macrophage in the presence of αEnv-PS-LUVs. αEnv-PS-LUVs bind to HIV-VLPs, are phagocytosed into macrophages via a PS-dependent mechanism and finally delivered to lysosomes. The presence of internalized HIV-VLPs and αEnv-PS-LUVs can be evaluated by fluorescence: HIV-VLPs are made by Env and Gag-EGFP (shown in green in the cartoon) and αEnv-PS-LUVs contain Vybrant DiI (shown in red in the cartoon). On the background, an electron micrograph of a macrophage treated with HIV-VLPs together with αEnv-PS-LUVs (taken from Figure 41).

Now, at this point, it has to be highlighted that, even if the previously described mechanism for VLPs release from LYs (LYs exocytosis) might be shared also by macrophages, phagocytosis of HIV-VLPs and subsequent delivery to acidic compartments (i.e. LYs) via PS-immunoliposomes is expected to follow a very specific internalization pathway proper to the mechanism of clearance of apoptotic cells by macrophages. This process, initiated by PS recognition, is known to represent a highly degradative pathway, characterized by an immediate targeting of the cargo to phago-lysosomes that undergo a progressive acidification of the phagosomal lumen and acquisition of vacuolar H^+-ATPases [129,152].

3.2.7 DISCUSSION: internalization of HIV-VLPs into macrophages via αEnv-PS-LUVs-mediated phagocytosis

Macrophages are believed to play a potential active role in the fight of the immune system against HIV-1. However, as soon as these cells are infected by the virus, many of their effector functions are impaired. This represents one of the principal causes of the development of AIDS pathogenesis. Specifically, phagocytosis of opsonized viral particles is compromised in infected macrophages [66,67,153]. On the other hand, PS-dependent phagocytosis seems not to be affected by the presence of the virus [80]. Also, in those cases where phagocytosis of apoptotic cells seemed affected by HIV-1 infection, the molecular mechanisms involved are not related to specific PS-recognition [154-156]. In this study, efficient internalization of HIV-VLPs into macrophages via αEnv-PS-LUVs -mediated phagocytosis was demonstrated.

3.2.7.1 Phagocytosis of HIV-VLPs via αEnv-PS-LUVs in macrophages

The internalization of HIV-VLPs into macrophages via αEnv-PS-LUVs was highly efficient and much higher compared to the cases of incubation of HIV-VLPs with αEnv-LUVs, PS-LUVs or with antibodies alone. The intracellular localization (rather than simple binding to cell surface) of the HIV-VLPs/immunoliposomes complexes can be deduced by the data in Figure 40. As previously stated in the Results (section 3.2.1), the confocal plane was positioned approximately in the middle of the cell plane, therefore excluding detection of liposomes or VLPs bound to the PM (well above or below the focal plane). PS-dependent internalization (rather than simple membrane binding) was already confirmed in the same system (i.e. PS-liposomes in macrophages) [94]. These results are compatible with a model according to which HIV-VLP bind to liposomes through a specific antibody. Subsequently, PS-containing liposomes are phagocytosed due to the presence of PS, carrying the bound viral particles into the macrophage. In the absence of antibodies, PS-LUVs are efficiently internalized but cannot carry HIV-VLPs into the phagocyte (see e.g. Figure 41). Furthermore, the mere presence of αEnv-Abs bound to HIV-VLPs does not elicit phagocytosis by itself. This result is reasonable, since the antibody used here (goat αEnv IgG) should not be specifically recognized by mouse macrophages.

Therefore, this *in vitro* system mirrors in this respect the behavior of HIV-infected macrophages characterized by impaired antibody-dependent phagocytosis.

3.2.7.2 Influence of PS amount in LUVs phagocytosis efficiency of both LUVs and HIV-VLPs

The specific amount of PS strongly correlates with the internalization of liposomes: LUVs made with 0 or 10 mol% PS have a similar degree of internalization and both are internalized to a much lesser degree than LUVs with 30-50 mol% PS. Qualitatively, these results are compatible with previous studies [94]. The amount of PS needed for optimal internalization in our experiments is somewhat different from that reported by Geelen et al. [94], probably due to e.g. differences in the cell line used, specific lipid composition, and/or liposome size. PS-mediated internalization of the PS-LUVs must be ascribed to the previously characterized capability of PS-liposomes to activate a specific phagocytosis signal in macrophages [149]. The PM of viable cells is characterized by an asymmetric distribution of phospholipids across the bilayer, PS being mostly localized into the inner leaflet of the PM. Exposure of the anionic phospholipid PS in the outer leaflet represents one of the most dramatic changes on the surface of apoptotic cells [74,77], eventually leading to phagocytosis by macrophages *in vivo*.

The dependence of HIV-VLPs uptake on the presence of PS in liposomes is less straightforward compared to uptake of the mere PS-liposomes, since this lipid is not strictly needed for HIV-VLPs internalization. In fact, a non-negligible internalization of HIV-VLPs in the presence of immunoliposomes without PS was observed. Although these data do not provide a definitive explanation for this observation, one possibility could be that HIV-VLPs and αEnv-LUVs form large aggregates that are non-specifically internalized by macrophages. Such aggregates seem to be enriched in HIV-VLPs rather than lipids (see Figure 45A and 45B – noticeable internalization of HIV-VLPs compared to that of immunoliposomes in absence of PS). Furthermore, non-specific internalization of HIV-VLPs does not occur in the absence of immunoliposomes (Figure 41). Nevertheless, it must be emphasized that PS should be present in a rationally designed liposomal system for viral particle phagocytosis since I) the presence of at least 30 mol% PS dramatically increases internalization of HIV-VLPs and II) the presence of PS triggers an internalization pathway which is

specific and supposedly not impaired in HIV-infected macrophages.

3.2.7.3 αEnv-PS-LUVs internalization: mechanism and target specificity

Different receptors on the macrophage membrane are known to interact with ligands (e.g. PS) on the apoptotic cell surface, resulting in the association of dead cells to the macrophages, which represents the first step of phagocytosis [157]. The recruitment of specific receptors also triggers cytoskeletal changes in the phagocytic cell structure required for the engulfment of apoptotic cells. Here, it was shown that inhibition of actin polymerization, and not of dynamin, correlates with a strong decrease in PS-LUVs uptake, suggesting that the mechanism of PS-LUVs internalization is indeed phagocytosis. In the context of a therapeutic approach against HIV-1, it is of great importance to ensure that the pathological agent (i.e. virus/immunoliposome complexes) is specifically delivered to the appropriate cell types where they can be properly disposed of, without toxic effects for the target cells. First it was verified that treatment with HIV-VLPs and αEnv-PS-LUVs is not toxic for macrophages (see Figure 48). Then it was investigated how specifically PS-LUVs are taken up by macrophages, comparing the internalization of PS-LUVs in macrophages and Madin-Darby Canine Kidney cells (MDCK), here used as an example of non-phagocytosing cells (see Figure 44). The results presented in this work show that MDCK cells internalize a significantly lower amount of PS-LUVs compared to macrophages.

3.2.7.4 Intracellular fate of internalized HIV-VLPs

After phagocytosis, depending on different factors (e.g. the intrinsic nature of the cargo, the type of the target cell, the internalization pathway), the internalized material is delivered to specific intracellular compartments. This will eventually determine the fate of the acquired content [158]. Subcellular localization is extremely important in HIV-1 infection as well, as it influences also its ability to infect the host and other cells [159]. Indeed, HIV-1 particles found in membrane-proximal compartments with neutral pH in macrophages (e.g. viral containing compartments (VCCs) and endosomal-like structures) [129] are still infectious and represent the

so-called virus-reservoirs, known to be one of the major causes of viral persistence in the host [18,160]. VCCs, shown in Figure 50, are tubule-vesicular membranous webs that extend throughout the macrophage and are frequently connected to the extracellular space [129].

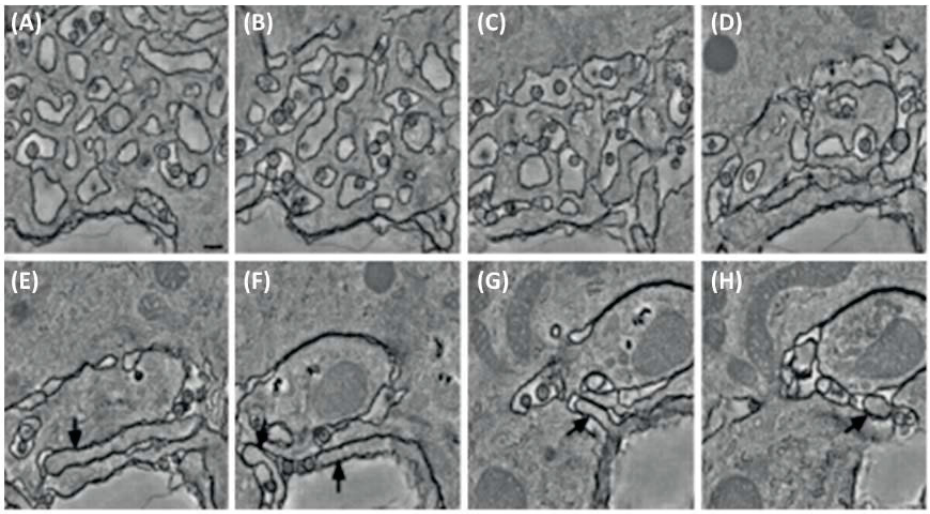

Figure 50. Virus-containing compartment (VCC) morphology. (A–H) Digital slices (from electron tomography) through a region of a HIV-1-infected macrophage depicting the morphological complexity and variability of the VCC. The arrows point to membranous protrusions that were initially thought to be a separate form of VCC but were later shown to be part of the overall three-dimensional VCC structure. Scale bar corresponds to 200 nm. From [129].

Confocal microscopy live imaging and correlative electron microscopy of macrophages showed that HIV-VLPs bound to αEnv-PS-LUVs are localized into membrane-delimited intracellular compartment morphologically similar to phagosomes and enriched in the LYs tracker Lysotracker. More specifically, image analysis (Figure 46C) showed that immunoliposomes - with or without PS - induce delivery of HIV-VLPs into LYs. This effect is significantly more reproducible in the presence of PS, as judged by the small standard deviation observed for the αEnv-PS-LUV sample (Figure 46C, compare to αEnv-LUVs). Lysotracker-stained compartments are very different from the above-mentioned VCCs, and are probably highly acidic vesicles. These results are in agreement with the fact that, as previous studies have shown, apoptotic cells, once inside the phagocyte, are processed via a phago-lysosomal pathway characterized by a progressive acidification of the phagosomal lumen and acquisition of vacuolar H^+-ATPases [129,152].

4 CONCLUSION AND OUTLOOK

4.1 Identification of a calcium-dependent pathway for VLPs release as potential new antiviral target

Although antiretroviral therapy effectively diminishes viral replication and substantially increases survival of patients, it has not been possible yet to achieve a cure. High viral replication rate, generation of extensive viral genetic diversity and spontaneous development of antiretroviral-drugs resistance (or interruption of antiretroviral therapy) result in rebound of virus replication and development of AIDS [84]. Furthermore, HIV-1 is able to escape from the immune surveillance establishing reservoirs in a small pool of latently infected cells. For all these reasons, resistance to the antiretroviral drugs, and the emergence of drug-resistant viral strains may occur, resulting, in the end, in treatment failure. The demand of new antiretroviral drugs and innovative therapies is therefore not decreasing and still remains an important objective for the research.

In recent years, medical and pharmaceutical research has supported, in contrast with conventional pathogen-targeting strategies, a new drug discovery paradigm [161]: it has been proposed that focusing on identifying and targeting the host factors hijacked by the pathogens might represent a novel possible successful strategy to develop new therapies. In other words, this kind of therapeutic approach against pathogens should not target molecular structures of the pathogen itself, but rather host structures or cellular mechanisms that directly or indirectly support one or more fundamental steps of the pathogen's life cycle [162]. Examples of drugs that have host factors as targets are various, and in some cases already available for treatment (see Table 3).

Pathogen	Host factor hijacked	Role played by the host factor in the pathogen life cycle	Drug of choice
SARS-Coronavirus	clathrin-dependent endocytosis machinery	Entry into the host cell	Chlorpromazine
Hepatitis C virus	Endoplasmic-reticulum glucosidase	Folding of the envelop proteins	Celgosivir
Vaccinia virus	Abl-kinase /Src-kinase	Actin motility	Gleevec
Plasmodium falciparum	20S proteasome	Proteasome activity	MLN-273

Table 3. Examples of antiviral or antiparassitic drugs that inhibit cellular factors requested for the pathogen's life cycle. The information summarized in this table were taken from [161].

Concerning anti-HIV-1 therapy, the CCR5 co-receptor has been suggested to represent an attractive anti-HIV target, since individuals with a natural CCR5Δ32 mutation (which has little apparent impact on immune status or general health) are highly protected against HIV-1 infection. Maraviroc (brand-named "Selzentry" or "Celsentri") is an antagonist of the CCR5 receptor, which inhibits the viral fusion process with the host PM [163]. This drug is commonly used in the therapy of AIDS patients.

In the last few years, the study of the interactions between HIV-1 and the host cell and the characterization of the viral life cycle in its different steps have seen some progresses, specifically thank to the technical advancements (e.g. super resolution microscopy) and the use of RNAi screening procedures [6]. In particular, the central process of ESCRT mediated budding seems to be now fairly well established [124]. In particular, the cellular factors exploited by Gag to achieve the viral assembly process include cellular structures, single proteins and protein complexes [164,165]. Such interactions between host and viral components may surely provide attractive new antiviral targets [84]. Nevertheless, identification of such host-directed targets requires a detailed biological and biochemical characterization. However, the different aspects of viral life cycle, particularly regarding the release of viral particles, still require further investigations. Specifically, despite the progress achieved in understanding viral structural properties and its single components, high-resolution structures of their complexes with cellular partners are very limited. Moreover, the fact that the virus is exploiting different assembly pathways in different target cells represents a further obstacle in the identification of potential target for a new antiretroviral therapy.

In this work, on the basis of previous preliminary observations [1,2,23], an intracellular pathway for viral release, which functions through the activity of cellular machineries common to all cell types was investigated. The here presented results allowed the identification of a model for a calcium-dependent release of VLPs which I) further confirms the relevance of intracellular calcium in the release of VLPs from the host cell, II) identifies a possible calcium-dependent pathway for rescue of LY/LE entrapped VLPs from degradation, which requests the activity of the lysosomal protein Syt-VII. The slight modulation in VLPs release upon TBHQ-treatment or knockdown of Syt-VII suggests that the role played by this pathway, in the context of HIV-1 release from the infected cell, might be not predominant. However, chemical compounds that modulate the intracellular calcium signaling, only mimicking the activity of extracellular (or intracellular) stimuli, might not be able to exactly reproduce real physiological conditions. The intracellular concentration of calcium might undergo oscillations that vary in the intensity and duration in dependence of the activated pathway. Furthermore, considering that perturbation of host-cell PM is a primary mechanism of HIV-1 cytopathology [166], it is reasonable that the virus itself, also through the continuous budding at the PM, might be able to induce a mechanism of PM-repair that requires the activity of lysosomal calcium signaling and ends in LYs-exocytosis and consequent release of LYs-entrapped VLPs.

The discovery of new cellular factors that play a role in the complex release mechanism of HIV-1 should pave the way for further investigations and hopefully will lead to identification of novel mechanisms and/or pathways critical for virus assembly. Such knowledge should facilitate the development of better approaches for the treatment of HIV-1.

4.2 Medical and biological relevance of the immunoliposomal system and further perspectives

Liposomes containing PS have been used in the past to target macrophages (e.g. for *in vivo* imaging [167]), and liposomes bound to antibodies have been largely used to target specific cells (e.g. during drug delivery [93,168]). This work adds to the existing body of knowledge by joining these two unrelated approaches in order to address the problem of the poor immune response against HIV-1. This is the first study in which the above-mentioned strategies are combined to produce a

nanobiotechnological system able to elicit phagocytosis and delivery of HIV-VLPs to acidic compartments (i.e. LYs) in macrophages.

Exploiting PS-mediated phagocytosis of HIV-1 particles would potentially help to support the immune system in the case of HIV-1 infection on multiple levels, with several potential advantages: first, the rapid clearance of HIV-1 particles from the circulation via macrophage-phagocytosis could diminish the high viral load observed in the first few months after the infection. Moreover, the direct delivery of the internalized particles to acidic compartments should allow for a more rapid destruction of the virus (Figure 46 and Figure 47). Second, PS-mediated phagocytosis of the viral particles, exploiting a specific cargo-internalization pathway different in respect to that activated by opsonized antigens, would allow circumventing the impaired phagocytosis via the FcγR pathway, which has been reported to be compromised in infected patients [68,69]. Furthermore, the mere binding of anti-HIV IgG to viral particles may even favor the persistence of the virus if trapped by follicular dendritic cells (FDC): a study has shown that optimal maintenance of HIV-1 infectivity requires both antibodies against particle-associated determinants and the FDC-FcγR [169]. Third, the influence of PS modulating the inflammatory response in macrophages, already demonstrated in previous studies [167,170], would strongly decrease the ongoing activation of the immune system and persistent inflammation, both of which are key driving forces in the loss of $CD4^+$ T-cells and progression to AIDS pathogenesis [41]. Specifically, in macrophages PS is able to down-regulate TNF-α production [171], whose up-regulated production is connected to HIV-associated dementia and other neuronal injuries [59,142]. Fourth, PS-mediated phagocytosis of apoptotic cells is known to induce antigen-presentation to the major histocompatibility complex class II on the macrophage surface [74,172]. Accidentally, a proper antigen presentation via major histocompatibility complex class II requires actin-dependent phagocytosis of the cargo [173], similarly to the internalization of the immunoliposomes described in this work. This may result in the stimulation of specific T-helper cells and, ultimately, stimulation of specific B-cells, which results in the subsequent secretion of antibodies. In conclusion, beside the development of a vaccine for HIV-1, which still seems extraordinarily challenging, and the advances in the identification of potent neutralizing antibodies [174,175], the immunoliposomes investigated in this work might provide the basis for the design of new and alternative therapeutic applications to combat HIV-1 in-

fection and positively stimulate the immune system.

Although in this work the capability of αEnv-PS-LUVs to produce efficient HIV-VLPs phagocytosis by macrophages was demonstrated and the potential role of this nanobiotechnological approach stimulating the immune system against HIV-1 and reducing persistent inflammation was illustrated, additional experiments on the potential of αEnv-PS-LUVs are required to further characterize the system presented here. For instance, proving αEnv-PS-LUVs functionality in other cells of the immune systems (e.g. DCs), testing the αEnv-PS-LUVs capability to also bind wild type HIV-1 virus, testing the usefulness of this system on other viruses, and *in vivo* studies represent future work that could be of great importance.

Appendix

Molecular structures of the lipids used in this work.

Images from the website of Avanti Polar Lipids, Inc.

L-α-phosphatidylcholine

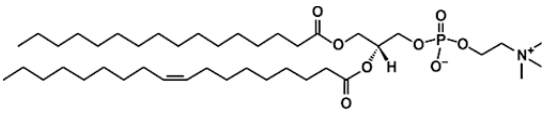

1,2-dipalmitoyl-sn-glycero-3-phosphoethanolamine-N-(cap-biotinyl)

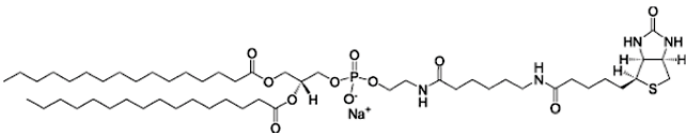

1-palmitoyl-2 (dipyrromethenebordondifluoride) undecanoyl-sn- glycero-3- phosphocholine

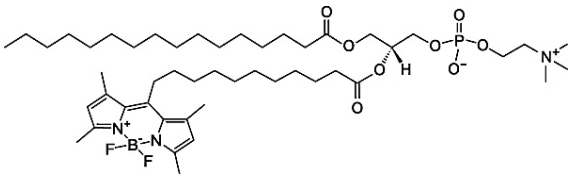

1,2-diacyl-sn-glycero-3- phospho-L-serine

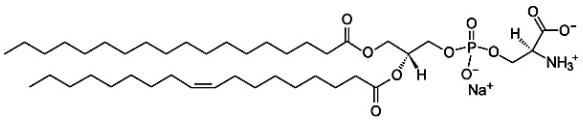

Abbreviations

Abs	Antibodies
AIDS	Acquiered immunodeficiency syndrome
ART	Anti-retroviral therapy
AZT	Azidothymidine
CA	Capside
CTL	Cytotoxic T-cell
DAG	Diacylglycerol
DC	Dendritic cell
DIC	Differential interference contrast (microscopy)
DMSO	Dimethyl sulfoxide
Env	Envelope
ER	Endoplasmic reticulum
ESCRT	Endosomal sorting complexes
	required for transport
FACS	Fluorescence-activated cell sorting
FcγR	Fc-gamma receptor
FDC	Follicular dendritic cell
Gag	G-antigen
GPCR	G-protein coupled receptor
HIV-1	Human immunodeficiency virus-1
IgG	Immunoglobulin G
IN	Integrase
LE	Late endosome
LTR	Long terminal repeat
LUV	Large unilamellar vesicles
LY	Lysosome
MA	Matrix
MTOC	Microtubule-organization center
MVB	Multivesicular bodies
NSF	N-ethylmaleimide-sensitive factor
NC	Nucleocapside
PI	Propidium iodide

PIP_2	Phosphatidylinositol(4,5)-bisphosphate
PKC	Protein-kinase C
PLC	Phospholipase C
PM	Plasma membrane
Pol	Polimarase
PR	Protease
PS	Phosphatidylserine
RES	Reticuloendotelial system
RF	Restriction factor
RT	Reverse transcriptase
SD	Standard deviation
SERCA	Sarco/endoplasmic reticulum Ca^{2+}-ATPase
SIV	Simian immunodeficiency virus
SNAP	Soluble NSF attachment protein
SNARE	SNAP receptor
Syt-VII	Synaptotagmin-VII
TBHQ	Tert-butylhydroquinone
Thaps	Thapsigargin
TKR	Tyrosine-kinase receptor
TNF	Tumor necrosis factor
TPC	Two pore channel
TRIM5	Tripartite motif-containing motif 5
VCC	Virus-containing compartment
VLP	Virus-like particle

Bibliography

1. Ehrlich LS, Medina GN, Khan MB, Powell MD, Mikoshiba K, Carter CA. Activation of the Inositol (1,4,5)-Triphosphate Calcium Gate Receptor Is Required for HIV-1 Gag Release. *Journal of Virology*. 84(13), 6438–6451 (2010).

2. Perlman M, Resh MD. Identification of an intracellular trafficking and assembly pathway for HIV-1 gag. *Traffic*. 7(6), 731–745 (2006).

3. Hemelaar J. The origin and diversity of theHIV-1 pandemic. *Trends in Molecular Medicine*. 18(3), 182–192 (2012).

4. Barré-Sinoussi F, Chermann JC, Rey F, *et al.* Isolation of a T-lymphotropic retrovirus from a patient at risk for acquired immune deficiency syndrome (AIDS). *Science*. 220(4599), 868–871 (1983).

5. Freed EO. HIV-1 Replication. *Somatic Cell and Molecular Genetics, Vol. , Nos. , November*. 1–21 (2002).

6. Balasubramaniam M, Freed EO. New Insights into HIV Assembly and Trafficking. *Physiology*. 26(4), 236–251 (2011).

7. Gallo S. The HIV Env-mediated fusion reaction. *Biochimica et Biophysica Acta (BBA) - Biomembranes*. 1614(1), 36–50 (2003).

8. Miyauchi K, Kim Y, Latinovic O, Morozov V, Melikyan GB. HIV Enters Cells via Endocytosis and Dynamin-Dependent Fusion with Endosomes. *Cell*. 137(3), 433–444 (2009).

9. McMichael AJ, Borrow P, Tomaras GD, Goonetilleke N, Haynes BF. The immune response during acute HIV-1 infection: clues for vaccine development. *Nature Reviews Immunology*. 10(1), 11–23 (2009).

10. Hubner W, McNerney GP, Chen P, *et al.* Quantitative 3D Video Microscopy of HIV Transfer Across T Cell Virological Synapses. *Science*. 323(5922), 1743–1747 (2009).

11. Benaroch P, Billard E, Gaudin R, Schindler M, Jouve M. HIV-1 assembly in macrophages. *Retrovirology*. 7(1), 29 (2010).

12. Kramer B, Pelchen-Matthews A, Deneka M, Garcia E, Piguet V, Marsh M. HIV interaction with endosomes in macrophages and dendritic cells. *Blood Cells, Molecules, and Diseases*. 35(2), 136–142 (2005).

13. Ganser-Pornillos BK, Yeager M, Sundquist WI. The structural biology of HIV assembly. *Current Opinion in Structural Biology*. 18(2), 203–217 (2008).

14. Ono A, Ablan SD, Lockett SJ, Nagashima K, Freed EO. Phosphatidylinositol (4,5) bisphosphate regulates HIV-1 Gag targeting to the plasma membrane. *Proc. Natl. Acad. Sci. U.S.A.* 101(41), 14889–14894 (2004).

15. Bhattacharya J, Repik A, Clapham PR. Gag Regulates Association of Human Immunodeficiency Virus Type 1 Envelope with Detergent-Resistant Membranes. *Journal of Virology*. 80(11), 5292–5300 (2006).

16. Hogue IB, Hoppe A, Ono A. Quantitative Fluorescence Resonance Energy Transfer Microscopy Analysis of the Human Immunodeficiency Virus Type 1 Gag-Gag Interaction: Relative Contributions of the CA and NC Domains and Membrane Binding. *Journal of Virology*. 83(14), 7322–7336 (2009).

17. Jolly C, Mitar I, Sattentau QJ. Requirement for an Intact T-Cell Actin and Tubulin Cytoskeleton for Efficient Assembly and Spread of Human Immunodeficiency Virus Type 1. *Journal of Virology*. 81(11), 5547–5560 (2007).

18. Carter CA, Ehrlich LS. Cell Biology of HIV-1 Infection of Macrophages. *Annu. Rev. Microbiol.* 62(1), 425–443 (2008).

19. Checkley MA, Luttge BG, Freed EO. HIV-1 Envelope Glycoprotein Biosynthesis, Trafficking, and Incorporation. *Journal of Molecular Biology*. 410(4), 582–608 (2011).

20. Patil A, Gautam A, Bhattacharya J. Evidence that Gag facilitates HIV-1 envelope association both in GPI-enriched plasma membrane and detergent resistant membranes and facilitates envelope incorporation onto virions in primary CD4+ T cells. *Virology Journal*. 7(1), 3 (2010).

21. Weissenhorn W, Göttlinger H. Essential Ingredients for HIV-1 Budding. *Cell Host and Microbe*. 9(3), 172–174 (2011).

22. Huang M, Orenstein JM, Martin MA, Freed EO. p6Gag is required for particle production from full-length human immunodeficiency virus type 1 molecular clones expressing protease. *Journal of Virology*. 69(11), 6810–6818 (1995).

23. Joshi A, Garg H, Ablan SD, Freed EO. Evidence of a Role for Soluble N-Ethylmaleimide-sensitive Factor Attachment Protein Receptor (SNARE) Machinery in HIV-1 Assembly and Release. *Journal of Biological Chemistry*. 286(34), 29861–29871 (2011).

24. Roxrud I, Stenmark H, Malerød L. ESCRT & Co. *Biology of the Cell*. 102(5), 293–318 (2012).

25. Baumgärtel V, Ivanchenko S, Dupont A, *et al.* Live-cell visualization of dynamics of HIV budding site interactions with an ESCRT component. *Nature Cell Biology*. 13(4), 469–474 (2011).

26. Sundquist WI, Krausslich HG. HIV-1 Assembly, Budding, and Maturation. *Cold Spring Harbor Perspectives in Medicine*. 2(7), a006924–a006924 (2012).

27. Freed EO. HIV-1 gag proteins: diverse functions in the virus life cycle. *Virology*. 251(1), 1–15 (1998).

28. Bell NM, Lever AML. HIV Gag polyprotein: processing andearly viral particle assembly. *Trends in Microbiology*. 21(3), 136–144 (2013).

29. Chukkapalli V, Ono A. Molecular Determinants that Regulate Plasma Membrane Association of HIV-1 Gag. *Journal of Molecular Biology*. 410(4), 512–524 (2011).

30. Ono A. HIV-1 assembly at the plasma membrane. *Vaccine*. 28, B55–B59 (2010).

31. Luban J. TRIM5 and the Regulation of HIV-1 Infectivity. *Molecular Biology International*. 2012(6), 1–6 (2012).

32. Solbak SMØ, Reksten TR, Röder R, *et al.* HIV-1 p6-Another viral interaction partner to the host cellular protein cyclophilin A. *Biochim. Biophys. Acta*. 1824(4), 667–678 (2012).

33. Jouvenet N, Zhadina M, Bieniasz PD, Simon SM. Dynamics of ESCRT protein recruitment during retroviral assembly. *Nature Cell Biology*. 13(4), 394–401 (2011).

34. Garrus JE, Schwedler von UK, Pornillos OW, *et al.* Tsg101 and the vacuolar protein sorting pathway are essential for HIV-1 budding. *Cell*. 107(1), 55–65 (2001).

35. Bieniasz PD. Late budding domains and host proteins in enveloped virus release. *Virology*. 344(1), 55–63 (2006).

36. Briggs JAG, Kräusslich H-G. The Molecular Architecture of HIV. *Journal of Molecular Biology*. 410(4), 491–500 (2011).

37. Jouvenet N, Simon SM, Bieniasz PD. Visualizing HIV-1 Assembly. *Journal of Molecular Biology*. 410(4), 501–511 (2011).

38. Saad JS, Miller J, Tai J, Kim A, Ghanam RH, Summers MF. Structural basis for targeting HIV-1 Gag proteins to the plasma membrane for virus assembly. *Proc. Natl. Acad. Sci. U.S.A.* 103(30), 11364–11369 (2006).

39. Simons K, Gerl MJ. Revitalizing membrane rafts: new tools and insights. *Nature Publishing Group*. 11(10), 688–699 (2010).

40. Yang P, Ai LS, Huang SC, *et al.* The Cytoplasmic Domain of Human Immunodeficiency Virus Type 1 Transmembrane Protein gp41 Harbors Lipid Raft Association Determinants. *Journal of Virology*. 84(1), 59–75 (2009).

41. Joshi A, Ablan SD, Soheilian F, Nagashima K, Freed EO. Evidence that Productive Human Immunodeficiency Virus Type 1 Assembly Can Occur in an Intracellular Compartment. *Journal of Virology*. 83(11), 5375–5387 (2009).

42. Booth AM, Fang Y, Fallon JK, Yang J-M, Hildreth JEK, Gould SJ. Exosomes and HIV Gag bud from endosome-like domains of the T cell plasma membrane. *The Journal of Cell Biology*. 172(6), 923–935 (2006).

43. Ehrlich LS, Medina GN, Carter CA. Sprouty2 Regulates PI(4,5)P2/Ca2+ Signaling and HIV-1 Gag Release. *Journal of Molecular Biology*. 410(4), 716–725 (2011).

44. Molle D, Segura-Morales C, Camus G, *et al.* Endosomal trafficking of HIV-1 gag and genomic RNAs regulates viral egress. *J. Biol. Chem.* 284(29), 19727–19743 (2009).

45. Ehrlich LS, Carter CA. HIV Assembly and Budding: Ca2+ Signaling and Non-ESCRT Proteins Set the Stage. *Molecular Biology International*. 2012, 1–12 (2012).

46. Visciano ML, Diomede L, Tagliamonte M, *et al.* Generation of HIV-1 Virus-Like Particles expressing different HIV-1 glycoproteins. *Vaccine*. 29(31), 4903–4912 (2011).

47. Deml L, Speth C, Dierich MP, Wolf H, Wagner R. Recombinant HIV-1 Pr55gag virus-like particles: potent stimulators of innate and acquired immune responses. *Molecular Immunology*. 42(2), 259–277 (2005).

48. Jalaguier P, Turcotte K, Danylo A, Cantin R, Tremblay MJ. Efficient Production of HIV-1 Virus-Like Particles from a Mammalian Expression Vector Requires the N-Terminal Capsid Domain. *PLoS ONE*. 6(11), e28314 (2011).

49. Greenstone HL, Nieland JD, de Visser KE, *et al.* Chimeric papillomavirus virus-like particles elicit antitumor immunity against the E7 oncoprotein in an HPV16 tumor model. *Proc. Natl. Acad. Sci. U.S.A.* 95(4), 1800–1805 (1998).

50. Hammonds J, Chen X, Zhang X, Lee F, Spearman P. Advances in methods for the production, purification, and characterization of HIV-1 Gag–Env pseudovirion vaccines. *Vaccine*. 25(47), 8036–8048 (2007).

51. Keele BF, Giorgi EE, Salazar-Gonzalez JF, *et al.* Identification and characterization of transmitted and early founder virus envelopes in primary HIV-1 infection. *Proceedings of the National Academy of Sciences*. 105(21), 7552–7557 (2008).

52. Brenchley JM, Paiardini M, Knox KS, *et al.* Differential Th17 CD4 T-cell depletion in pathogenic and nonpathogenic lentiviral infections. *Blood*. 112(7), 2826–2835 (2008).

53. Gasper-Smith N, Crossman DM, Whitesides JF, *et al.* Induction of plasma (TRAIL), TNFR-2, Fas ligand, and plasma microparticles after human immunodeficiency virus type 1 (HIV-1) transmission: implications for HIV-1 vaccine design. *Journal of Virology*. 82(15), 7700–7710 (2008).

54. Brenchley JM, Schacker TW, Ruff LE, *et al.* CD4+ T cell depletion during all stages of HIV disease occurs predominantly in the gastrointestinal tract. *J. Exp. Med.* 200(6), 749–759 (2004).

55. Wilson JD, Ogg GS, Allen RL, *et al.* Direct visualization of HIV-1-specific cytotoxic T lymphocytes during primary infection. *AIDS*. 14(3), 225–233 (2000).

56. Borrow P, Lewicki H, Hahn BH, Shaw GM, Oldstone MB. Virus-specific CD8+ cytotoxic T-lymphocyte activity associated with control of viremia in primary human immunodeficiency virus type 1 infection. *Journal of Virology*.

68(9), 6103–6110 (1994).

57. Markowitz M, Louie M, Hurley A, *et al.* A novel antiviral intervention results in more accurate assessment of human immunodeficiency virus type 1 replication dynamics and T-cell decay in vivo. *Journal of Virology*. 77(8), 5037–5038 (2003).

58. Sedaghat AR, Siliciano JD, Brennan TP, Wilke CO, Siliciano RF. Limits on replenishment of the resting CD4+ T cell reservoir for HIV in patients on HAART. *PLoS Pathog*. 3(8), e122 (2007).

59. Lee C. HIV-1 gp120-induced TNF- production by primary human macrophages is mediated by phosphatidylinositol-3 (PI-3) kinase and mitogen-activated protein (MAP) kinase pathways. *Journal of Leukocyte Biology*. 78(4), 1016–1023 (2005).

60. Ancuta P, Kamat A, Kunstman KJ, *et al.* Microbial translocation is associated with increased monocyte activation and dementia in AIDS patients. *PLoS ONE*. 3(6), e2516 (2008).

61. Mosser DM, Edwards JP. Exploring the full spectrum of macrophage activation. *Nature Publishing Group*. 8(12), 958–969 (2008).

62. Koppensteiner H, Brack-Werner R, Schindler M. Macrophages and their relevance in Human Immunodeficiency Virus Type I infection. *Retrovirology*. 9, 82 (2012).

63. Herbein G, Gras G, Khan K, Abbas W. Macrophage signaling in HIV-1 infection. *Retrovirology*. 7(1), 34 (2010).

64. Ackerman ME, Dugast AS, McAndrew EG, *et al.* Enhanced Phagocytic Activity of HIV-Specific Antibodies Correlates with Natural Production of Immunoglobulins with Skewed Affinity for Fc R2a and Fc R2b. *Journal of Virology*. 87(10), 5468–5476 (2013).

65. Lahouassa H, Daddacha W, Hofmann H, *et al.* SAMHD1 restricts the replication of human immunodeficiency virus type 1 by depleting the intracellular pool of deoxynucleoside triphosphates. *Nat. Immunol.* 13(3), 223–228 (2012).

66. Kedzierska K, Mak J, Mijch A, *et al.* Granulocyte-macrophage colony-stimulating factor augments phagocytosis of Mycobacterium avium complex by human immunodeficiency virus type 1-infected monocytes/macrophages in vitro and in vivo. *J. Infect. Dis.* 181(1), 390–394 (2000).

67. Biggs BA, Hewish M, Kent S, Hayes K, Crowe SM. HIV-1 infection of human macrophages impairs phagocytosis and killing of Toxoplasma gondii. *J. Immunol.* 154(11), 6132–6139 (1995).

68. Kedzierska K, Ellery P, Mak J, Lewin SR, Crowe SM, Jaworowski A. HIV-1 down-modulates gamma signaling chain of Fc gamma R in human macrophages: a possible mechanism for inhibition of phagocytosis. *J. Immunol.* 168(6), 2895–2903 (2002).

69. Holl V, Hemmerter S, Burrer R, *et al.* Involvement of Fc gamma RI (CD64) in the mechanism of HIV-1 inhibition by polyclonal IgG purified from infected patients in cultured monocyte-derived macrophages. *J. Immunol.* 173(10), 6274–6283 (2004).

70. Leeansyah E, Wines BD, Crowe SM, Jaworowski A. The mechanism underlying defective Fcgamma receptor-mediated phagocytosis by HIV-1-infected human monocyte-derived macrophages. *J. Immunol.* 178(2), 1096–1104 (2007).

71. Nimmerjahn F, Ravetch JV. Fcγ receptors as regulators of immune responses. *Nature Reviews Immunology*. 8(1), 34–47 (2008).

72. Ahmad R, Sindhu ST, Toma E, *et al.* Evidence for a correlation between antibody-dependent cellular cytotoxicity-mediating anti-HIV-1 antibodies and prognostic predictors of HIV infection. *J. Clin. Immunol.* 21(3), 227–233 (2001).

73. Crowley MT, Costello PS, Fitzer-Attas CJ, *et al.* A critical role for Syk in signal transduction and phagocytosis mediated by Fcgamma receptors on macrophages. *J. Exp. Med.* 186(7), 1027–1039 (1997).

74. Stuart LM, Ezekowitz RAB. Phagocytosis: elegant complexity. *Immunity*. 22(5), 539–550 (2005).

75. Krahling S, Callahan MK, Williamson P, Schlegel RA. Exposure of phosphatidylserine is a general feature in the phagocytosis of apoptotic lymphocytes by macrophages. *Cell Death Differ.* 6(2), 183–189 (1999).

76. Hoffmann PR. Phosphatidylserine (PS) induces PS receptor-mediated macropinocytosis and promotes clearance of apoptotic cells. *The Journal of Cell Biology*. 155(4), 649–660 (2001).

77. Armstrong A, Ravichandran KS. Phosphatidylserine receptors: what is the new RAGE? *Nature Publishing Group*. 12(4), 287–288 (2011).

78. Kay JG, Grinstein S. Sensing Phosphatidylserine in Cellular Membranes. *Sensors*. 11(2), 1744–1755 (2011).

79. Maiti SN, Balasubramanian K, Ramoth JA, Schroit AJ. Beta-2-glycoprotein 1-dependent macrophage uptake of apoptotic cells. Binding to lipoprotein receptor-related protein receptor family members. *J. Biol. Chem.* 283(7), 3761–3766 (2008).

80. Lodge R, Ouellet M, Barat C, Andreani G, Kumar P, Tremblay MJ. HIV-1 Promotes Intake of Leishmania Parasites by Enhancing Phosphatidylserine-Mediated, CD91/LRP-1-Dependent Phagocytosis in Human Macrophages. *PLoS ONE*. 7(3), e32761 (2012).

81. Montagnier L. 25 years after HIV discovery: Prospects for cure and vaccine. *Virology*. 397(2), 248–254 (2010).

82. Date AA, Destache CJ. A review of nanotechnological approaches for the

prophylaxis of HIV/AIDS. *Biomaterials*. 34(26), 6202–6228 (2013).

83. Permanyer M, Ballana E, Ruiz A, *et al.* Antiretroviral Agents Effectively Block HIV Replication after Cell-to-Cell Transfer. *Journal of Virology*. 86(16), 8773–8780 (2012).

84. Deeks SG, Lewin SR, Havlir DV. The end of AIDS: HIV infection as a chronic disease. *Lancet*. 382(9903), 1525–1533 (2013).

85. GREENE W, DEBYSER Z, IKEDA Y, *et al.* Novel targets for HIV therapy. *ANTIVIRAL RESEARCH*. 80(3), 251–265 (2008).

86. Parboosing R, Maguire GEM, Govender P, Kruger HG. Nanotechnology and the Treatment of HIV Infection. *Viruses*. 4(12), 488–520 (2012).

87. Lisziewicz J, Tőke ER. Nanomedicine applications towards the cure of HIV. *Nanomedicine: Nanotechnology, Biology and Medicine*. 9(1), 28–38 (2013).

88. Chiappetta DA, Hocht C, Taira C, Sosnik A. Efavirenz-loaded polymeric micelles for pediatric anti-HIV pharmacotherapy with significantly higher oral bioavailability [corrected]. *Nanomedicine (Lond)*. 5(1), 11–23 (2010).

89. Kovochich M, Marsden MD, Zack JA. Activation of latent HIV using drug-loaded nanoparticles. *PLoS ONE*. 6(4), e18270 (2011).

90. Kinman L, Brodie SJ, Tsai CC, *et al.* Lipid-drug association enhanced HIV-1 protease inhibitor indinavir localization in lymphoid tissues and viral load reduction: a proof of concept study in HIV-2287-infected macaques. *JAIDS Journal of Acquired Immune Deficiency Syndromes*. 34(4), 387–397 (2003).

91. Abdool Karim Q, Abdool Karim SS, Frohlich JA, *et al.* Effectiveness and safety of tenofovir gel, an antiretroviral microbicide, for the prevention of HIV infection in women. *Science*. 329(5996), 1168–1174 (2010).

92. Ensign LM, Schneider C, Suk JS, Cone R, Hanes J. Mucus penetrating nanoparticles: biophysical tool and method of drug and gene delivery. *Adv. Mater. Weinheim*. 24(28), 3887–3894 (2012).

93. Etzerodt A, Maniecki MB, Graversen JH, Møller HJ, Torchilin VP, Moestrup SK. Efficient intracellular drug-targeting of macrophages using stealth liposomes directed to the hemoglobin scavenger receptor CD163. *Journal of Controlled Release*. 1–9 (2012).

94. Geelen T, Yeo SY, Paulis LE, Starmans LW, Nicolay K, Strijkers GJ. Internalization of paramagnetic phosphatidylserine-containing liposomesby macrophages. *Journal of Nanobiotechnology*. 10(1), 1–1 (2012).

95. Phillips NC, Tsoukas C. Liposomal encapsulation of azidothymidine results in decreased hematopoietic toxicity and enhanced activity against murine acquired immunodeficiency syndrome. *Blood*. 79(5), 1137–1143 (1992).

96. Coombs PJ, Taylor ME, Drickamer K. Two categories of mammalian galactose-binding receptors distinguished by glycan array profiling. *Glycobiology*.

16(8), 1C–7C (2006).

97. Flasher D, Konopka K, Chamow SM, *et al.* Liposome targeting to human immunodeficiency virus type 1-infected cells via recombinant soluble CD4 and CD4 immunoadhesin (CD4-IgG). *Biochim. Biophys. Acta*. 1194(1), 185–196 (1994).

98. Pollock S, Dwek RA, Burton DR, Zitzmann N. N-Butyldeoxynojirimycin is a broadly effective anti-HIV therapy significantly enhanced by targeted liposome delivery. *AIDS*. 22(15), 1961–1969 (2008).

99. Gallo RC, Sarin PS, Gelmann EP, *et al.* Isolation of human T-cell leukemia virus in acquired immune deficiency syndrome (AIDS). *Science*. 220(4599), 865–867 (1983).

100. van Gils MJ, Sanders RW. Broadly neutralizing antibodies against HIV-1 Templates for a vaccine. *Virology*. 435(1), 46–56 (2013).

101. Mascola JR, Montefiori DC. The Role of Antibodies in HIV Vaccines. *Annu. Rev. Immunol.* 28(1), 413–444 (2010).

102. Luzio JP, Pryor PR, Bright NA. Lysosomes: fusion and function. *Nature Publishing Group*. 8(8), 622–632 (2007).

103. Helma J, Schmidthals K, Lux V, *et al.* Direct and Dynamic Detection of HIV-1 in Living Cells. *PLoS ONE*. 7(11), e50026 (2012).

104. Horowitz LF, Hirdes W, Suh B-C, Hilgemann DW, Mackie K, Hille B. Phospholipase C in living cells: activation, inhibition, Ca2+ requirement, and regulation of M current. *The Journal of General Physiology*. 126(3), 243–262 (2005).

105. Barbosa CMV, Bincoletto C, Barros CC, Ferreira AT, Paredes-Gamero EJ. PLCγ2 and PKC are important to myeloid lineage commitment triggered by M-SCF and G-CSF. *J. Cell. Biochem.* 115(1), 42–51 (2014).

106. Bunney TD, Katan M. PLC regulation: emerging pictures for molecular mechanisms. *Trends in Biochemical Sciences*. 36(2), 88–96 (2011).

107. Chan CK, Liao SY, Zhang YL, Xu A, Tse HF, Vanhoutte PM. Protective effects of histamine on Gq-mediated relaxation in regenerated endothelium. *AJP: Heart and Circulatory Physiology*. 306(2), H286–90 (2014).

108. Huotari J, Helenius A. Endosome maturation. *The EMBO Journal*. 30(17), 3481–3500 (2011).

109. Clapham DE. Calcium Signaling. *Cell*. 131(6), 1047–1058 (2007).

110. Eaddy AC, Schnellmann RG. Visualization and quantification of endoplasmic reticulum Ca2+ in renal cells using confocal microscopy and Fluo5F. *Biochemical and Biophysical Research Communications*. 404(1), 424–427 (2011).

111. Idone V, Tam C, Goss JW, Toomre D, Pypaert M, Andrews NW. Repair of

injured plasma membrane by rapid Ca2+-dependent endocytosis. *The Journal of Cell Biology*. 180(5), 905–914 (2008).

112. Piper RC, Luzio JP. CUPpling calcium to lysosomal biogenesis. *Trends in Cell Biology*. 14(9), 471–473 (2004).

113. Luzio JP, Gray SR, Bright NA. Endosome–lysosome fusion. *Biochem. Soc. Trans*. 38(6), 1413 (2010).

114. Czibener C, Sherer NM, Becker SM, *et al.* Ca2+ and synaptotagmin VII-dependent delivery of lysosomal membrane to nascent phagosomes. *The Journal of Cell Biology*. 174(7), 997–1007 (2006).

115. Coxon CH, Lewis AM, Sadler AJ, *et al.* NAADP regulates human platelet function. *Biochem. J.* 441(1), 435–442 (2011).

116. Bego MG, Dubé M, Mercier J, Cohen EA. Effect of calcium-modulating cyclophilin ligand on human immunodeficiency virus type 1 particle release and cell surface expression of tetherin. *Journal of Virology*. 83(24), 13032–13036 (2009).

117. Perez-Caballero D, Zang T, Ebrahimi A, *et al.* Tetherin Inhibits HIV-1 Release by Directly Tethering Virions to Cells. *Cell*. 139(3), 499–511 (2009).

118. Pornillos O. HIV Gag mimics the Tsg101-recruiting activity of the human Hrs protein. *The Journal of Cell Biology*. 162(3), 425–434 (2003).

119. Subach FV, Subach OM, Gundorov IS, *et al.* Monomeric fluorescent timers that change color from blue to red report on cellular trafficking. *Nat Chem Biol*. 5(2), 118–126 (2009).

120. Franker MAM, Hoogenraad CC. Microtubule-based transport - basic mechanisms, traffic rules and role in neurological pathogenesis. *Journal of Cell Science*. 126(11), 2319–2329 (2013).

121. Churchill GC, Okada Y, Thomas JM, Genazzani AA, Patel S, Galione A. NAADP mobilizes Ca(2+) from reserve granules, lysosome-related organelles, in sea urchin eggs. *Cell*. 111(5), 703–708 (2002).

122. Calcraft PJ, Ruas M, Pan Z, *et al.* NAADP mobilizes calcium from acidic organelles through two-pore channels. *Nature*. 459(7246), 596–600 (2009).

123. Martinez I, Chakrabarti S, Hellevik T, Morehead J, Fowler K, Andrews NW. Synaptotagmin VII regulates Ca(2+)-dependent exocytosis of lysosomes in fibroblasts. *The Journal of Cell Biology*. 148(6), 1141–1149 (2000).

124. Meng B, Lever AM. Wrapping up the bad news – HIV assembly and release. *Retrovirology*. 10(1), 1–1 (2013).

125. Morita E, Sandrin V, McCullough J, Katsuyama A, Hamilton IB, Sundquist WI. ESCRT-III Protein Requirements for HIV-1 Budding. *Cell Host and Microbe*. 1–8 (2011).

126. Ivanchenko S, Godinez WJ, Lampe M, *et al.* Dynamics of HIV-1 Assembly

and Release. *PLoS Pathog*. 5(11), e1000652 (2009).

127. Ehrlich LS, Medina GN, Carter CA. ESCRT Machinery Potentiates HIV-1 Utilization of the PI(4,5)P2-PLC-IP3R-Ca2+ Signaling Cascade. *Journal of Molecular Biology*. 413(2), 347–358 (2011).

128. Rothbauer U, Zolghadr K, Tillib S, *et al.* Targeting and tracing antigens in live cells with fluorescent nanobodies. *Nat Meth*. 3(11), 887–889 (2006).

129. Tan J, Sattentau QJ. The HIV-1-containing macrophage compartment: a perfect cellular niche? *Trends in Microbiology*. 21(8), 405–412 (2013).

130. Jouvenet N, Bieniasz PD, Simon SM. Imaging the biogenesis of individual HIV-1 virions in live cells. *Nature*. 454(7201), 236–240 (2008).

131. Gaudin R, de Alencar BC, Arhel N, Benaroch P. HIV trafficking in host cells: motors wanted! *Trends in Cell Biology*. 1–11 (2013).

132. Kadiu I, Gendelman HE. Human Immunodeficiency Virus type 1 Endocytic Trafficking Through Macrophage Bridging Conduits Facilitates Spread of Infection. *J Neuroimmune Pharmacol*. 6(4), 658–675 (2011).

133. Freed EO, Martin MA. Virion incorporation of envelope glycoproteins with long but not short cytoplasmic tails is blocked by specific, single amino acid substitutions in the human immunodeficiency virus type 1 matrix. *Journal of Virology*. 69(3), 1984–1989 (1995).

134. Joshi A, Nagashima K, Freed EO. Defects in cellular sorting and retroviral assembly induced by GGA overexpression. *BMC Cell Biol*. 10(1), 72 (2009).

135. Verma A, Bhatt AN, Farooque A, Khanna S, Singh S, Dwarakanath BS. Calcium ionophore A23187 reveals calcium related cellular stress as â€œI-Bodiesâ€ : An old actor in a new role. *Cell Calcium*. 1–13 (2011).

136. Scott CC, Gruenberg J. Ion flux and the function of endosomes and lysosomes: pH is just the start: the flux of ions across endosomal membranes influences endosome function not only through regulation of the luminal pH. *Bioessays*. 33(2), 103–110 (2011).

137. Dickinson GD, Churchill GC, Brailoiu E, Patel S. Deviant Nicotinic Acid Adenine Dinucleotide Phosphate (NAADP)-mediated Ca2+ Signaling upon Lysosome Proliferation. *Journal of Biological Chemistry*. 285(18), 13321–13325 (2010).

138. Lloyd-Evans E, Platt FM. Lysosomal Ca2+ homeostasis: Role in pathogenesis of lysosomal storage diseases. *Cell Calcium*. 50(2), 200–205 (2011).

139. Bucci C, Thomsen P, Nicoziani P, McCarthy J, van Deurs B. Rab7: a key to lysosome biogenesis. *Mol. Biol. Cell*. 11(2), 467–480 (2000).

140. Zhou Y, Frey TK, Yang JJ. Viral calciomics: Interplays between Ca2+ and virus. *Cell Calcium*. 46(1), 1–17 (2009).

141. Ekokoski E, Aitio O, rnquist KT, Yli-Kauhaluoma J, Tuominen RK. HIV-1 Tat-

peptide inhibits protein kinase C and protein kinase A through substrate competition. *European Journal of Pharmaceutical Sciences*. 1–8 (2010).

142. Mayne M, Holden CP, Nath A, Geiger JD. Release of calcium from inositol 1,4,5-trisphosphate receptor-regulated stores by HIV-1 Tat regulates TNF-alpha production in human macrophages. *J. Immunol.* 164(12), 6538–6542 (2000).

143. Uhlén P, Fritz N. Biochemistry of calcium oscillations. *Biochemical and Biophysical Research Communications*. 396(1), 28–32 (2010).

144. Gao F, Li Y, Decker JM, *et al.* Codon usage optimization of HIV type 1 subtype C gag, pol, env, and nef genes: in vitro expression and immune responses in DNA-vaccinated mice. *AIDS Res. Hum. Retroviruses*. 19(9), 817–823 (2003).

145. Lindwasser OW, Resh MD. Human immunodeficiency virus type 1 Gag contains a dileucine-like motif that regulates association with multivesicular bodies. *Journal of Virology*. 78(11), 6013–6023 (2004).

146. Underhill DM, Goodridge HS. Information processing during phagocytosis. *Nature Publishing Group*. 12(7), 492–502 (2012).

147. Ribes S, Ebert S, Regen T, *et al.* Toll-Like Receptor Stimulation Enhances Phagocytosis and Intracellular Killing of Nonencapsulated and Encapsulated Streptococcus pneumoniae by Murine Microglia. *Infection and Immunity*. 78(2), 865–871 (2010).

148. Gronski MA, Kinchen JM, Juncadella IJ, Franc NC, Ravichandran KS. An essential role for calcium flux in phagocytes for apoptotic cell engulfment and the anti-inflammatory response. *Cell Death Differ.* 16(10), 1323–1331 (2009).

149. Fidler IJ, Raz A, Fogler WE, Kirsh R, Bugelski P, Poste G. Design of liposomes to improve delivery of macrophage-augmenting agents to alveolar macrophages. *Cancer Res.* 40(12), 4460–4466 (1980).

150. Liu X, Huang N, Li H, Jin Q, Ji J. Surface and Size Effects on Cell Interaction of Gold Nanoparticles with Both Phagocytic and Nonphagocytic Cells. *Langmuir*. 29(29), 9138–9148 (2013).

151. Laskar A, Yuan X-M, Li W. Dimethyl sulfoxide prevents 7β-hydroxycholesterol-induced apoptosis by preserving lysosomes and mitochondria. *J. Cardiovasc. Pharmacol.* 56(3), 263–267 (2010).

152. Viegas MS, Estronca LMBB, Vieira OV. Comparison of the Kinetics of Maturation of Phagosomes Containing Apoptotic Cells and IgG-Opsonized Particles. *PLoS ONE*. 7(10), e48391 (2012).

153. Michailidis C, Giannopoulos G, Vigklis V, Armenis K, Tsakris A, Gargalianos P. Impaired phagocytosis among patients infected by the human immunodeficiency virus: implication for a role of highly active anti-retroviral therapy. *Clinical & Experimental Immunology*. 167(3), 499–504 (2012).

154. Poggi A, Carosio R, Rubartelli A, Zocchi MR. Beta(3)-mediated engulfment of apoptotic tumor cells by dendritic cells is dependent on CAMKII: inhibition by HIV-1 Tat. *Journal of Leukocyte Biology*. 71(3), 531–537 (2002).

155. Torre D, Gennero L, Baccino FM, Speranza F, Biondi G, Pugliese A. Impaired Macrophage Phagocytosis of Apoptotic Neutrophils in Patients with Human Immunodeficiency Virus Type 1 Infection. *Clinical and Vaccine Immunology*. 9(5), 983–986 (2002).

156. Lima RG, Van Weyenbergh J, Saraiva EMB, Barral-Netto M, Galvão-Castro B, Bou-Habib DC. The replication of human immunodeficiency virus type 1 in macrophages is enhanced after phagocytosis of apoptotic cells. *J. Infect. Dis.* 185(11), 1561–1566 (2002).

157. Lauber K, Blumenthal SG, Waibel M, Wesselborg S. Clearance of apoptotic cells: getting rid of the corpses. *Mol. Cell*. 14(3), 277–287 (2004).

158. Torchilin VP. Recent advances with liposomes as pharmaceutical carriers. *Nat Rev Drug Discov*. 4(2), 145–160 (2005).

159. Jouve M, Sol-Foulon N, Watson S, Schwartz O, Benaroch P. HIV-1 Buds and Accumulates in "Nonacidic" Endosomes of Macrophages. *Cell Host and Microbe*. 2(2), 85–95 (2007).

160. Ha S-D, Park S, Hattlmann CJ, Barr SD, Kim SO. Inhibition or deficiency of cathepsin B leads defects in HIV-1 Gag pseudoparticle release in macrophages and HEK293T cells. *ANTIVIRAL RESEARCH*. 1–10 (2011).

161. Schwegmann A, Brombacher F. Host-Directed Drug Targeting of Factors Hijacked by Pathogens. *Science Signaling*. 1(29), re8–re8 (2008).

162. Debyser Z, Desimmie BA, Taltynov O, Demeulemeester J, Christ F. Validation of host factors of HIV integration as novel drug targets for anti-HIV therapy. *Med. Chem. Commun.* 5(3), 314 (2014).

163. Opar A. New HIV drug classes on the horizon. Nat Rev Drug Discov. 6(4), 258–259 (2007).

164. Goff SP. Host factors exploited by retroviruses. *Nat Rev Micro*. 5(4), 253–263 (2007).

165. Weiss ER, Göttlinger H. The Role of Cellular Factors in Promoting HIV Budding. *Journal of Molecular Biology*. 410(4), 525–533 (2011).

166. Cloyd MW, Lynn WS. Perturbation of host-cell membrane is a primary mechanism of HIV cytopathology. *Virology*. 181(2), 500–511 (1991).

167. Wu Z, Nakanishi H. Phosphatidylserine-Containing Liposomes: Potential Pharmacological Interventions Against Inflammatory and Immune Diseases Through the Production of Prostaglandin E2 After Uptake by Myeloid Derived Phagocytes. *Arch. Immunol. Ther. Exp.* 59(3), 195–201 (2011).

168. Goldenbogen B, Brodersen N, Gramatica A, *et al.* Reduction-Sensitive Liposomes from a Multifunctional Lipid Conjugate and Natural Phospholipids:

Reduction and Release Kinetics and Cellular Uptake. *Langmuir*. 27(17), 10820–10829 (2011).

169. Smith-Franklin BA, Keele BF, Tew JG, *et al.* Follicular dendritic cells and the persistence of HIV infectivity: the role of antibodies and Fcgamma receptors. *J. Immunol.* 168(5), 2408–2414 (2002).

170. Harel-Adar T, Ben Mordechai T, Amsalem Y, Feinberg MS, Leor J, Cohen S. Modulation of cardiac macrophages by phosphatidylserine-presenting liposomes improves infarct repair. *Proceedings of the National Academy of Sciences*. 108(5), 1827–1832 (2011).

171. Fadok VA, Bratton DL, Rose DM, Pearson A, Ezekewitz RA, Henson PM. A receptor for phosphatidylserine-specific clearance of apoptotic cells. *Nature*. 405(6782), 85–90 (2000).

172. Henson PM, Bratton DL, Fadok VA. The phosphatidylserine receptor: a crucial molecular switch? *Nat. Rev. Mol. Cell Biol.* 2(8), 627–633 (2001).

173. Delwig von A, Bailey E, Gibbs DM, Robinson JH. The route of bacterial uptake by macrophages influences the repertoire of epitopes presented to CD4 T cells. *Eur. J. Immunol.* 32(12), 3714–3719 (2002).

174. Kwong PD, Mascola JR. Human Antibodies that Neutralize HIV-1: Identification, Structures, and B Cell Ontogenies. *Immunity*. 37(3), 412–425 (2012).

175. Crispin M, Bowden TA. Antibodies expose multiple weaknesses in the glycan shield of HIV. *Nature Publishing Group*. 20(7), 771–772 (2013).

List of figures and tables

Figures

Tables

Acknowledgments

First, I would like to thank **Prof. Dr. Andreas Herrmann** for giving me the great opportunity to work in his lab, where I spent the best three years of my life (until now, at least). He constantly supported and supervised my work, encouraging me particularly when I was doubting my skills.

Heartfelt thanks are for **Salvo**, a dearest friend and a colleague, who strongly contributed to my work with his vast experience, and always reassured and supported me with his endless patience. *Ringraziu a Santa Lucia, ca mi fici canusciri a Salvo.*

For the experimental support, I want to thank **Maik J. Lehmann** for performing electron microscopy imaging and **Roberto Petazzi**, who produced part of the liposomes used in this work and performed fundamental measurements at the FACS. Thanks also to **Marie Behrent**, who worked at the characterization of the calcium staining under my supervision.

Thanks to **Anja**, who supervised the work of my master thesis, introducing me into the world of biophysics. Her teaching inspired me in the following years, giving me fundamental ideas for my work.

I own special thanks to **Julia Heymann** for performing the translation in German of the Abstract of this thesis and for her constant kindness and generosity.

Special thanks to my two "desk-mates": **Christian** and **Joanna.** You are just the best desk-mates of the world. Thank you for the precious scientific discussions and the gorgeous time spent together, at work and in the free time. *Joanna, I would have put a cross on that post-it if you haven't done it first, and Christian, dear "Kumpel", I just wish you all the best, ever.*

Thanks to all the **members of the Molecular Biophysics Lab** for their friendliness and for keeping a great atmosphere at work. But especially, I would like to thank **Roland**, who taught me, at the beginning of my PhD, not to be scared of a

confocal microscope and with whom I shared very important moments of the last three years. *Our friendship means a lot to me*. Heartfelt thanks are also for **Caro**, for her immense sweetness and kindness and with whom I had the pleasure to share some exciting trips around the world. I want to thank also **Aouefa**, *who is a bit magic and can make some light in the darkness*, **Lotte,** the girl from Neukölln (it has always been *mega lustig* with you!) and **Fabian** (*der Leutnant*), for solving the troubles I was having with my MacBook and for the great time at work. Many thanks go also to **Gabi** for the support with FACS, her kindness (and the fabulous tomatoes from her balcony), **Luisa** for her constant good mood, and **Chris** for her generosity and for helping me in a difficult moment with her encouraging advices.

I would like to thank also **Dr. Thomas Korte**, **Gudrun**, **Sabine** and **Silvia** for the technical support in the every-day-lab's life and **Frau Piater**, for the kind help with the German bureaucracy.

This work was supported by the **European Commission - Marie Curie Initial Training Network**.

*Ringrazio di cuore **i miei genitori** per tutto quello che hanno sempre fatto per me. Senza il loro amore e la loro costante fiducia nei miei confronti, questo lavoro non sarebbe stato realizzabile.*

*Ganz lieben Dank auch an **Jan** und **Sebastian**. Jungs, wie hätte ich es ohne euch schaffen können?*

Publications

Publications and manuscripts

αEnv-decorated phosphatidylserine liposomes trigger phagocytosis of HIV-virus-like particles in macrophages. ***Gramatica A.**, Petazzi R.A., Lehmann M.J., Ziomkowska J., Herrmann A., Chiantia S. Nanomedicine. 2014 Mar 1. pii: S1549-9634(14)00043-4. doi: 10.1016/j.nano.2014.02.008. [Epub ahead of print].*

Reduction-sensitive liposomes from a multifunctional lipid conjugate and natural phospholipids: reduction and release kinetics and cellular uptake. *Goldenbogen B., Brodersen N., **Gramatica A**., Loew M., Liebscher J., Herrmann A., Egger H., Budde B., Arbuzova A. Langmuir. 2011 Sep 6;27(17):10820-9. doi: 10.1021/la201160y. Epub 2011 Aug 5.*

The HIV-1 Envelope Transmembrane Domain Binds TLR2 Through a Distinct Dimerization Motif and Inhibits TLR2 Mediated Responses. *Reuven E.M., Ali M., Rotem E., Schwarzer R. **Gramatica A.,** Futerman A.H., Shai Y. (In revision by PLOS Pathogens).*

The cholesterol-binding motif of the HIV-1 glycoprotein gp41 regulates lateral sorting and oligomerization. *Schwarzer R., Levental I., **Gramatica A.**, Scolari S., Buschmann V., Veit M., Herrmann A. (In revision by Cellular Microbiology).*

Release of intracellular calcium after gH-α4β1-integrin interaction promotes alphaherpesviruses entry. *Azab W., **Gramatica A.**, Herrmann A., Osterreider N. (in preparation).*

Patent

Composition for targeting cancer by the controlled release of an active substance. *Egger H., Budde B., Temming K., Arbuzova A.,* **Gramatica A.**, *Herrmann A., Liebscher J., Brodersen N. Publication number: CA000002814097A1.*

Oral and poster presentations

Oral presentations

Final Virus-Entry Meeting *(26.08.13–30.08.13) Tel Aviv (Israel)*

Annual Virus-Entry Meeting *(13.02.13–15.02.13) Greifensee, (Switzerland)*

Annual Virus-Entry Meeting *(11.05.12–13.05.12) Punta Prima, Menorca (Spain)*

Annual Virus-Entry Meeting *(07.07.11–10.07.11) Stockholm (Sweden)*

Poster presentations

57th Annual Meeting of the Biophysical Society

(02.02.13 – 06.02.13) Philadelphia, Pennsylvania (USA)

7th International Virus Assembly Symposium

(13.05.12 – 17.05.12) Punta Prima, Menorca (Spain)

56th Annual Meeting of the Biophysical Society

(25.02.12 – 29.02.12) San Diego, California (USA)

7th International Conference on Methods and Applications of Fluorescence

(11.09.11 – 14.09.11) Strasbourg (France)

Eidestattliche Erklärung

Ich erkläre, dass ich die vorliegende Arbeit selbständig und nur unter Verwendung der angegebenen Literatur und Hilfsmittel angefertigt habe. Wurden Ergebnisse in Kooperation produziert, ist dies entsprechend angegeben.☐Ich besitze keinen entsprechenden Doktorgrad und habe mich anderwärts nicht um einen Doktorgrad beworben. Die dem Promotionsverfahren zugrunde liegende Promotionsordnung ist mir bekannt.

Berlin, den 06.05.14

Andrea Gramatica